

TKK Dissertations 2  
Espoo 2005

**SIMULATION OF ELECTRICAL MACHINES, CIRCUITS  
AND CONTROL SYSTEMS USING FINITE ELEMENT  
METHOD AND SYSTEM SIMULATOR**

Doctoral Dissertation

**Sami Kanerva**



**Helsinki University of Technology  
Department of Electrical and Communications Engineering  
Laboratory of Electromechanics**

TKK Dissertations 2  
Espoo 2005

**SIMULATION OF ELECTRICAL MACHINES, CIRCUITS  
AND CONTROL SYSTEMS USING FINITE ELEMENT  
METHOD AND SYSTEM SIMULATOR**

Doctoral Dissertation

**Sami Kanerva**

Dissertation for the degree of Doctor of Science in Technology to be presented with due permission of the Department of Electrical and Communications Engineering for public examination and debate in Auditorium S4 at Helsinki University of Technology (Espoo, Finland) on the 29th of April, 2005, at 12 noon.

**Helsinki University of Technology  
Department of Electrical and Communications Engineering  
Laboratory of Electromechanics**

**Teknillinen korkeakoulu  
Sähkö- ja tietoliikennetekniikan osasto  
Sähkömekaniikan laboratorio**

Distribution:

Helsinki University of Technology

Department of Electrical and Communications Engineering

Laboratory of Electromechanics

P.O.Box 3000

FI - 02015 TKK

URL: <http://www.sahko.hut.fi/>

Tel. +358-9-4511

E-mail: [electromechanics@hut.fi](mailto:electromechanics@hut.fi)

© 2005 Sami Kanerva

ISBN 951-22-7609-7

ISBN 951-22-7610-0 (PDF)

ISSN 1795-2239

ISSN 1795-4584 (PDF)

URL: <http://lib.hut.fi/Diss/2005/isbn9512276100/>

TKK-DISS-1981

Picaset Oy

Helsinki 2005



HELSINKI UNIVERSITY OF TECHNOLOGY P.O. BOX 1000, FIN-02015 HUT <a href="http://www.hut.fi">http://www.hut.fi</a>		ABSTRACT OF DOCTORAL DISSERTATION	
Author			
Name of the dissertation			
Date of manuscript		Date of the dissertation	
Monograph		Article dissertation (summary + original articles)	
Department			
Laboratory			
Field of research			
Opponent(s)			
Supervisor (Instructor)			
Abstract			
Keywords			
UDC		Number of pages	
ISBN (printed)		ISBN (pdf)	
ISBN (others)		ISSN	
Publisher			
Print distribution			
The dissertation can be read at <a href="http://lib.hut.fi/Diss/">http://lib.hut.fi/Diss/</a>			

# Preface

The research related to this thesis was carried out in the Laboratory of Electromechanics, Helsinki University of Technology. This study is a part of the long-term project to couple the finite element code of the laboratory (FCSMEK) with a system simulator. The work was financed by the National Technology Agency of Finland (Tekes), ABB Oy, Fortum Power and Heat Oy and the Graduate School in Electrical Engineering (GSEE).

First of all, I would like to express my gratitude to Emeritus Professor Tapani Jokinen, who originally suggested this topic, to my supervisor Professor Antero Arkkio, and to the head of the laboratory, Professor Asko Niemenmaa.

For many people, this work may seem my "personal" project, since I have been continuously working on this topic for several years. However, I was not alone. Slavomir Seman from the Laboratory of Electromechanics has made a remarkable contribution to this work by testing the methods, creating simulation models, providing results and bringing out the user's point of view. I also owe a debt of gratitude to Jukka Kaukonen, Jukka Järvinen, Juhani Mantere and Áron Szücs from ABB Oy, Halina Burzanowska, Christian Stulz and Bilal Gerhard from ABB Switzerland Ltd, and all the colleges in the Laboratory of Electromechanics. In addition, I would like to express my special appreciation to Marika Schröder, Kimmo Hamunen, Jarmo Perho and Ari Haavisto for keeping the many every-day matters running smoothly.

Naturally, I thank my loving family for bringing so much happiness into my life.

Finally, the financial support of the Finnish Cultural Foundation, Imatran Voima Foundation and Tekniikan edistämissäätiö is gratefully acknowledged.

Helsinki, 2005

Sami Kanerva

# Contents

<b>Abstract</b>	<b>3</b>
<b>Preface</b>	<b>4</b>
<b>Contents</b>	<b>5</b>
<b>Symbols and definitions</b>	<b>8</b>
<b>1 Introduction</b>	<b>11</b>
1.1 Overview of the coupled field-circuit problems . . . . .	11
1.1.1 Numerical methods . . . . .	12
1.1.2 Modelling electrical machines by field and circuit equations . . . . .	13
1.1.3 Coupling with external circuits . . . . .	14
1.1.4 Coupling with power electronics . . . . .	14
1.1.5 Coupling with closed-loop control systems . . . . .	16
1.1.6 Software for coupled simulation . . . . .	16
1.2 Aim of the work . . . . .	17
1.3 Scientific contribution . . . . .	17
1.4 Outline of the thesis . . . . .	18
<b>2 Computational methods</b>	<b>19</b>
2.1 Finite element model for electrical machines . . . . .	19
2.1.1 Equations for magnetic field and windings . . . . .	19
2.1.2 Transient time-stepping simulation . . . . .	23
2.2 Direct coupling of field and circuit equations . . . . .	27
2.3 Coupling by the current output approach . . . . .	28
2.3.1 FEM model as a functional block . . . . .	28
2.3.2 Implementation for SIMULINK . . . . .	29
2.4 Coupling by the circuit parameter approach . . . . .	30
2.4.1 Electromotive force and dynamic inductance . . . . .	30
2.4.2 Extraction of the circuit parameters . . . . .	31
2.4.3 Implementation for SIMULINK . . . . .	32
2.5 Conclusion . . . . .	33

<b>3</b>	<b>Case study: doubly-fed induction generator</b>	<b>34</b>
3.1	Description of the system . . . . .	34
3.1.1	Finite element model of the generator . . . . .	34
3.1.2	Electrical supply . . . . .	35
3.2	Simulation models . . . . .	37
3.2.1	Circuit parameter approach . . . . .	37
3.2.2	Direct coupling . . . . .	39
3.3	Simulation results . . . . .	40
3.3.1	Steady state . . . . .	40
3.3.2	Voltage dip in stator . . . . .	41
3.3.3	Effect of the simulation parameters . . . . .	43
3.4	Discussion . . . . .	45
<b>4</b>	<b>Case study: cage induction motor with compensation capacitors</b>	<b>48</b>
4.1	Description of the system . . . . .	48
4.1.1	FEM model of the cage induction motor . . . . .	48
4.1.2	Circuit model . . . . .	48
4.2	Simulation models . . . . .	51
4.2.1	Current output approach . . . . .	51
4.2.2	Circuit parameter approach . . . . .	52
4.2.3	Direct coupling . . . . .	53
4.3	Simulation results . . . . .	55
4.3.1	Ideal voltage supply . . . . .	55
4.3.2	Grid and compensating capacitors . . . . .	58
4.4	Experimental validation . . . . .	61
4.4.1	Test setup . . . . .	61
4.4.2	Measured results . . . . .	62
4.5	Discussion . . . . .	63
<b>5</b>	<b>Case studies of controlled frequency converter supply</b>	<b>65</b>
5.1	Induction motor drive with detailed DTC algorithm . . . . .	65
5.1.1	Background . . . . .	65
5.1.2	Description of the system model . . . . .	66
5.1.3	Results . . . . .	67
5.1.4	Conclusion . . . . .	68
5.2	Doubly-fed induction generator in a variable-speed wind turbine . . . . .	70
5.2.1	Background . . . . .	70
5.2.2	Description of the system model . . . . .	71
5.2.3	Results . . . . .	72
5.2.4	Conclusion . . . . .	75
5.3	Discussion . . . . .	76

<b>6</b>	<b>Discussion</b>	<b>78</b>
6.1	Summary of the results . . . . .	78
6.2	Significance of the work . . . . .	79
6.3	Optimal environment for the coupled simulation of electrical machines, circuits and control systems . . . . .	80
<b>7</b>	<b>Conclusion</b>	<b>82</b>
	<b>References</b>	<b>84</b>
<b>A</b>	<b>Implementation of the FEM computation in Simulink</b>	<b>90</b>
A.1	S-functions in general . . . . .	90
A.2	S-function for the FEM computation . . . . .	91
A.2.1	Exceptional concepts . . . . .	91
A.2.2	Outline of the implementation . . . . .	91
A.2.3	Data transfer methodology . . . . .	92

## Symbols and definitions

$A$	magnetic vector potential
$a$	nodal value of the magnetic vector potential
$B$	magnetic flux density, coefficient related with rotor bar equations
$C$	capacitance
$e$	unit vector ( $e$ ), electromotive force in electrical machine ( $d\psi/dt$ )
$E$	electric field strength
$F$	coefficient related with field and winding equations
$f$	frequency
$G$	coefficient related with the circuit equations
$H$	magnetic field strength
$I$	effective RMS value of current
$i$	current, index
$J$	current density, Jacobian, moment of inertia
$j$	index
$K$	coefficient related with the connection of the windings
$k$	index of a time step
$L$	inductance
$l$	length
$M$	coefficient related with the connection of the windings
$N$	number of turns or nodes
$n$	number of phases or rotor bars, rotational speed
$P$	coefficient related with the connection of the windings, power
$p$	number of pole pairs
$Q$	coefficient related with winding equations
$R$	resistance
$r$	residual function
$S$	cross section area, coefficient related with field equations
$s$	slip
$T$	torque
$t$	time
$U$	effective RMS value of voltage
$u$	line-to-neutral voltage
$v$	line-to-line voltage

$W$	coefficient related with phase winding equations
$x$	general variable
$z$	coordinate axis
$\alpha$	cutoff frequency of the high-pass filter used in numerical integration
$\gamma$	number of symmetry sectors in the finite element mesh
$\Delta$	difference
$\theta$	angular position of rotor
$\lambda$	weight function
$\nu$	reluctivity
$\sigma$	conductivity
$\phi$	electric scalar potential
$\psi$	magnetic flux linkage
$\Omega$	integration area
$\omega$	angular frequency

## Subscripts

b	rotor bar
c	capacitance
e	end winding
f	field
g	grid
L	load
m	mechanical
max	maximum
min	minimum
N	rated value
n	node
neg	negative
pos	positive
r	rotor
s	stator
sc	short circuit
w	winding
z	z-axis
0	coefficient referring to the previous time step
$\Delta$	increment

## Superscripts

abs	absolute
circ	circuit parameter approach
cur	current output approach
D	delta connection
dir	direct coupling
dyn	dynamic
$k$	current time step
$k - 1$	previous time step
meas	measured
$n$	iteration step
rel	relative
T	transpose
Y	star connection

## Abbreviations

AC	alternating current
DC	direct current
DFIG	doubly-fed induction generator
DTC	direct torque control
FEM	finite element method
RMS	root mean square
TR	transformer

Vectors are typed as lowercase bold italic, for example  $\mathbf{a}$ . Matrices and vector fields are typed as uppercase bold italic, for example  $\mathbf{S}$ ,  $\mathbf{H}$ . Independent variables are denoted by prime, for example  $x'$ .

MATLAB and SIMULINK are registered trademarks of MathWorks, Inc. FLUX2D is a registered trademark of Cedrat. Maxwell2D and SIMPLORER are registered trademarks of Ansoft Corporation. FEMLAB is a registered trademark of Comsol, Inc.

# 1 Introduction

During the past few decades, the numerical computation of magnetic fields has gradually become a standard in electrical machine design. At the same time, the amount of power electronics coupled with electrical machines has continuously increased. The design of converters and electrical machines has traditionally been carried out separately, but the demands for increased efficiency and performance at lower cost push the product development activities towards a combined design process. Especially in large motor drives and variable-speed generators, both machine and converter must be individually tailored to work together and thereby guarantee the best possible performance for the application. In such a task, a combined simulation environment, where the magnetic field analysis of the electrical machine is coupled with a detailed model of the converter is required.

The finite element method (FEM) currently represents the state-of-the-art in the numerical magnetic field computation relating to electrical machines. The converter models are generally composed of relatively simple electrical circuits and a control system with varying complexity. In the scope of this thesis, a typical motor or generator can be modelled with high accuracy by two-dimensional FEM, which is coupled with the circuit equations for the windings. The converter circuits usually contain a few passive circuit elements, such as inductors and capacitors, and also switching components, which are often modelled as ideal switches. For such circuits, coupling with the FEM computation is quite simple and reported widely in the literature. The control systems, on the other hand, are nowadays based on complex estimators and feedback loops, and they are typically implemented by digital signal processors. Consequently, the control system simulation is usually carried out in system simulators, like SIMULINK, using very simple analytical models for electrical machines.

In order to achieve the desired system-simulation environment for electrical machine and controlled converters, the FEM computation must be coupled with the circuit and control simulation. For this purpose, new knowledge about the coupling mechanisms is required. Based on the previous studies and comparative analysis of newly developed methods, this thesis aims at proposing an optimal methodology for coupling the FEM models of electrical machines with external circuits and closed-loop control systems.

## 1.1 Overview of the coupled field-circuit problems

In the following literature review, the coupled field-circuit problems are studied from the viewpoint of electrical machines and converters. The main field of interest is the coupling of two-dimensional finite element analysis with the circuit and control equations. In the early 1980's, formulations for such coupling were developed for modelling voltage-supplied electrical machines. Inclusion of external circuits with power electronics was presented widely during

the late 1980's and early 1990's. However, most of the studies concerned rather simple geometries and circuits, because the computational facilities were limited and most of the authors had to develop the program codes themselves. Together with the increasing computational power and development of the software, the complexity of the modelled systems has also increased. Nowadays, the trend is to model large systems as a whole, including electromagnetics, thermal fields, kinematics and control systems. However, there is still a lot of work ahead to achieve this goal and the coupling mechanisms need to be studied further.

The formulations, terminology and numerical methods in the field-circuit problems are discussed by Tsukerman et al. (1993). The most usual approach is the magnetic vector potential formulation with filamentary and solid conductors. The filamentary conductors, sometimes referred as stranded conductors, consist of several turns of thin wire carrying the same current. In order to simplify the analysis, the eddy currents in filamentary conductors are not taken into account, but a constant current density is assumed. In the solid conductors, or massive conductors, eddy currents represent a significant part of the total excitation and they cannot be omitted from the analysis.

The numerical solution of the coupled problem is generally accomplished directly or indirectly. The difference lies in, whether the field and circuit equations are solved simultaneously or sequentially. Eustache et al. (1996) have discussed the coupled problems more generally, especially pointing out the benefits and applicability of indirect coupling procedures. When the time constants in the subdomains differ significantly from each other, it is advantageous to decouple the domains and utilize different time steps. Another major advantage is that the decoupled models can be constructed separately by the experts in different fields. Hameyer et al. (1999) classified several types of coupled problems on the basis of physical, numerical or geometrical coupling. When considering the coupling between magnetic fields and electrical circuits, the coupling is physically strong, which means that they cannot be considered separately without causing a significant error in the analysis. However, they can be analyzed indirectly in the case of different time constants. In this thesis, similar definitions are adopted for strong, weak, direct and indirect coupling, as presented in the references mentioned above.

### **1.1.1 Numerical methods**

The numerical methods for the solution of strongly coupled problems with finite elements are studied extensively in the literature. In the time-stepping analysis of FEM-based nonlinear differential equations, the solution process requires methods for modelling the time-dependence, handling the nonlinearity and solving the resulting system of equations. Many aspects of this process are discussed by Albanese and Rubinacci (1992), for example.

The simple difference methods, like backward Euler, Galerkin or Crank-Nicholson, are the most commonly used methods for the time-stepping simulation. While these utilize results from two adjacent time steps, there are also numerous multi-step methods performing numerical integration over several time steps and providing higher accuracy. When phenomena of substantially different time scales are coupled together, the problem is mathematically considered as stiff. Most of the multi-step methods usually fail for such problems, but the implicit difference methods often converge. Further discussion on stiff problems is presented by Gear (1971).

For nonlinear equations, an iterative scheme is required for the numerical solution. The classical Newton-Raphson method, with its several modifications, is used widely for this purpose, as well as the block iterative Picard methods (Cervera et al., 1996; Driesen et al., 2002). In order to improve the convergence, the iteration is often damped by relaxation procedures, which are discussed by several authors (Nakata et al., 1992; Fujiwara et al., 1993; O'Dwyer and O'Donnell, 1995; Driesen et al., 1999; Vande Sande et al., 2003).

The final system of equations arising from the finite element method is typically sparse, symmetric and positive definite. When coupled field-circuit problems are considered, however, the system of equations is indefinite and often ill-conditioned. This must be taken into account in choosing suitable methods for preconditioning and factorization (De Gersem et al., 2000).

### **1.1.2 Modelling electrical machines by field and circuit equations**

In the finite element model of an electrical machine, the magnetic field is excited by the currents in the coils. However, it is often more appropriate to model the feeding circuit as a voltage source, which leads to the combined solution of the field and circuit equations. At first, time-harmonic formulations using complex variables were presented for sinusoidal supply; later on, approaches for time-stepping simulation were derived in order to model arbitrary voltage waveforms or transients. The phase windings in the stator and rotor are generally modelled as filamentary conductors, and the rotor bars in cage induction machines or damper windings in synchronous machines are modelled as solid conductors with eddy currents.

Williamson and Ralph (1983) modelled an induction motor with a constant voltage source, assuming uniformly distributed sinusoidal currents in the stator and rotor coils. The model was extended by including eddy currents in the formulation (Williamson and Begg, 1985), and introducing a time-stepping methodology for cage induction machines (Williamson et al., 1990) and wound-rotor induction machines (Smith et al., 1990). The coupling between the magnetic field and the feeding circuit was accomplished by coupling impedances, which were determined by the finite element method and inserted into the circuit equations. In nonlinear cases, the correct inductance values were determined iteratively from the field and circuit equations.

Most of the approaches for modelling electrical machines were based on the direct coupling between the field and circuit equations. Shen et al. (1985) coupled the eddy-current formulation with circuit equations and applied the method on a shaded-pole motor, assuming sinusoidal variation of the field and circuit variables, and linear characteristics of the iron parts. After including the nonlinearity of the iron and impedances of the end-ring, the method was also applied to a cage induction machine using either the time-harmonic (Vassent et al., 1991a) or time-stepping approach (Vassent et al., 1991b). Strangas and Theis (1985) presented a time-stepping approach for analyzing a shaded-pole motor. They coupled the field equations directly with the circuit equations of the stator coils, shading rings and the rotor cage. The same method was also applied to a cage induction motor (Strangas, 1985) and a permanent magnet motor (Strangas and Ray, 1988). A similar method was also presented by Preston et al. (1988) and applied to an induction motor. Arkkio (1987) presented a methodology for analyzing cage induction machines using both time-harmonic and time-stepping approaches. This methodology is also the computational basis for this work and is described thoroughly in Chapter 2.

### 1.1.3 Coupling with external circuits

Based on the approaches for electrical machines presented above, the inclusion of external circuits is relatively simple, since it only requires adding new elements into the circuit equations of the windings. For this purpose, many authors have presented general methods, in which any circuit models composed of resistors, inductors, capacitors, diodes or other semiconductors can be coupled with the electromagnetic model of the electrical machine. The mathematical formulations for the circuit equations are usually based on loop currents or nodal voltages, but most of the formulations combine both approaches. The main reason for this is that the currents of filamentary conductors and inductances, as well as the voltages of solid conductors and capacitances, are the most natural selections for unknown variables in the coupled formulation, and therefore result in the minimum number of equations.

Meunier et al. (1988) presented a generalized formulation for coupling two-dimensional finite element analysis with solid or filamentary conductors using sinusoidal voltage or current sources. Lombard and Meunier (1993) developed the method further for time-stepping analysis allowing resistive and inductive components in the external circuit. The unknown variables of the formulation were the magnetic vector potential, current in the filamentary conductors and inductors, and voltage drop over the solid conductors. Tsukerman et al. (1992) presented a similar approach, allowing also capacitors in the external circuit. However, the voltage drop over the capacitance was not included as an unknown variable but integrated from the current instead. Salon et al. (1990) developed a method, which also takes movement into account, and Bedrosian (1993) developed an indirect method, which separated the finite element and circuit equations in order to gain a more efficient simulation by retaining the sparsity and positive-definiteness of the finite element matrix.

Many authors have considered the field-circuit coupling from the circuit theoretical point of view. The methods presented by Sadowski et al. (1995) and Charpentier et al. (1998) were based on the state-space approach, where the inductor currents and capacitor voltages were considered as the unknown variables in the circuit model. Similar equations were also obtained using the modified loop approach (Väänänen, 1994) and the modified nodal approach (Wang, 1996; Costa et al., 2000). Väänänen (1996) formulated the field equations to represent a multiport circuit element, which was coupled to the electric circuit by the currents and voltages of the filamentary and solid conductors. Abe and Cardoso (1998) coupled the field and circuit equations by a special nodal formulation presented originally by Dommel (1969), in which the inductors and capacitors were modelled as current sources in parallel with a variable resistor. Fu et al. (2004) presented both nodal and loop formulations, which were applied to several example cases. The selection of the appropriate formulation was case-dependent, since additional equations were introduced in the nodal formulation by the filamentary conductors, and similarly in the loop formulation by the solid conductors.

### 1.1.4 Coupling with power electronics

The simulation of power electronics together with electrical machines can be carried out in several ways. The simplest approach is to define the supply voltage waveform with respect

to time or position and use this pre-defined supply in the simulation. However, modelling the real interaction between the electrical machine and the converter also requires models for the semiconductors. Usually, the switching elements are represented in the circuit model as binary-valued resistors, the value of which depends on the state of the switch. A distinction is often made between diodes and externally controlled switches because of the differences in defining the switching instant. In the simulation of diodes, the time step must be adapted to the switching instants in order to prevent negative overshoots in the current. For the externally controlled switches, synchronization of the time steps is simple, since the switching instants are already known in advance.

Arkkio (1990) simulated a cage induction motor and a frequency converter, in which the voltage waveform was determined before the simulation. Preston et al. (1991a) used a similar approach for the simulation of a switched reluctance motor drive, where the excitation current was defined according to the rotor position. In the simulation of a synchronous generator and rectifier, the field and circuit equations were decoupled and solved iteratively, and a procedure for searching the switching instants in the rectifier was introduced (Preston et al., 1991b).

Piriou and Razek (1988) modelled the operation of a diode by means of an exponential function and applied it to the simulation of a simple circuit consisting of a magnetic coil, voltage source and diode. Later on, the method was extended for rotating machines and three-dimensional geometries (Piriou and Razek, 1990a; Piriou and Razek, 1990b; Piriou and Razek, 1993). Väänänen (1994, 1996) modelled the diodes by a resistance in parallel with a controllable current source, providing a smooth transition region between the conducting and non-conducting states. The controllable switches were modelled in the same manner, but the switching instants had to be defined before the simulation. The method was applied to the simulation of a switched reluctance motor drive, a permanent magnet generator and a rectifier, and a cage induction motor supplied by a frequency converter.

Williamson and Volschenk (1995) simulated a generator and a rectifier using the same approach that had previously been applied to induction machines (Williamson et al., 1990; Smith et al., 1990). The diodes were modelled as binary-valued resistors and the time steps were selected according to the rate of change in the magnetic properties and the switching instants of the rectifier.

Sadowski et al. (1993) presented a field-circuit simulation of a load-commutated inverter supplying a permanent magnet motor. Switches were modelled as binary-valued resistors, and the converter operation was divided into conduction and commutation sequences. The resistance and inductance values in the phases were changed according to the states of the switches. The method was developed further and the state-space approach was adopted (Sadowski et al., 1995). Kuo-Peng et al. (1997) developed a general method using an automatic procedure to construct the state-space equation for arbitrary circuit topologies and demonstrated the method by simulating a fly-back converter with a saturable transformer. Linear forces and movement was included for modelling contactors (Kuo-Peng et al., 2000) and, finally, the method was extended for rotating machines by taking into account the polyphase structures and rotational movement (Oliveira et al., 2001; Oliveira et al., 2002).

### 1.1.5 Coupling with closed-loop control systems

Inclusion of a closed-loop control system within the field-circuit model has not been studied very widely, since implementing the feedback loop into the time-stepping analysis is a rather complex task. The basic scheme is to synchronize the time steps with the control system, which, in turn, controls the switching components of the converter. The most common approach is to pass the output data from the field-circuit simulation after each time step to the control system, which makes the decision to set the switching state for the next step. Naturally, this causes a one-step delay in the operation of the control system, but the error is usually negligible due to the discrete characteristics of the controlled converter circuit. Another possibility is to couple the control system equations directly with the field and circuit equations, when the switching instants are not governed by the time stepping, but the time steps will be adapted according to the desired control.

Demenko (1994) used direct field-circuit coupling to simulate a permanent magnet motor drive with a simple control strategy, where the speed and position of the rotor were used for controlling the switches after each time step. Ito et al. (1997) simulated a similar system by coupling the field analysis indirectly with the circuit and mechanical equations. The control logic was also based on the angular position, but no details were presented. In the study of Ahn et al. (2000), vector control of the current was coupled with the field-circuit analysis of a linear induction motor by running the vector control model between the time steps. Ho et al. (2001) modelled a current hysteresis controller with a brushless DC motor drive in a similar manner, but an adaptive time-step control was added in order to keep the current within the hysteresis limit. A similar approach was also applied by Jabbar et al. (2004) to a spindle motor drive with a current hysteresis controller.

Kuo-Peng et al. (1999) included the closed-loop control systems into the software for coupled field-circuit simulation, and applied the method to a nonlinear coil and transistor inverter with a current hysteresis controller. As a continuation, Roel Ortiz et al. (2001) presented an approach in which the control signals for the switches are generated during the simulation and the time steps are automatically adjusted according to the control. The method was applied to a saturable inductor and a full bridge inverter with sliding mode control. Manot et al. (2002) presented an application of the method to model an induction heating device supplied by a resonant converter.

### 1.1.6 Software for coupled simulation

In most of the studies, the software used for the computation has been developed in universities for research purposes. The main reasons for this are the lack of suitable commercial software with a reasonable price and the need to modify the program code freely. In many cases, the development of a finite element code was started in 1970's or 1980's and then constantly developed to suit the current research interests. However, commercial FEM software is nowadays available with various possibilities of coupling the field analysis with circuits or other fields, but they are still not always suitable for university research due to unaffordable licence fees and confidential computational algorithms or program code.

One of the first commercial field analysis software with circuit coupling was FLUX2D by Cedrat, which had a connection with the system simulator SIMPLORER. Later on, the link with SIMPLORER was cancelled, but coupling between FLUX2D and SIMULINK is now available (Cedrat, 2005). Another major contribution to commercial software is carried out by Ansoft, presenting coupling between Maxwell2D and SIMPLORER (Ansoft, 2005). In addition, Ansys, MagneForce and Infolytica provide software performing circuit simulation together with finite element analysis (Ansys, 2005; MagneForce, 2005; Infolytica, 2005), and Comsol provides FEMLAB, a multiphysics software for coupling any fields that can be described by partial differential equations (Comsol, 2005). Naturally, there are numerous software vendors that are not included in this study, but usually they are not actively operating in the field of electrical machines or do not provide the field-circuit coupling.

## 1.2 Aim of the work

The original motivation for this work was to simplify the procedure of modelling and simulating electrical machines and controlled power electronics. In this thesis, therefore, a methodology is presented for coupling two-dimensional FEM computation of electrical machines with the system simulator SIMULINK. The main objective is to provide methods for constructing a large-scale simulation model in SIMULINK, with the FEM computation included as a simple functional block representing the electrical machine. The benefits obtained by such a methodology are ease of model construction and simulation, flexible options for post processing and the possibility of extending the finite element analysis for experts in power electronics or control systems without a comprehensive knowledge of FEM computation.

Another important goal of the work is to explore the coupling mechanisms between the magnetic fields, circuits and control systems. Two numerical approaches will be presented: the current output approach and circuit parameter approach, and their applicability for such a task will be evaluated. The results obtained in this work will be analyzed in order to find an optimal environment and methodology for the simulation of coupled magnetic fields, circuits and control systems.

## 1.3 Scientific contribution

The scientific contribution of this study comprises the following:

1. A methodology for coupling time-stepping finite element analysis with a system simulator is presented.
2. The development and evaluation of two numerical coupling methods based on current output or circuit parameters.
3. A simulation of closed-loop control systems with the finite element analysis using different time steps for the subdomains.

4. Confirmation of the applicability of the methodology by examples relating to real industrial applications.
5. The proposal of an optimal environment and methodology for coupled simulation of magnetic field, circuits and control systems.

## **1.4 Outline of the thesis**

The aim of this chapter is to introduce the topic, relevant literature and the contents of the thesis. Chapter 2 reviews the computational methods for the finite element analysis and presents the two coupling methods, current output approach and circuit parameter approach.

In Chapter 3, the accuracy of the circuit parameter approach is evaluated by simulating a doubly-fed induction generator and comparing the results to those obtained by directly coupled simulation. Chapter 4 presents an example of a cage induction motor with compensation capacitors and a simple grid model. The example is used for evaluating both the current output approach and the circuit parameter approach by comparing the simulation results with each other and directly coupled simulation. Chapter 5 presents two examples of frequency converter supply, which are based on real industrial applications. Both the current output approach and circuit parameter approach are used for the simulation and their performance is analyzed.

The results are discussed in each chapter and gathered together in Chapter 6, in which an optimal environment and methodology for coupled simulation of magnetic field, circuits and control systems is also proposed. Finally, the conclusion of the thesis is presented in Chapter 7.

## 2 Computational methods

This chapter describes the computational methods that are used in simulating the example cases in the following chapters. The finite element model for electrical machines, combining the magnetic field equations with the voltage equations of the windings, is coupled with external circuit equations using either direct or non-iterative indirect coupling. Two different approaches are presented for indirect coupling: the current output approach and circuit parameter approach, both of which are also implemented for SIMULINK.

### 2.1 Finite element model for electrical machines

In the model of the electrical machine, the magnetic field in the iron core, windings and air gap is solved by the two-dimensional finite element method and coupled with the voltage equations of the stator and rotor windings. The resulting equations are solved by a time-stepping approach, while the Newton-Raphson iteration is utilized for handling the nonlinearities.

#### 2.1.1 Equations for magnetic field and windings

##### Two-dimensional quasi-static magnetic field

The magnetic field in an electrical machine is governed by Maxwell's equations

$$\nabla \times \mathbf{H} = \mathbf{J} \quad (2.1)$$

$$\nabla \times \mathbf{E} = -\frac{\partial \mathbf{B}}{\partial t} \quad (2.2)$$

where

$\mathbf{H}$  is the magnetic field strength

$\mathbf{J}$  is the current density

$\mathbf{E}$  is the electric field strength

$\mathbf{B}$  is the magnetic flux density.

It is assumed that the polarization and displacement currents are negligible because of the low frequencies used with the electrical machines. Therefore, those components are omitted from (2.1) and the analysis is referred to as quasi-static.

Using the reluctivity  $\nu$ , we have the material equation

$$\mathbf{H} = \nu \mathbf{B} \quad (2.3)$$

where  $\nu$  is a material-dependent, possibly nonlinear function of the magnetic field. If the material is not isotropic,  $\nu$  must be replaced by a tensor taking into account the effect of the magnetizing direction. The magnetic vector potential  $\mathbf{A}$  defines the magnetic flux density as

$$\mathbf{B} = \nabla \times \mathbf{A} \quad (2.4)$$

and the substitution of (2.4) and (2.3) into (2.1) gives the fundamental equation of the vector potential formulation for magnetic field

$$\nabla \times (\nu \nabla \times \mathbf{A}) = \mathbf{J} \quad (2.5)$$

The two-dimensional model is based on the assumption that the magnetic vector potential and current density have only  $z$ -axis components and their values are determined in the  $xy$ -plane

$$\mathbf{A} = A(x, y) \mathbf{e}_z \quad (2.6)$$

$$\mathbf{J} = J(x, y) \mathbf{e}_z \quad (2.7)$$

where  $\mathbf{e}_z$  denotes the unit vector in the  $z$ -axis direction. As a result, (2.5) becomes

$$-\nabla \cdot (\nu \nabla A) = J \quad (2.8)$$

### Source of the field

Although the two-dimensional analysis is utilized, let us first consider a general case. The current density on the right-hand side of (2.5) can be determined from the material equation

$$\mathbf{J} = \sigma \mathbf{E} \quad (2.9)$$

where  $\sigma$  is the conductivity. Combining (2.2) with (2.4) gives

$$\nabla \times \mathbf{E} = -\frac{\partial}{\partial t} \nabla \times \mathbf{A} \quad (2.10)$$

which is satisfied by defining the current density as

$$\mathbf{J} = -\sigma \frac{\partial \mathbf{A}}{\partial t} - \sigma \nabla \phi \quad (2.11)$$

where  $\phi$  is the electric scalar potential.

For solid conductors in the axial direction, for instance rotor bars in cage induction machines or synchronous machines, the gradient of electric scalar potential in (2.11) can be defined as

$$\nabla \phi = \frac{\partial u_b}{\partial z} \mathbf{e}_z = -\frac{u_b}{l_b} \mathbf{e}_z \quad (2.12)$$

where  $u_b$  denotes the voltage across the rotor bar and  $l_b$  is the total length of the bar. Accordingly, the current density in rotor bars is

$$J_b = -\sigma \frac{\partial A}{\partial t} + \sigma \frac{u_b}{l_b} \quad (2.13)$$

For phase windings with several coils in series, the eddy current approach (2.11) would lead to extremely inconvenient models due to the high number of thin conductors in each slot. In such cases, the skin effect is excluded and the current density is

$$J_w = \frac{N_w i_w}{S_w} \quad (2.14)$$

where  $N_w$  is the number of turns in a coil,  $i_w$  the current in the coil and  $S_w$  the cross section of the coil area.

### Material properties

The magnetic properties of the laminated iron core are modelled by the reluctivity  $\nu$ , which is a single-valued nonlinear function of the flux density  $B$ , thus excluding the effect of magnetic hysteresis from the analysis. Since the eddy currents are greatly reduced by the laminated structure, the conductivity is set to zero in the laminated iron core.

The shaft and pole shoes, which are typically made of alloy steel, are modelled as conductive iron with a nonlinear magnetization curve. In order to model the eddy currents, the current density is given by (2.11), when the gradient of electric scalar potential is zero.

Resulting from the analysis above, the magnetic field in different materials can be presented in the form

$$-\nabla \cdot (\nu \nabla A) = \begin{cases} 0 & \text{in air and laminated iron} \\ N_w i_w / S_w & \text{in phase windings} \\ -\sigma \frac{\partial A}{\partial t} + \sigma u_b / l_b & \text{in rotor bars} \\ -\sigma \frac{\partial A}{\partial t} & \text{in conductive iron} \end{cases} \quad (2.15)$$

### Stator and rotor windings

The computational model of the electrical machine can be greatly improved by coupling the circuit equations of the stator and rotor windings with the two-dimensional field equation (2.15). In the circuit equations, the dependence between current and voltage is solved and the circuit quantities are coupled with the magnetic field by means of flux linkage. Also, the end-windings outside the core region are modelled by including an additional inductance in the circuit model.

In a cage rotor, each rotor bar requires its own equation. Integration of the current density in a rotor bar (2.13) over its cross section  $S_b$  gives

$$i_b = - \int_{S_b} \sigma \frac{\partial A}{\partial t} dS + \int_{S_b} \sigma \frac{u_b}{l_b} dS \quad (2.16)$$

When constant conductivity  $\sigma$  and uniform cross section area  $S_b$  are assumed in the bar and the bar-end inductance  $L_{be}$  is included, the above equation can be presented in the form

$$u_b = l_b \int_{S_b} \frac{\partial A}{\partial t} dS + R_b i_b + L_{be} \frac{di_b}{dt} \quad (2.17)$$

where  $R_b$  denotes the resistance of the bar including the end region. All the rotor bars are connected by short-circuit rings in both ends of the rotor core. This is taken into account by defining the end-ring resistance  $R_{sc}$  and the end-ring inductance  $L_{sc}$

$$\mathbf{u}_{sc} = \mathbf{R}_{sc} \mathbf{i}_{sc} + \mathbf{L}_{sc} \frac{d\mathbf{i}_{sc}}{dt} \quad (2.18)$$

where  $\mathbf{u}_{sc}$  and  $\mathbf{i}_{sc}$  are vectors of voltage and current in the end-ring that connects the bars to each other. Details of the end-ring model are presented by Arkkio (1987).

The phase windings in the stator or rotor consist of several coils connected in series and distributed in several slots in the stator or rotor core. When the number of positively oriented coil sides is  $N_{pos}$  and the number of negatively oriented coil sides is  $N_{neg}$ , integration of the current density over all the coil sides in a phase winding gives a voltage equation

$$u_w = l_w \left[ \sum_{n=1}^{N_{pos}} \frac{N_{wn}}{S_{wn}} \int_{S_{wn}} \frac{\partial A}{\partial t} dS - \sum_{n=1}^{N_{neg}} \frac{N_{wn}}{S_{wn}} \int_{S_{wn}} \frac{\partial A}{\partial t} dS \right] + R_w i_w + L_{we} \frac{di_w}{dt} \quad (2.19)$$

where  $l_w$  is the length of the coils in the core region,  $N_{wn}$  is the number of turns in the coil side  $n$  and  $S_{wn}$  is the cross section area of the coil side  $n$ . Voltage  $u_w$  is applied to the whole winding and current  $i_w$  flows through all coils that belong to the phase winding. Resistance  $R_w$  includes all coils and the end region outside the iron core.  $L_{we}$  is the inductance outside the core region.

## Finite element method

Several different methods can be utilized in the numerical solution of the magnetic field equation (2.15), such as reluctance networks, the boundary element method, finite difference method or finite element method. In this work, the numerical analysis is based on the finite element method (FEM). The two-dimensional geometry is covered by a finite element mesh, consisting of first- or second-order triangular elements. If possible, the cross section of the electrical machine is divided in  $\gamma$  symmetry sectors, from which only one is modelled by FEM and symmetry constraints are set on the periodic boundary.

In the finite element method, the approximation for the vector potential is

$$A = \sum_{j=1}^{N_n} \lambda_j a_j \quad (2.20)$$

where  $N_n$  is the total number of free nodes in the finite element mesh,  $\lambda_j$  the shape function associated with node  $j$  and  $a_j$  the magnetic vector potential in node  $j$ . For nodes located on the

outer surface of the stator, the vector potential value is fixed to zero. Therefore, these nodes are not included in the computation.

The shape function  $\lambda_j$  has value 1 at node  $j$  and 0 at all the other nodes. Between the nodes in the surrounding elements, the shape function is fitted by first- or second-order polynomials, depending on the order of the elements. Outside the associated elements, the value of a single shape function is zero.

The numerical field equation is derived by Galerkin's method, where (2.15) is multiplied by shape functions and integrated over the whole finite element mesh. Details of the method are presented by, for example, Silvester and Ferrari (1990). For node  $i$ , we get

$$\int_{\Omega} \left[ \sum_{j=1}^{N_n} \left( \nu \nabla \lambda_i \cdot \nabla \lambda_j a_j + \sigma \lambda_i \lambda_j \frac{\partial a_j}{\partial t} \right) - \sigma \lambda_i u_b - \lambda_i \frac{N_w i_w}{S_w} \right] d\Omega = 0 \quad (2.21)$$

where  $\Omega$  represents the whole area of the finite element mesh. It should be noted, however, that the last three terms of (2.21) are only present in the areas where  $\sigma$ ,  $u_b$  or  $i_w$  is defined and has non-zero values.

The same approximation (2.20) is also applied to the winding equations (2.17) and (2.19). The resulting equations are

$$u_b = l_b \int_{S_b} \sum_{j=1}^{N_n} \lambda_j \frac{\partial a_j}{\partial t} dS + R_b i_b + L_{be} \frac{di_b}{dt} \quad (2.22)$$

$$u_w = \gamma l_w \sum_{j=1}^{N_n} \left[ \sum_{n=1}^{N_{pos}} \frac{N_{wn}}{S_{wn}} \int_{S_{wn}} \frac{\partial a_j}{\partial t} dS - \sum_{n=1}^{N_{neg}} \frac{N_{wn}}{S_{wn}} \int_{S_{wn}} \frac{\partial a_j}{\partial t} dS \right] + R_w i_w + L_{we} \frac{di_w}{dt} \quad (2.23)$$

where  $\gamma$  is the number of symmetry sectors in the finite element mesh.

## 2.1.2 Transient time-stepping simulation

### Numerical integration

The field and winding equations are coupled directly and solved in time-domain using constant time steps denoted by  $\Delta t$ . The time derivatives are modelled by trapezoidal approximation, in which the derivative is determined as a mean value from two successive steps. When  $x^k$  represents any variable at the current time step and  $x^{k-1}$  is the same variable at the previous step, the derivatives are approximated by

$$\frac{dx^k}{dt} + \frac{dx^{k-1}}{dt} \approx \frac{2}{\Delta t} (x^k - x^{k-1}) \quad (2.24)$$

The equations for the time-stepping simulation are derived by adding the equations from two successive steps together and replacing the derivatives with expression (2.24). The method

itself is very simple, and it has not been necessary to utilize more sophisticated methods as no accuracy or convergence problems have occurred. Using this approach, the field equations (2.21) are formed for each node in the finite element mesh, the rotor bar equations (2.22) are formed for each rotor bar in the solution sector and the phase winding equations (2.23) are formed for each phase winding in the stator or rotor. The resulting group of equations can be presented as residual functions

$$\begin{aligned} \mathbf{r}_f &= \mathbf{S}\mathbf{a}^k + \mathbf{F}_b^\top \mathbf{u}_b^k + \mathbf{F}_{ws}^\top \mathbf{K}_{ws}^\top \mathbf{i}_{ws}^k + \mathbf{F}_{wr}^\top \mathbf{K}_{wr}^\top \mathbf{i}_{wr}^k \\ &+ \mathbf{S}_0 \mathbf{a}^{k-1} + \mathbf{F}_b^\top \mathbf{u}_b^{k-1} + \mathbf{F}_{ws}^\top \mathbf{K}_{ws}^\top \mathbf{i}_{ws}^{k-1} + \mathbf{F}_{wr}^\top \mathbf{K}_{wr}^\top \mathbf{i}_{wr}^{k-1} = 0 \end{aligned} \quad (2.25)$$

$$\mathbf{r}_b = \mathbf{F}_b \mathbf{a}^k + \mathbf{B} \mathbf{u}_b^k - \mathbf{F}_b \mathbf{a}^{k-1} + \mathbf{B} \mathbf{u}_b^{k-1} + \mathbf{Q}_{b0} \mathbf{i}_b^{k-1} = 0 \quad (2.26)$$

$$\begin{aligned} \mathbf{r}_{ws} &= \mathbf{K}_{ws} \mathbf{F}_{ws} \mathbf{a}^k + \mathbf{K}_{ws} \mathbf{W}_s \mathbf{K}_{ws}^\top \mathbf{i}_{ws}^k + \mathbf{Q}_{ws} \mathbf{v}_{ws}^k \\ &- \mathbf{K}_{ws} \mathbf{F}_{ws} \mathbf{a}^{k-1} + \mathbf{K}_{ws} \mathbf{W}_{s0} \mathbf{K}_{ws}^\top \mathbf{i}_{ws}^{k-1} + \mathbf{Q}_{ws} \mathbf{v}_{ws}^{k-1} = 0 \end{aligned} \quad (2.27)$$

$$\begin{aligned} \mathbf{r}_{wr} &= \mathbf{K}_{wr} \mathbf{F}_{wr} \mathbf{a}^k + \mathbf{K}_{wr} \mathbf{W}_r \mathbf{K}_{wr}^\top \mathbf{i}_{wr}^k + \mathbf{Q}_{wr} \mathbf{v}_{wr}^k \\ &- \mathbf{K}_{wr} \mathbf{F}_{wr} \mathbf{a}^{k-1} + \mathbf{K}_{wr} \mathbf{W}_{r0} \mathbf{K}_{wr}^\top \mathbf{i}_{wr}^{k-1} + \mathbf{Q}_{wr} \mathbf{v}_{wr}^{k-1} = 0 \end{aligned} \quad (2.28)$$

where  $\mathbf{a}$  is a vector containing the nodal values of the magnetic vector potential,  $\mathbf{u}_b$  a vector of the rotor bar voltages,  $\mathbf{i}_{ws}$  a vector of the stator phase currents and  $\mathbf{i}_{wr}$  a vector of the rotor phase currents. In general, subscript ‘f’ refers to the magnetic field, ‘b’ to the rotor bars, ‘ws’ to the stator phase winding and ‘wr’ to the rotor phase winding. Superscripts  $k$  and  $k - 1$  refer to the current and previous time steps, respectively.

The coefficient matrices  $\mathbf{S}$  and  $\mathbf{S}_0$  are nonlinear functions of vector potential, defined as

$$S_{ij} = \int_{\Omega} \left[ \nu(\mathbf{a}^k) \nabla \lambda_i \cdot \nabla \lambda_j + \frac{2\sigma}{\Delta t} \lambda_i \lambda_j \right] d\Omega \quad (2.29)$$

$$S_{0,ij} = \int_{\Omega} \left[ \nu(\mathbf{a}^{k-1}) \nabla \lambda_i \cdot \nabla \lambda_j - \frac{2\sigma}{\Delta t} \lambda_i \lambda_j \right] d\Omega \quad (2.30)$$

where the reluctivity  $\nu(\mathbf{a})$  is determined from the vector potential separately for each element, depending on the flux density and material. The conductivity  $\sigma$  has a non-zero value only in rotor bars and shaft. The dimensions of  $\mathbf{S}$  and  $\mathbf{S}_0$  are  $N_n \times N_n$ , when  $N_n$  is the number of free nodes in the finite element analysis.

For the rotor bars, matrix  $\mathbf{F}_b$  is defined as

$$F_{b,ij} = -\frac{1}{l_b} \int_{\Omega} \sigma \lambda_j d\Omega \quad (2.31)$$

when node  $j$  belongs to rotor bar  $i$ . Otherwise, the entries of  $\mathbf{F}_b$  are zero. The dimension of  $\mathbf{F}_b$  is  $n_b \times N_n$ , where  $n_b$  is the number of rotor bars in the solution sector. Matrices  $\mathbf{B}$  and  $\mathbf{Q}_{b0}$  are

$$\mathbf{B} = \frac{\Delta t}{2l_b R_b} \left\{ \mathbf{1} + \frac{R_b}{2} \left[ \left( R_{sc} + 2 \frac{L_{sc}}{\Delta t} \right) \mathbf{1} + \left( R_{be} + 2 \frac{L_{be}}{\Delta t} \right) \mathbf{M}_b \right]^{-1} \mathbf{M}_b \right\} \quad (2.32)$$

$$\mathbf{Q}_{b0} = \frac{\Delta t}{2l_b} \mathbf{1} - \frac{\Delta t}{2l_b} \left[ \left( R_{sc} + 2 \frac{L_{sc}}{\Delta t} \right) \mathbf{1} + \left( R_{be} + 2 \frac{L_{be}}{\Delta t} \right) \mathbf{M}_b \right]^{-1} \cdot \left[ \left( R_{sc} - 2 \frac{L_{sc}}{\Delta t} \right) \mathbf{1} + \left( R_{be} - 2 \frac{L_{be}}{\Delta t} \right) \mathbf{M}_b \right] \quad (2.33)$$

where  $R_{sc}$  and  $L_{sc}$  are the resistance and inductance between adjacent rotor bars in the short-circuit ring and, respectively,  $R_{be}$  and  $L_{be}$  are the resistance and inductance of the bar end outside the iron core. The unit matrix is denoted by  $\mathbf{1}$  and the connection matrix  $\mathbf{M}_b$  is

$$\mathbf{M}_b = \begin{bmatrix} 2 & -1 & 0 & \cdots & 0 & \pm 1 \\ -1 & 2 & -1 & \cdots & 0 & 0 \\ 0 & -1 & 2 & \cdots & 0 & 0 \\ \vdots & \vdots & \vdots & \ddots & \vdots & \vdots \\ 0 & 0 & 0 & \cdots & 2 & -1 \\ \pm 1 & 0 & 0 & \cdots & -1 & 2 \end{bmatrix} \quad (2.34)$$

with the dimension  $n_b \times n_b$ . The entries in the upper right corner and lower left corner are 1 for negative symmetry constraint and  $-1$  for positive symmetry constraint in the finite element mesh. The rotor bar current  $i_b^k$  is determined after the field solution from

$$i_b^k = - \left[ \left( R_{sc} + 2 \frac{L_{sc}}{\Delta t} \right) \mathbf{1} + \left( R_{be} + 2 \frac{L_{be}}{\Delta t} \right) \mathbf{M}_b \right]^{-1} \cdot \left\{ \frac{1}{2} \mathbf{M}_b (\mathbf{u}_b^k + \mathbf{u}_b^{k-1}) + \left[ \left( R_{sc} - 2 \frac{L_{sc}}{\Delta t} \right) \mathbf{1} + \left( R_{be} - 2 \frac{L_{be}}{\Delta t} \right) \mathbf{M}_b \right] i_b^{k-1} \right\} \quad (2.35)$$

For phase windings in the stator or rotor, the matrix  $F_w$  is defined as

$$F_{w,ij} = - \int_{\Omega} \lambda_j d\Omega \quad (2.36)$$

when node  $j$  belongs to phase winding  $i$  and zero otherwise. The dimension of  $F_w$  is  $n_w \times N_n$ , where  $n_w$  is the number of phases.

In the star connection, the connection matrix  $K_w$  is

$$\mathbf{K}_w = \begin{bmatrix} 1 & 0 & 0 & \cdots & 0 & -1 \\ 0 & 1 & 0 & \cdots & 0 & -1 \\ 0 & 0 & 1 & \cdots & 0 & -1 \\ \vdots & \vdots & \vdots & \ddots & \vdots & \vdots \\ 0 & 0 & 0 & \cdots & 1 & -1 \end{bmatrix} \quad (2.37)$$

and  $M_w$  is

$$\mathbf{M}_w = \begin{bmatrix} 1 & 1 & 1 & \cdots & 1 & 0 \\ 0 & 1 & 1 & \cdots & 1 & 0 \\ 0 & 0 & 1 & \cdots & 1 & 0 \\ \vdots & \vdots & \vdots & \ddots & \vdots & \vdots \\ 0 & 0 & 0 & \cdots & 1 & 0 \end{bmatrix} \quad (2.38)$$

with the dimension  $n_w-1 \times n_w$  for both. In the delta connection, both  $\mathbf{K}_w$  and  $\mathbf{M}_w$  are unity matrices with the dimension  $n_w \times n_w$ .

Matrices  $\mathbf{W}$ ,  $\mathbf{W}_0$  and  $\mathbf{Q}_w$  are

$$W_{ii} = -\frac{R_{w,i}\Delta t + 2L_{we,i}}{2\gamma l_w} \quad (2.39)$$

$$W_{0,ii} = -\frac{R_{w,i}\Delta t - 2L_{we,i}}{2\gamma l_w} \quad (2.40)$$

$$\mathbf{Q}_w = \frac{\Delta t}{2\gamma l_w} \mathbf{M}_w \quad (2.41)$$

$\mathbf{W}$  and  $\mathbf{W}_0$  are diagonal matrices with dimensions  $n_w \times n_w$ .

The vector of magnetic flux linkages  $\boldsymbol{\psi}_w^k$  in the phase windings can be determined from the field solution by

$$\boldsymbol{\psi}_w^k = \gamma l_w \mathbf{F}_w \mathbf{a}^k \quad (2.42)$$

It should be noted that the definitions of the currents depend on the connection. In the star connection, the current vector  $\mathbf{i}_w$  contains  $n_w-1$  independent line currents and the last component is determined from Kirchhoff's current law, because the sum of the currents has to be zero. In the delta connection, the elements of  $\mathbf{i}_w$  are the currents in the phase windings, which are different from the line currents. The elements of the voltage vector  $\mathbf{v}_w$  are always line-to-line voltages.

### Nonlinear iterative solution

Due to the characteristics of the iron core, equations (2.25)–(2.28) form a nonlinear system of equations that is solved by the iterative Newton–Raphson approach. The solution is based on the Jacobian and the residuals, which are determined at each iteration step and used for solving the incremental changes in the variables. The iteration is finished when the increments in the simulation variables per iteration step fall below the convergence limit.

Resulting from the stages described above, the final system of equations for the nonlinear time-stepping simulation of the electrical machine is

$$\begin{bmatrix} \mathbf{J}(\mathbf{a}^{k,n}) & \mathbf{F}_b^T & \mathbf{F}_{ws}^T \mathbf{K}_{ws}^T & \mathbf{F}_{wr}^T \mathbf{K}_{wr}^T \\ \mathbf{F}_b & \mathbf{B} & \mathbf{0} & \mathbf{0} \\ \mathbf{K}_{ws} \mathbf{F}_{ws} & \mathbf{0} & \mathbf{K}_{ws} \mathbf{W}_s \mathbf{K}_{ws}^T & \mathbf{0} \\ \mathbf{K}_{wr} \mathbf{F}_{wr} & \mathbf{0} & \mathbf{0} & \mathbf{K}_{wr} \mathbf{W}_r \mathbf{K}_{wr}^T \end{bmatrix} \begin{bmatrix} \Delta \mathbf{a}^{k,n} \\ \Delta \mathbf{u}_b^{k,n} \\ \Delta \mathbf{i}_{ws}^{k,n} \\ \Delta \mathbf{i}_{wr}^{k,n} \end{bmatrix} = - \begin{bmatrix} \mathbf{r}_f^n \\ \mathbf{r}_b^n \\ \mathbf{r}_{ws}^n \\ \mathbf{r}_{wr}^n \end{bmatrix} \quad (2.43)$$

where the superscript  $n$  denotes the iteration step. The Jacobian  $\mathbf{J}(\mathbf{a})$  is defined at each iteration step by

$$J_{ij} = S_{ij} + \int_{\Omega} \sum_{k=1}^{N_n} \left( \frac{\partial v(\mathbf{a}^{k,n})}{\partial a_j} \nabla \lambda_i \cdot \nabla \lambda_k \right) d\Omega \quad (2.44)$$

and the residual functions are determined by (2.26)–(2.28) using values from the  $n$ :th iteration step.

## Motion and electromagnetic torque

Unless a constant speed is assumed, the movement of the rotor during time steps is solved from the equations of motion

$$J \frac{d\omega_m}{dt} = T_e - T_L \quad (2.45)$$

$$\omega_m = \frac{d\theta_m}{dt} \quad (2.46)$$

where  $J$  is the moment of inertia,  $\omega_m$  is the angular speed and  $\theta_m$  is the angular position of the rotor.  $T_e$  is the electromagnetic torque and  $T_L$  is the load torque. The new position of the rotor is determined at the beginning of each time step and a new mesh is created in the air gap.

The electromagnetic torque is determined by the virtual work principle

$$T_e = \frac{\partial}{\partial \theta_m} \int_{\Omega} \left( \int_0^H \mathbf{B} \cdot d\mathbf{H} \right) d\Omega \quad (2.47)$$

where the integration area  $\Omega$  covers only the air gap. The implementation for finite element analysis follows the approach presented by Coulomb (1983), in which the virtual movement is determined by means of a coordinate transformation matrix without altering the air-gap mesh.

### Initial state

The initial magnetic field for the time-stepping simulation is determined by complex time-harmonic analysis (Arkkio, 1987). The simulation variables and sources are determined by sinusoidal harmonic components, while a complex notation with amplitude and phase is used for the variables. An effective reluctivity is considered, as described in (Luomi et al., 1986).

The resulting AC field solution is transformed into a DC field by taking the real values of the variables and replacing the effective reluctivity with the absolute reluctivity. However, the field solution obtained does not exactly correspond to the real initial field, but a steady state can usually be reached after simulating a few periods of the supply frequency.

All information about the finite element mesh, materials and magnetic field are stored in a text file. The file contains the coordinates of the nodes, association between the nodes and elements, material characteristics, values of vector potential and current density, dimensions and parameters of the electrical machines and some other parameters that are required for the FEM computation.

## 2.2 Direct coupling of field and circuit equations

The most reliable, but not very user-friendly, method for coupling external circuit equations with the FEM equations (2.25)–(2.43) is to formulate a single system of equations modelling the

whole system. All the equations will be solved simultaneously and the mathematical coupling between the equations is strong. This approach, called direct coupling, is used for verification and evaluation of the indirect methods presented in Sections 2.3 and 2.4. The coupled field-circuit equations are later presented in detail for the case studies, whereas only basic principles are discussed here.

Typical circuit connections in the phase winding of an electrical machine comprise resistors, inductors, capacitors and different types of power electronic switching components. In this thesis, however, ideal switch models are utilized. The fundamental equations for resistance  $\mathbf{R}$ , inductance  $\mathbf{L}$  and capacitance  $\mathbf{C}$  in multi-phase systems are

$$\mathbf{u} = \mathbf{R}\mathbf{i} \quad (2.48)$$

$$\mathbf{u} = \mathbf{L}\frac{d\mathbf{i}}{dt} \quad (2.49)$$

$$\mathbf{i} = \mathbf{C}\frac{d\mathbf{u}}{dt} \quad (2.50)$$

where  $\mathbf{u}$  and  $\mathbf{i}$  represent the vectors of voltage and current. The connection between the circuit elements and electrical machine can be modelled by connection matrices, as (2.37) or (2.38).

In direct coupling, the circuit equations must be formulated separately for each case using the same methods for numerical integration and nonlinear iteration. With the trapezoidal approximation utilized in the finite element analysis, the fundamental circuit equations (2.48)–(2.50) become

$$\mathbf{u}^k - \mathbf{R}\mathbf{i}^k + \mathbf{u}^{k-1} - \mathbf{R}\mathbf{i}^{k-1} = 0 \quad (2.51)$$

$$\mathbf{u}^k - \frac{2}{\Delta t}\mathbf{L}\mathbf{i}^k + \mathbf{u}^{k-1} + \frac{2}{\Delta t}\mathbf{L}\mathbf{i}^{k-1} = 0 \quad (2.52)$$

$$\mathbf{i}^k - \frac{2}{\Delta t}\mathbf{C}\mathbf{u}^k + \mathbf{i}^{k-1} + \frac{2}{\Delta t}\mathbf{C}\mathbf{u}^{k-1} = 0 \quad (2.53)$$

The final system of equations, naturally, requires as many additional equations as there are additional independent variables, but a Jacobian is not required in a case of linear circuit models. An example with detailed equations is presented in Chapter 4.

## 2.3 Coupling by the current output approach

### 2.3.1 FEM model as a functional block

In the current output approach, the FEM model of the electrical machine is represented by a functional block, solving (2.25)–(2.28). Figure 2.1 presents a schematic of the block, in which the line currents  $\mathbf{i}_{ws}$  and  $\mathbf{i}_{wr}$  are solved from the phase voltages  $\mathbf{v}_{ws}$  and  $\mathbf{v}_{wr}$  in the stator and rotor. The load torque  $T_L$  is also given as an input, unless a constant mechanical speed is considered. The additional outputs are the electromagnetic torque  $T_e$ , mechanical speed  $\omega_m$ , angular position  $\theta_m$  and flux linkages  $\psi_{ws}$  and  $\psi_{wr}$  in stator and rotor phase windings. For a

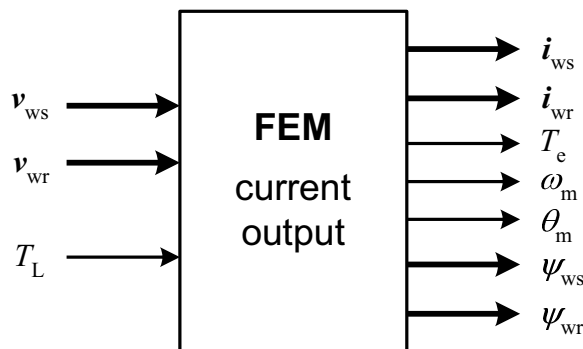


Figure 2.1: FEM model of the electrical machine as a functional block.

cage rotor, no inputs or outputs are required, because there are no connections with the external circuit.

Since the FEM block represents a voltage-controlled current source, coupling with external circuit models is straightforward. Using the current output approach, the whole circuit model is formulated as a block diagram, which is an ideal approach for modelling frequency converters, for example, or other controlled systems. Nevertheless, block diagrams are inconvenient for passive components, like resistors, inductors or capacitors. Because of this, even simple circuit models may result in complex diagrams using this approach.

### 2.3.2 Implementation for SIMULINK

The functional block of Fig. 2.1 is implemented for SIMULINK as an S-function (Kanerva, 2001). The program code is written in Fortran and linked with MATLAB by predefined subroutines that are required to create a functional block for SIMULINK (Simulink, 2005). Those subroutines define the sampling times, inputs, outputs and state variables for continuous or discrete computation.

As described in Section 2.1, constant time step  $\Delta t$  is used in the FEM computation. The sampling time of the FEM block is set to that value, but the step sizes are not limited elsewhere in the model. As a result, models run with major and minor time steps and the mathematical coupling between the FEM model and the external model is weak. This gives flexibility in the model construction and the possibility of setting individual sampling times in different parts of the model, resulting in an effective usage of computation resources for simulation. Naturally, this also requires careful analysis and knowledge of the physical system on the part of the user.

The input and output variables are defined as stated above and are updated discretely at the major steps as set for the finite element analysis. The average of the input voltage from two adjacent steps is replaced by a single value taken from the middle point between the steps. This is not equivalent to the selected trapezoidal integration method, but it has not caused any problems with accuracy or convergence. During the minor time steps, the output remains constant. The state variables are not required at all, because the vector potential and current are solved explicitly inside the FEM block.

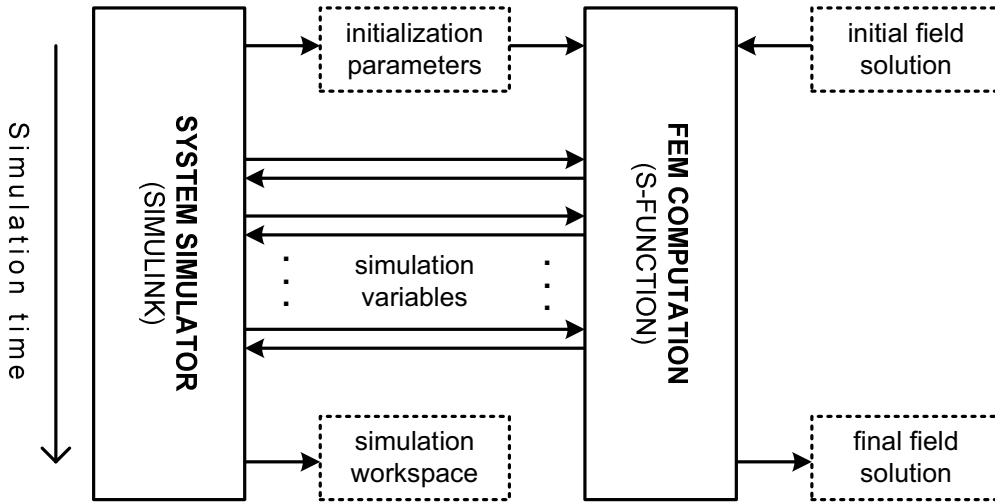


Figure 2.2: Schematic of the data transfer between the FEM block and SIMULINK.

The data transfer between the FEM block and SIMULINK is illustrated in Fig. 2.2. Before the simulation, the initialization parameters are stored in a file, from which the FEM block reads the parameters before the first time step. The initial state of the magnetic field is also restored from a separate file at the same time. During the time-stepping simulation, the simulation variables are passed directly back and forth between the FEM block and SIMULINK. After the simulation, the magnetic field is stored in a file with the same format as the one with the initial field. The simulation variables can be stored in MATLAB's workspace or in a separate file.

## 2.4 Coupling by the circuit parameter approach

### 2.4.1 Electromotive force and dynamic inductance

The concept of the circuit parameter approach can be clarified by means of an example of a rotating coil. The magnetic flux linkage  $\psi$  is defined as the product of inductance  $L$  and current  $i$

$$\psi(i, \theta, t) = L(i, \theta) i(\theta, t) \quad (2.54)$$

where  $\theta$  is the angular position. The inductance is a function of current and position due to magnetic saturation, saliency and slotting. The current changes with time, but has also a dependence on position, representing the transformation between rotating and stationary frames of reference. Hence, the time derivative of the flux linkage is

$$\frac{d\psi}{dt} = \left( \frac{\partial L}{\partial i} \frac{\partial i}{\partial t} + \frac{\partial L}{\partial \theta} \frac{\partial \theta}{\partial t} \right) i + L \left( \frac{\partial i}{\partial \theta} \frac{\partial \theta}{\partial t} + \frac{\partial i}{\partial t} \right) \quad (2.55)$$

By reordering the components, (2.55) can be presented in the following form:

$$\frac{d\psi}{dt} = \left( L + \frac{\partial L}{\partial i} i \right) \frac{\partial i}{\partial t} + \left( \frac{\partial L}{\partial \theta} i + L \frac{\partial i}{\partial \theta} \right) \frac{\partial \theta}{\partial t} \quad (2.56)$$

On the other hand,

$$\frac{d\psi}{dt} = \frac{\partial\psi}{\partial i} \frac{\partial i}{\partial t} + \frac{\partial\psi}{\partial\theta} \frac{\partial\theta}{\partial t} = L^{\text{dyn}} \frac{\partial i}{\partial t} + e \quad (2.57)$$

By identification of (2.56) and (2.57), the components multiplying the current derivative in (2.56) together form the dynamic inductance  $L^{\text{dyn}}$ , while the rest is considered as the electromotive force  $e$ , which is directly proportional to the angular speed. The final form of (2.57) is similar to the linear circuit model, but now the magnetic saturation is included in the inductance and the effects of saliency and slotting are included in the electromotive force. Further discussion about the definitions of inductance is presented by Demerdash and Nehl (1999).

For a system with  $n_w$  phase windings, the parameters are defined in matrix form. The dynamic inductance  $L_w^{\text{dyn}}$  comprises the self and mutual inductances of all phase windings; its dimension is  $n_w \times n_w$ . The electromotive force  $e_w$  is defined as a vector with  $n_w$  components.

The mutual inductances between stator and rotor windings, as well as the inductances of the rotor bars with short-circuit rings, are not included in  $L_w^{\text{dyn}}$  for better accuracy. It was found that the discrete movement of the rotor in time-stepping simulation caused a significant error in the mutual inductances. Instead, the effects relating to coupling between the stator and rotor are contained in  $e_w$ . For a cage rotor, only the stator inductances are present in  $L_w^{\text{dyn}}$  in order to keep the size of the matrix reasonable. The error caused by this simplification is discussed in Chapter 4.

Besides  $L_w^{\text{dyn}}$  and  $e_w$ , the model of the electrical machine includes coil resistances and end-winding inductances. In the circuit parameter approach, the coil resistances form a diagonal matrix  $R_w$  and the end-winding inductances are added in the diagonal of  $L_w^{\text{dyn}}$ . Hence, the electrical machine satisfies the voltage equation

$$M_w v = K_w e_w + K_w L_w^{\text{dyn}} K_w^T \frac{di_w}{dt} + K_w R_w K_w^T i_w \quad (2.58)$$

where  $M_w$  and  $K_w$  are the connection matrices defined in Section 2.1, modelling the star or delta connection.

## 2.4.2 Extraction of the circuit parameters

The circuit parameters  $L_w^{\text{dyn}}$  and  $e_w$  are determined from the field solution at each major time step. The finite element analysis is run as described in Section 2.1 and the model is linearized at the operating point for the parameter calculation. This is done by fixing the Jacobian (2.44) and reluctivities for each element to correspond with the magnetic field distribution at the moment.

After fixing the magnetic properties, an incremental current  $i_{w\Delta}$  is applied in each phase winding, one by one. The resulting change in the vector potential  $a_\Delta$  is calculated from the linear system of equations (2.43), where the Jacobian (2.44) holds the value from the last iteration step of the nonlinear solution. This ensures that the calculated inductance is incremental, thus

representing the tangent of the magnetization curve. The incremental flux linkage  $\psi_{w\Delta}$  for all phase windings is determined by (2.42) and the entries of  $L_w^{\text{dyn}}$  are

$$L_{ij}^{\text{dyn}} = \frac{\psi_{w\Delta,i}}{i_{w\Delta,j}} \quad (2.59)$$

The same procedure is repeated for each phase winding, which means that the determination of the dynamic inductance matrix for  $n_w$  phase windings requires  $n_w$  additional solutions of the linear system of field equations.

The electromotive force  $e_w$  is determined by subtracting the effect of the current derivative from the total flux derivative

$$e_w = \frac{d\psi_w}{dt} - L_w^{\text{dyn}} \frac{di_w}{dt} \quad (2.60)$$

where the derivatives are approximated by

$$\frac{d\psi_w}{dt} \approx \frac{\psi_w^k - \psi_w^{k-1}}{\Delta t} \quad (2.61)$$

$$\frac{di_w}{dt} \approx \frac{i_w^k - i_w^{k-1}}{\Delta t} \quad (2.62)$$

This approach was chosen, because the flux derivative versus angular position could not be determined in a way that would correspond with the definition (2.59) of dynamic inductance. It was discovered that if the parameters  $L_w^{\text{dyn}}$  and  $e_w$  are defined by methods not corresponding with each other, a significant error is generated in the results when the phase currents are integrated from the voltage equation (2.58).

### 2.4.3 Implementation for SIMULINK

Implementation of the circuit parameter approach for SIMULINK is similar to the implementation of the current output approach, but the outputs are different. Figure 2.3 presents a functional

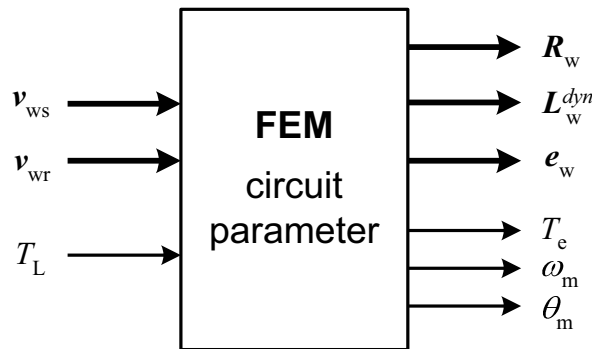


Figure 2.3: FEM model of the electrical machine as a functional block with circuit parameters as output.

block of the FEM model, in which the outputs are the dynamic inductance, phase resistance and electromotive force. Naturally, the signals consist of the single elements of the matrices or vectors, but are illustrated as concatenated signals for simplicity. The resistance  $\mathbf{R}_w$  is normally constant throughout the simulation, whereas  $\mathbf{L}_w^{\text{dyn}}$  and  $\mathbf{e}_w$  are updated at each time step defined for the FEM computation.

The connection of the FEM block with external circuit models requires coupling of the voltage equation (2.58) with the circuit equations of the external model. In SIMULINK, the resulting equations are formulated as a block diagram. Nevertheless, it should be noted that the circuit parameter approach doesn't necessarily require block diagram structures, but it could also be implemented for other types of simulators using different approaches for modelling electrical circuits.

## 2.5 Conclusion

In this chapter, the computational methods were presented for modelling and simulation of electrical machines and external circuits. The magnetic field in the electrical machine is modelled by two-dimensional FEM and solved together with the circuit equations of the windings. The external circuit model is coupled with the electrical machine model either directly, when all the equations are solved simultaneously in the common system of equations, or indirectly in SIMULINK, using the current output approach or circuit parameter approach.

In the current output approach, the phase currents of the electrical machine are solved together with the magnetic field, when the supply voltages are given as inputs. In the circuit parameter approach, the electrical machine is characterized by the electromotive force, dynamic inductance and resistance, which are solved by FEM at each time step for the given supply voltages. Both the approaches are implemented as S-functions representing functional blocks in SIMULINK.

In the following chapters, the methods are applied to different case studies concerning electrical machines, circuits and control systems. The simulation results obtained by the different methods are compared with each other in order to draw conclusions about their accuracy and applicability to different cases.

## 3 Case study: doubly-fed induction generator

In this case study, a 1.7 MW wound-rotor induction generator is modelled by FEM and coupled with SIMULINK by the circuit parameter approach (Section 2.4). The stator and rotor windings of the generator are supplied by ideal sinusoidal voltage sources, and the system is simulated in steady state and during a voltage dip in stator supply. The simulation results are compared with the results obtained by directly coupled field and circuit equations. The purpose of this chapter is to verify the theory and implementation of the circuit parameter approach, evaluate the accuracy of the method, and analyze the effect of the time step length on the results.

### 3.1 Description of the system

#### 3.1.1 Finite element model of the generator

The ratings of the doubly-fed induction generator are presented in Table 3.1. There are four poles and three phases in the stator and rotor windings. The maximum rotor voltage  $U_{r,\max}$  corresponds to the locked-rotor operation and defines the transformer ratio between stator and rotor, together with the rated stator voltage  $U_{s,N}$ . The amplitude and phase of the rotor voltage is adjusted according to the rotational speed and power factor.

The finite element mesh of the generator covers one quarter of the cross section, as illustrated in Fig. 3.1. The mesh consists of 949 nodes forming 1848 linear triangular elements. Linear elements are utilized in the presented simulations in order to reduce the computation time. In the test simulations, it was also found that neither the order of the elements nor the density of the mesh significantly affected the results. The stator and rotor windings are modelled as series-connected coils with uniform current density. The coupled field-circuit equations of the generator are similar to (2.25)–(2.44) on pages 24–26, except that there are no rotor bars in the model.

T	3.1: R	-
$P_N$	rated power	1.7 MW
$U_{s,N}$	rated stator voltage	690 V (delta)
$U_{r,\max}$	maximum rotor voltage	2472 V (star)
$f_N$	rated stator frequency	50 Hz
$n_N$	nominal speed	1500 rpm

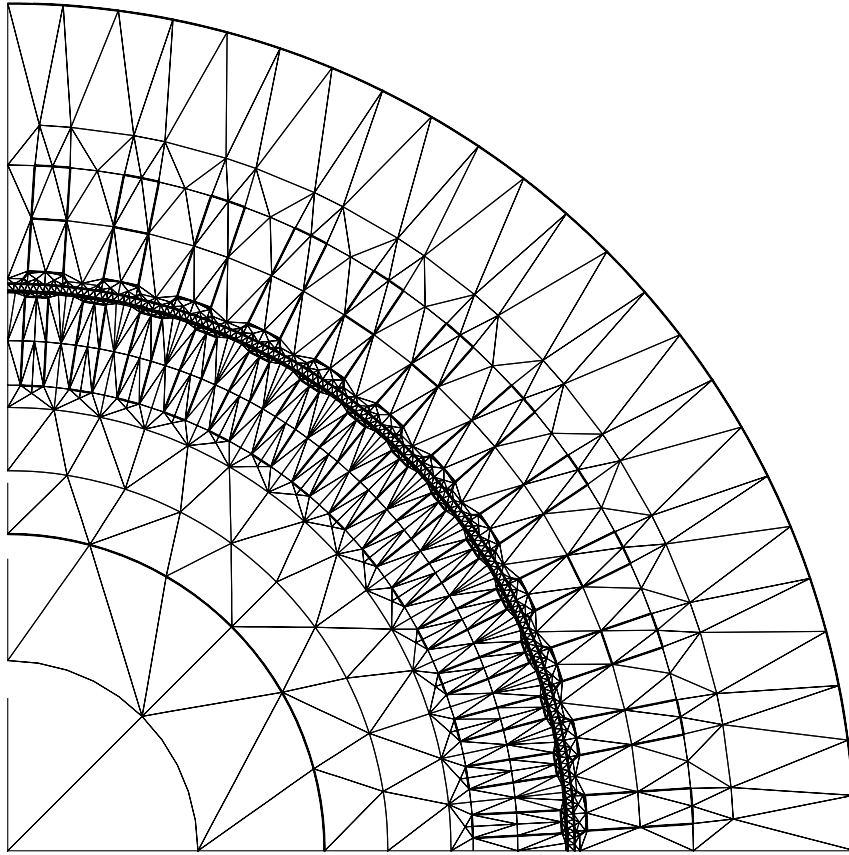


Figure 3.1: Finite element mesh of the doubly-fed induction generator.

### 3.1.2 Electrical supply

The supply voltage of the generator is sinusoidal and symmetric in both stator and rotor. In real applications, the rotor phase winding is usually connected to a frequency converter or adjustable resistor, but sinusoidal waveforms are used here in order to provide a better basis for comparison between the computational methods.

The stator supply frequency is 50 Hz and the rotor supply frequency is determined by the slip. When the number of pole-pairs is  $p$ , the angular speed of the rotor  $\omega_m$  and the stator supply frequency  $f_s$ , the rotor supply frequency is

$$f_r = \left(1 - \frac{p \cdot \omega_m}{2\pi f_s}\right) f_s \quad (3.1)$$

where the sign of  $f_r$  determines the phase order of the sinusoidal rotor voltages. For positive values of  $f_r$ , the phase order is the same in the stator and rotor and the magnetic field induced by the rotor currents also rotates in the same direction as the stator field. For negative values of  $f_r$ , the phase order in the rotor is the opposite.

The amplitude of the rotor supply voltage is determined by the turns ratio between the stator and rotor, slip and the voltage drop in the impedance of the rotor winding. Generally, the rotor voltage is directly proportional to the rotor frequency, but also the voltage drop in the winding

needs to be considered. At the beginning of the simulation, the phase angles of the stator and rotor voltages are set to zero and the mechanical power is determined by the angular position of the rotor  $\theta_m$ . The values for stator and rotor voltages, angular position, slip and electrical power describing the initial state of different operating points are presented in Table 3.2.

In the time-stepping simulation, sinusoidal voltages with constant amplitude and frequency are applied until there is no visible fluctuation in the current. A sudden voltage dip is applied in the stator by changing the amplitude of the stator voltage, whereas the frequency and the phase remain. The rotor voltage and the rotational speed are preserved during the fault. An example of the supply voltage in stator and rotor at slip  $s = -50\%$  is presented in Fig. 3.2, where a 50% voltage dip is introduced in the stator voltage at  $t = 20$  ms.

T 3.2: P

slip		-10%	-10%	-50%	-50%
power		0 MW	1.7 MW	0 MW	1.7 MW
$U_s$	[V <sub>RMS</sub> ]	690	690	690	690
$U_r$	[V <sub>RMS</sub> ]	235	249	1245	1250
$\theta_m$	[deg]	-77.5	-81.5	-79.8	-82.3

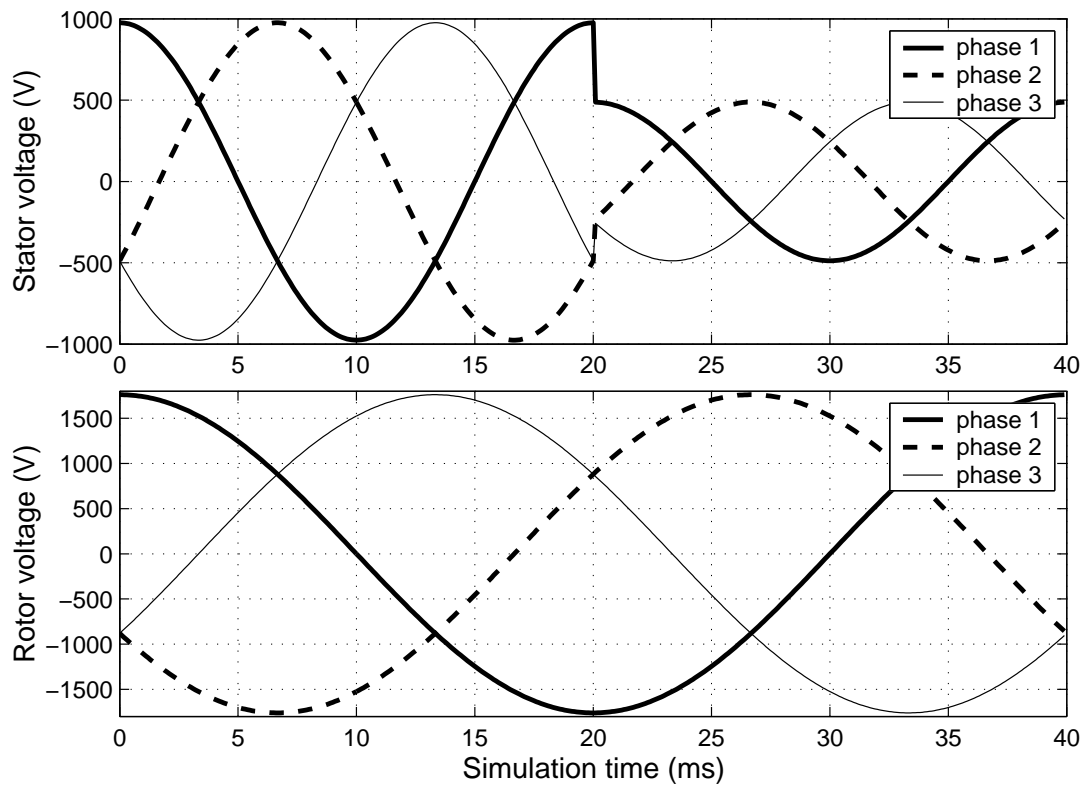


Figure 3.2: Supply voltages in stator and rotor for slip  $s = -50\%$ , where a 50% voltage dip is introduced in the stator voltage at  $t = 20$  ms.

## 3.2 Simulation models

### 3.2.1 Circuit parameter approach

Using the circuit parameter approach, the doubly-fed induction generator is governed by the circuit equation

$$\mathbf{M}_w \mathbf{v} = \mathbf{K}_w \mathbf{e}_w + \mathbf{K}_w \mathbf{L}_w^{\text{dyn}} \mathbf{K}_w^T \frac{d\mathbf{i}'_w}{dt} + \mathbf{K}_w \mathbf{R}_w \mathbf{K}_w^T \mathbf{i}'_w \quad (3.2)$$

where  $\mathbf{v}$  is the vector of line-to-line supply voltages in the stator and rotor windings

$$\mathbf{v} = \begin{bmatrix} v_{s12} \\ v_{s23} \\ v_{s31} \\ v_{r12} \\ v_{r23} \\ v_{r31} \end{bmatrix} \quad (3.3)$$

$\mathbf{e}_w$  is the vector of electromotive forces in the stator and rotor windings

$$\mathbf{e}_w = \begin{bmatrix} e_{ws1} \\ e_{ws2} \\ e_{ws3} \\ e_{wr1} \\ e_{wr2} \\ e_{wr3} \end{bmatrix} \quad (3.4)$$

and  $\mathbf{i}'_w$  is the vector of independent currents in the stator and rotor windings

$$\mathbf{i}'_w = \begin{bmatrix} i_{ws1}^{\text{D}} \\ i_{ws2}^{\text{D}} \\ i_{ws3}^{\text{D}} \\ i_{wr1}^{\text{Y}} \\ i_{wr2}^{\text{Y}} \end{bmatrix} \quad (3.5)$$

In (3.5), the current in the delta-connected stator winding is denoted by  $i_{ws}^{\text{D}}$  and current in the star-connected rotor winding by  $i_{wr}^{\text{Y}}$ . Because of the star connection, only two of the three rotor currents are considered as independent variables. The connection matrices  $\mathbf{M}_w$  and  $\mathbf{K}_w$  are

$$\mathbf{M}_w = \begin{bmatrix} 1 & 0 & 0 & & & \\ 0 & 1 & 0 & & & \\ 0 & 0 & 1 & & & \\ & & & 1 & 1 & 0 \\ & & & 0 & 1 & 0 \end{bmatrix} \quad (3.6)$$

$$\mathbf{K}_w = \begin{bmatrix} 1 & 0 & 0 \\ 0 & 1 & 0 \\ 0 & 0 & 1 \\ & & & 1 & 0 & -1 \\ & & & 0 & 1 & -1 \end{bmatrix} \quad (3.7)$$

and the matrices  $\mathbf{L}_w^{\text{dyn}}$  and  $\mathbf{R}_w$  for the dynamic inductance and coil resistance are

$$\mathbf{L}_w^{\text{dyn}} = \begin{bmatrix} L_{ws11}^{\text{dyn}} & L_{ws12}^{\text{dyn}} & L_{ws13}^{\text{dyn}} \\ L_{ws21}^{\text{dyn}} & L_{ws22}^{\text{dyn}} & L_{ws23}^{\text{dyn}} \\ L_{ws31}^{\text{dyn}} & L_{ws32}^{\text{dyn}} & L_{ws33}^{\text{dyn}} \\ & & & L_{wr11}^{\text{dyn}} & L_{wr12}^{\text{dyn}} & L_{wr13}^{\text{dyn}} \\ & & & L_{wr21}^{\text{dyn}} & L_{wr22}^{\text{dyn}} & L_{wr23}^{\text{dyn}} \\ & & & L_{wr31}^{\text{dyn}} & L_{wr32}^{\text{dyn}} & L_{wr33}^{\text{dyn}} \end{bmatrix} \quad (3.8)$$

$$\mathbf{R}_w = \begin{bmatrix} R_{ws1} & & & & & \\ & R_{ws2} & & & & \\ & & R_{ws3} & & & \\ & & & R_{wr1} & & \\ & & & & R_{wr2} & \\ & & & & & R_{wr3} \end{bmatrix} \quad (3.9)$$

The subscripts 's' and 'r' in the above equations refer to the stator and rotor, and the numbers from 1 to 3 refer to the phases.

### Implementation for system simulator

The block diagram of the mathematical system is depicted in Fig. 3.3. The parameters  $\mathbf{e}_w$ ,  $\mathbf{L}_w^{\text{dyn}}$  and  $\mathbf{R}_w$  are determined at the major time steps by the S-function, which performs the FEM computation as described in Section 2.4. The supply voltage  $\mathbf{v}$  is given as an input for the S-function and the phase current  $\mathbf{i}_w$  is solved at the minor time steps from (3.2) by numerical integration

$$\frac{d\mathbf{i}'_w}{dt} = \left( \mathbf{K}_w \mathbf{L}_w^{\text{dyn}} \mathbf{K}_w^T \right)^{-1} \left( \mathbf{M}_w \mathbf{v} - \mathbf{K}_w \mathbf{e}_w - \mathbf{K}_w \mathbf{R}_w \mathbf{K}_w^T \mathbf{i}'_w \right) - \alpha \mathbf{i}'_w \quad (3.10)$$

where a high-pass filter with cutoff frequency  $\alpha$  is used for drift compensation.

It should be noted that the parameter  $\alpha$  is purely related to the numerical integration, which is by nature an open-loop integration in Simulink. In such a case, even negligible numerical errors will accumulate in the integrand, since there is no feedback signal to cancel the error. The parameter must be selected in such a way that it removes the erroneous drifting, which typically occurs at much lower frequency than is present in the signal, but it must not interfere with the actual signals. It was observed that an appropriate value for  $\alpha$  is about one tenth of the fundamental frequency in the steady-state simulation. During the voltage dip simulation, however, the compensation is not used in order to preserve the DC components in the currents.

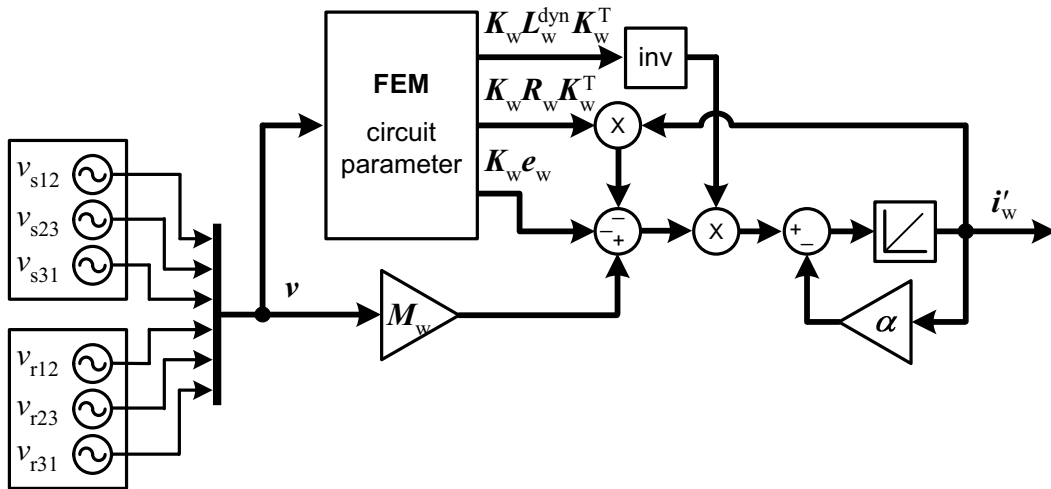


Figure 3.3: Simulation model of the doubly-fed induction generator using the circuit parameter approach.

### 3.2.2 Direct coupling

The direct coupling between the magnetic field equations and the circuit equations of the phase windings is used here for verification. The phase currents in stator and rotor are solved from (2.43) together with the magnetic vector potential using the line voltages as input variables.

Since there are no external circuit elements connected to the windings, there is no difference between the direct coupling and the current output approach in terms of numerical computation. Therefore, the simulation model is implemented using the current output approach, as depicted in Fig. 3.4.

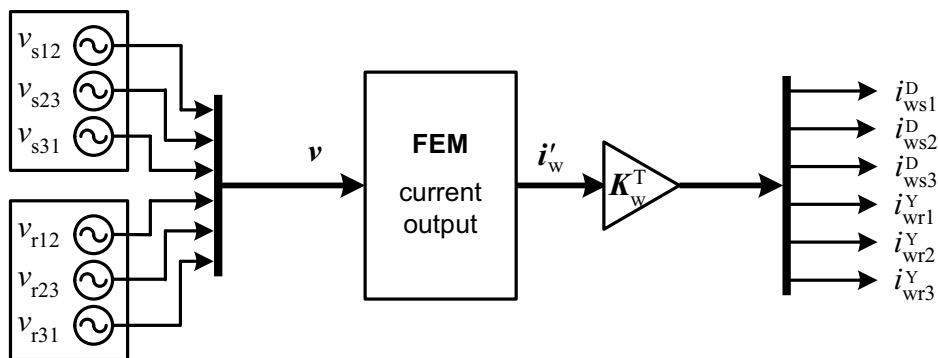


Figure 3.4: Simulation model of the doubly-fed induction generator using the current output approach, in which the field and circuit equations of the generator are coupled directly.

### 3.3 Simulation results

The system described above was simulated in steady-state operation and during a symmetric fault in the stator supply using both the circuit parameter approach and direct coupling. The FEM model was composed of linear elements in all simulations. The results obtained by the circuit parameter approach were compared with the results of the directly coupled simulation in order to evaluate the accuracy of the circuit parameter approach in different cases. In this respect, the direct coupling represents the correct and verified method of simulation, even though the results might differ from the actual measurements.

#### 3.3.1 Steady state

The steady-state operation of the generator was simulated at full load (1.7 MW) and no load (0 MW), when the slip was  $-10\%$  and  $-50\%$ . The supply voltages in the stator and rotor are the same as presented earlier in Table 3.2. In the circuit parameter approach, the FEM computation was processed with  $100 \mu\text{s}$  time steps, which are later referred to as major steps. The circuit equations of the windings were simulated with minor steps, the length of which were  $10 \mu\text{s}$ . The cutoff frequency  $\alpha$  used in the numerical integration had the value  $15 \text{ Hz}$  for the stator current and zero for the rotor current. In the direct coupling, the field and circuit equations were simulated with common  $100 \mu\text{s}$  time steps.

The initial state for the time-stepping simulation was estimated by time-harmonic analysis, where complex variables were used. After the initialization, the time-stepping simulation was continued until the phase currents were stable. For simplicity, a constant angular speed was assumed.

The differences between the circuit parameter approach and the direct coupling are illustrated in Table 3.3, where  $i^{\text{circ}}$  denotes the effective (RMS) value of the steady-state current obtained by the circuit parameter approach and  $i^{\text{dir}}$  is the corresponding value from the directly coupled simulation. The absolute difference between the results is denoted by  $\Delta i^{\text{abs}}$  and the relative difference with respect to direct coupling is  $\Delta i^{\text{rel}}$ . The results show that the absolute difference

T 3.3: C

slip		$-10\%$	$-10\%$	$-50\%$	$-50\%$
power		0 MW	1.7 MW	0 MW	1.7 MW
		st / rt	st / rt	st / rt	st / rt
$i^{\text{circ}}$	[A]	135 / 117	1186 / 361	119 / 115	738 / 240
$i^{\text{dir}}$	[A]	144 / 117	1204 / 361	118 / 115	756 / 243
$\Delta i^{\text{abs}}$	[A]	$-9.5 / -0.1$	$-18.5 / -0.5$	$+0.7 / +0.1$	$-17.9 / -2.4$
$\Delta i^{\text{rel}}$	[%]	$-6.6 / -0.1$	$-1.5 / -0.04$	$+0.6 / +0.1$	$-2.4 / -0.3$

in the stator current varies with the slip or load, giving quite acceptable values for all cases. In the rotor current, the difference is smaller and also dependent on the frequency.

In addition to the amplitude difference, a slight phase difference is also present in the currents. This is illustrated in Fig. 3.5, where the difference is plotted as a function of time for the case with  $-50\%$  slip and 1.7 MW power. The stator current difference varies around zero producing a difference in both phase and amplitude. In the rotor current, there are some DC components in the difference, because no high-pass filtering was used in the rotor current integration. A closer analysis of the differences is presented in Section 3.3.3.

The simulations were run on a desktop computer with a 500 MHz Pentium III processor. Using the direct coupling, the computational time required for the simulation of one time step was 0.22 seconds and there were an average of 6.5 iterations per time step. With the circuit parameter approach, the number of iterations per step was approximately the same, but the computational time was about 25 per cent higher than it was for the direct coupling. This is mainly due to the numerical integration carried out in Simulink. Since the FEM computation is programmed in Fortran and compiled for Simulink as an S-function, its execution time does not significantly differ from the corresponding stand-alone application.

### 3.3.2 Voltage dip in stator

The transient operation of the generator was simulated by applying a symmetric 50% or 100% voltage dip in the stator voltage, when the rotor supply continued with the same amplitude and frequency. The faults were applied in each of the steady-state conditions described above. The major and minor steps were 100  $\mu$ s and 10  $\mu$ s as above, but the parameter  $\alpha$  was set to zero in order to preserve the DC components that are present by nature in sudden faults. As in the steady-state simulation, a constant angular speed was also assumed in the fault simulation.

The results from the circuit parameter approach and direct coupling were again compared with each other; the results are presented in Tables 3.4 and 3.5. Since the fault currents do not any more have constant amplitude, the analysis is only carried out for the maximum peak current after the fault. According to the results, the absolute difference still remains in the same range as it was in the steady-state simulation, even though the current value is more than ten times higher. Therefore, the relative difference between the circuit parameter approach and direct coupling is practically negligible.

In Figure 3.6, the current waveforms and the difference between the methods are presented for  $-50\%$  slip and 1.7 MW power. Again, the results show an approximately constant difference in the phase and amplitude during the whole fault.

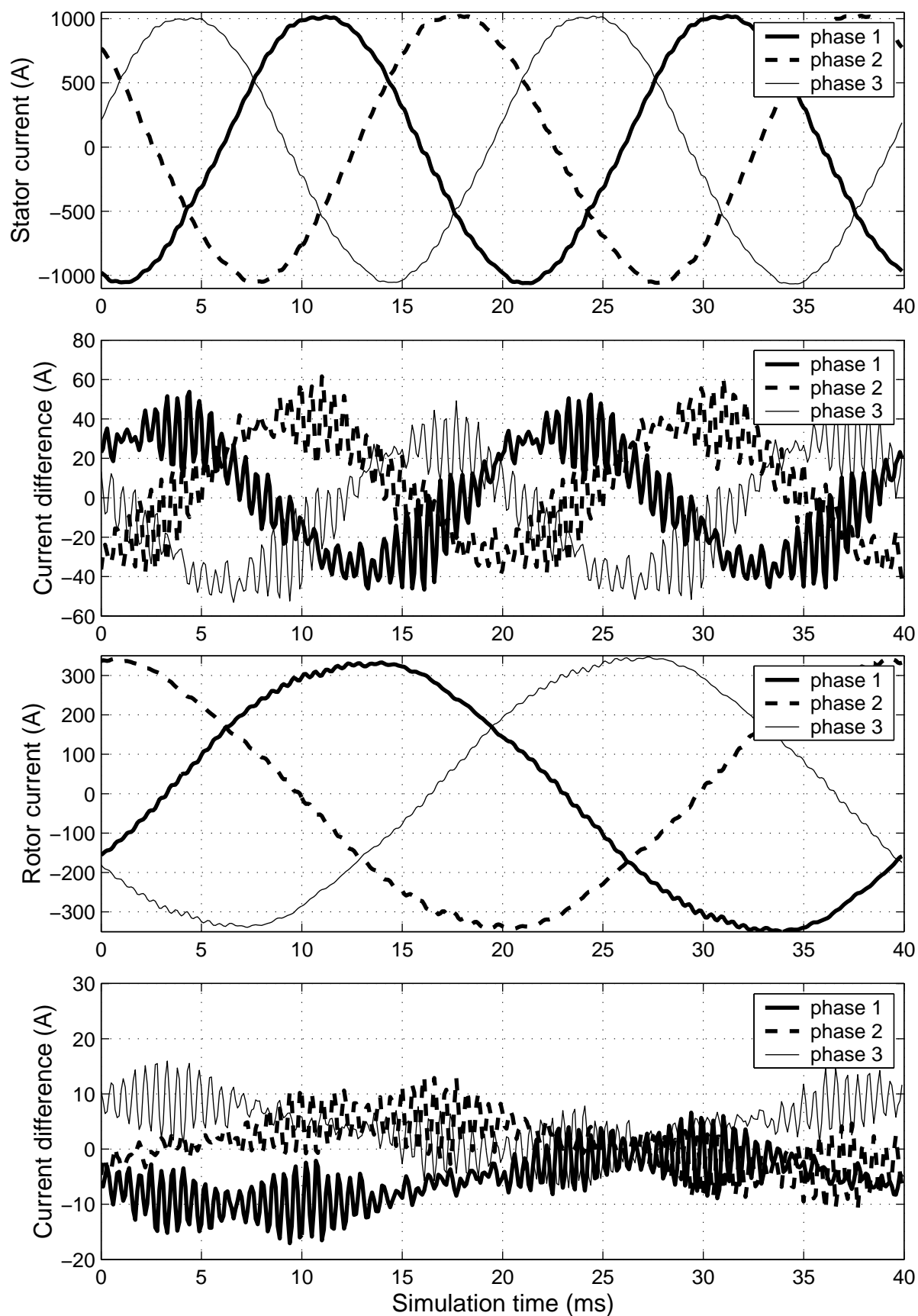


Figure 3.5: Stator and rotor currents in steady state ( $P = 1.7$  MW,  $s = -50\%$ ) obtained by circuit parameter approach, and absolute difference in the currents compared with the direct coupling.

T 3.4: C

slip	-10%	-50%	-10%	-50%
voltage dip	50%	50%	100%	100%
	st / rt	st / rt	st / rt	st / rt
$i^{\text{circ}}$ [A]	12360 / 3150	13022 / 3756	29670 / 7165	31688 / 8721
$i^{\text{dir}}$ [A]	12369 / 3150	13033 / 3765	29673 / 7165	31694 / 8731
$\Delta i^{\text{abs}}$ [A]	-8.9 / +0.05	-11.2 / -9.0	-2.9 / +0.05	-6.1 / -10.2
$\Delta i^{\text{rel}}$ [%]	-0.07 / +0.00	-0.09 / -0.07	-0.01 / +0.00	-0.02 / -0.03

T 3.5: C

slip	-10%	-50%	-10%	-50%
voltage dip	50%	50%	100%	100%
	st / rt	st / rt	st / rt	st / rt
$i^{\text{circ}}$ [A]	12782 / 2991	13112 / 3852	29958 / 7135	31685 / 8789
$i^{\text{dir}}$ [A]	12744 / 2992	13103 / 3858	29912 / 7135	31670 / 8796
$\Delta i^{\text{abs}}$ [A]	+37 / -0.3	+8.7 / -6.3	+45.6 / -0.2	+14.8 / -7.4
$\Delta i^{\text{rel}}$ [%]	+0.29 / -0.00	+0.07 / -0.05	+0.15 / -0.00	+0.05 / -0.02

### 3.3.3 Effect of the simulation parameters

In the analysis presented above, the major and minor steps were kept constant through all the simulations. Therefore, the differences between the computational methods could not be analyzed thoroughly, which meant that additional simulations with altered parameters had to be run for selected cases in order to get a proper insight into the numerical methods and their differences.

#### Minor steps

Figure 3.7 presents a close-up of the stator current waveforms obtained by the directly coupled simulation and the circuit parameter approach when the length of the minor step is either 10  $\mu\text{s}$  or 100  $\mu\text{s}$ . The major step is 100  $\mu\text{s}$  in all cases.

When the minor step in the circuit parameter approach is 10  $\mu\text{s}$ , the output is smoother than in the directly coupled simulation, but there is a clear difference in both amplitude and phase. As the minor step is increased into an equal value with the major step, the current waveform follows very closely the directly coupled simulation, but the delay of one major step remains.

This phenomenon can be explained simply by the separation of the field and circuit equations in the circuit parameter approach: When the parameters  $L_w^{\text{dyn}}$  and  $e_w$  are determined by FEM, the computation is based on time instants  $t^{k-1}$  and  $t^k$ , referring to the previous and current time

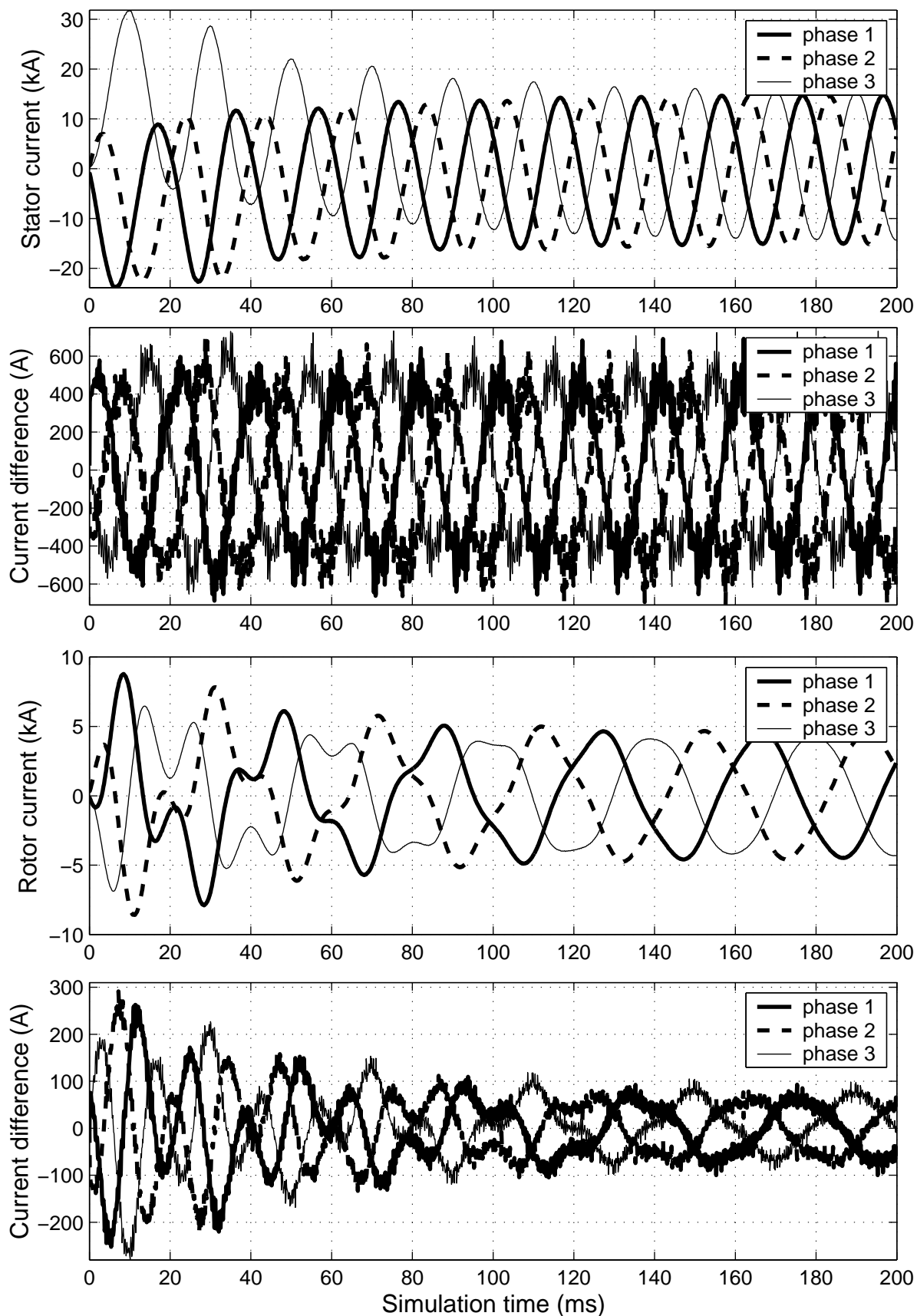


Figure 3.6: Stator phase currents after 100% voltage drop in stator ( $P = 1.7$  MW,  $s = -50\%$ ) obtained by the circuit parameter approach, and absolute difference in the currents compared with the direct coupling.

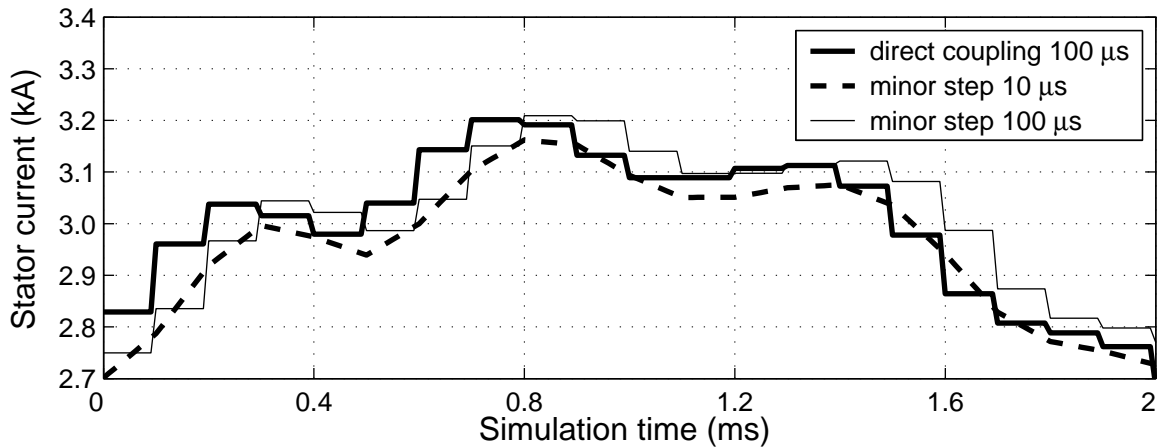


Figure 3.7: Influence of the minor step size on the stator current.

steps. However, the circuit model (3.2) in the system simulator receives this information at time instant  $t^k$  and utilizes it from that point onward, causing the one-step delay.

The size of the difference can be slightly adjusted by changing the minor step size, but the origin of the problem remains and cannot be removed, since the coupling is non-iterative. Adding an iteration loop between the FEM computation and the system simulator would change the situation, but the method would also become much more complex and would not any more provide any significant advantage over direct coupling.

### Major steps

Based on the previous analysis of the minor steps, it is clear that decreasing the length of the major steps would also decrease the difference between the methods. This is also shown in Fig. 3.8, which presents examples of the same period of simulation with either  $50 \mu\text{s}$  or  $200 \mu\text{s}$  steps for the FEM computation. The minor step size was  $10 \mu\text{s}$  in both the cases.

When considering the appropriate step length for the direct coupling, the harmonic contents of the supply voltage and phase current are the most relevant factors. In order to model the slot harmonics properly in this case, the length of a step should be  $100 \mu\text{s}$  or less.

## 3.4 Discussion

In this case study, the FEM model of a doubly-fed induction generator was used for verifying the indirect field-circuit coupling by the circuit parameter approach, in which the magnetic field equations are represented by circuit parameters  $L_w^{\text{dyn}}$  and  $e_w$  and the circuit equations of the windings are simulated separately from the field equations using the above parameters. The supply voltages in the stator and rotor windings were considered as ideal and sinusoidal in order to ensure that any differences in the results truly originated from the method itself. The

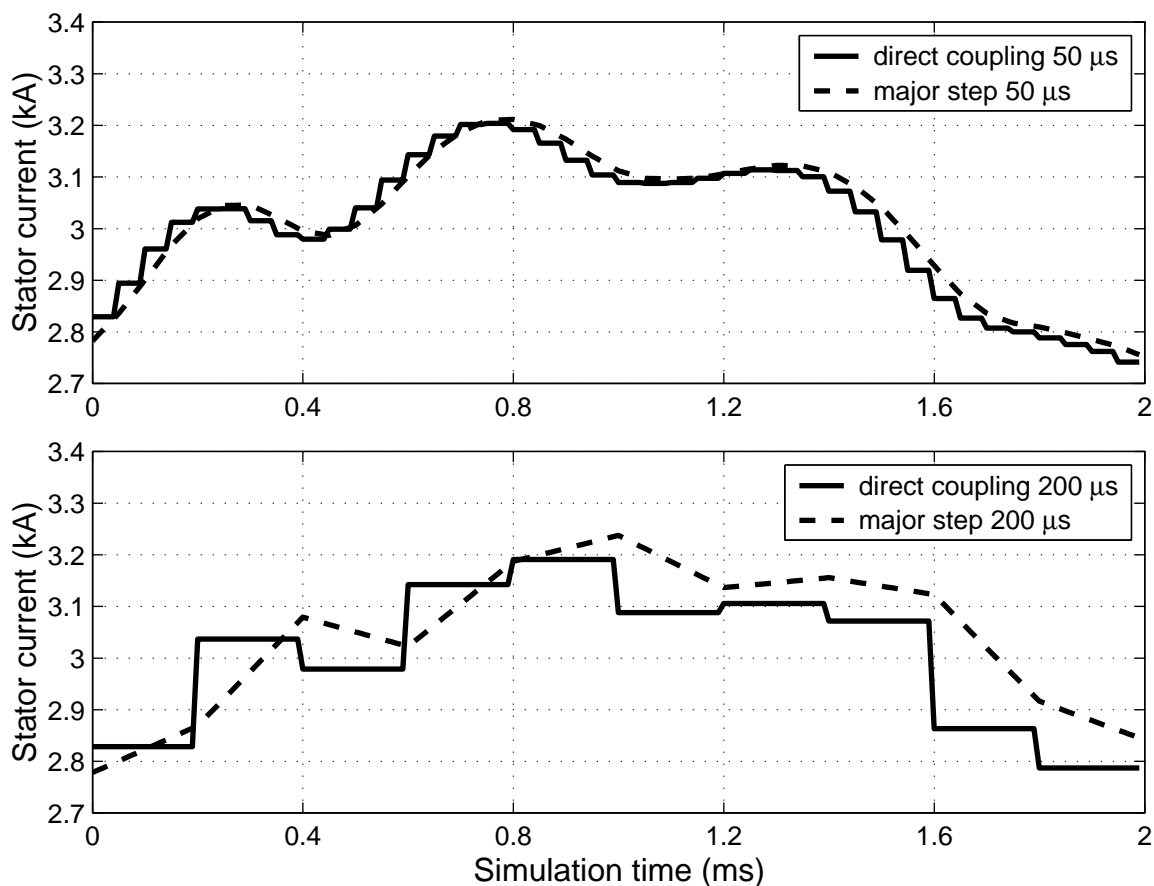


Figure 3.8: Influence of the major step size on the stator current.

verification was based on a comparison between the simulation results obtained by the circuit parameter approach and the direct coupling of the field and circuit equations.

Agreement with the direct coupling was good, but there were also some differences that can be explained by the non-iterative indirect coupling. Accordingly, the results justify the following conclusions:

1. The theory and implementation are correct in the circuit parameter approach.
2. The non-iterative indirect coupling causes a delay of one major step, which can be adjusted by the step size but cannot be removed.

In practice, however, the model is always more complex than the presented example and it is therefore necessary to consider, whether the one-step delay is crucial at the system level. In the case of passive circuits, the proper selection of the step size probably suffices, but some control system models might be sensitive to such a delay. Nevertheless, these topics cannot be answered by means of the presented example, but will be discussed in the following chapters.

Since one of the reasons for developing new approaches instead of direct coupling is to simplify the process of model construction, this example case should be evaluated from the users'

point of view also. In this respect, the implementation for SIMULINK is troublesome, since the circuit models must be presented as block diagrams. However, the methodology itself is applicable to other types of simulators that could provide different kinds of possibilities. The numerical integration by open-loop integrators is also problematic because of drifting, but that problem can be solved by proper compensation or filtering. In this work, the drift compensation is not analyzed in detail, since the subject is not within the scope of the thesis.

As mentioned in the introduction, the original motivation for separating the solutions of field and circuit equations has been the convenience of large-scale system modelling. Because of its simplicity, this example does not provide much insight into that aspect; however, the examples presented in the following chapters do focus more on system-level simulation.

## 4 Case study: cage induction motor with compensation capacitors

In this case study, a 37kW three-phase cage induction motor is connected directly to the grid, while the reactive power is compensated by a capacitor bank. The stator of the cage induction motor is in the star connection and the capacitors are in the delta connection. The cage induction motor is modelled by FEM and the field computation is coupled with the circuit model by the current output approach (Section 2.3), circuit parameter approach (Section 2.4) and direct coupling (Section 2.2). The simulation results are validated by laboratory measurements. The purpose of this chapter is to study the performance of the current output approach and circuit parameter approach in the simulation of electrical machines and passive circuit elements.

### 4.1 Description of the system

#### 4.1.1 FEM model of the cage induction motor

Table 4.1 presents the ratings of the cage induction motor. The number of phases is three, the number of poles is four and there are 40 non-skewed rotor bars. The finite element mesh of the motor consists of 960 nodes forming 1510 linear triangular elements, as illustrated in Fig. 4.1.

T 4.1: R

$P_N$	rated power	37 kW
$U_N$	rated voltage	400 V (star)
$I_N$	rated current	73 A
$f_N$	rated frequency	50 Hz
$n_N$	nominal speed	1470 rpm

#### 4.1.2 Circuit model

##### Cage induction motor

The circuit model of the cage induction motor is based on the FEM equations defined in Chapter 2. When considering the current output approach or direct coupling, the electromotive force  $e_{ws}$  in the following analysis corresponds to the vector potential derivative in the stator winding

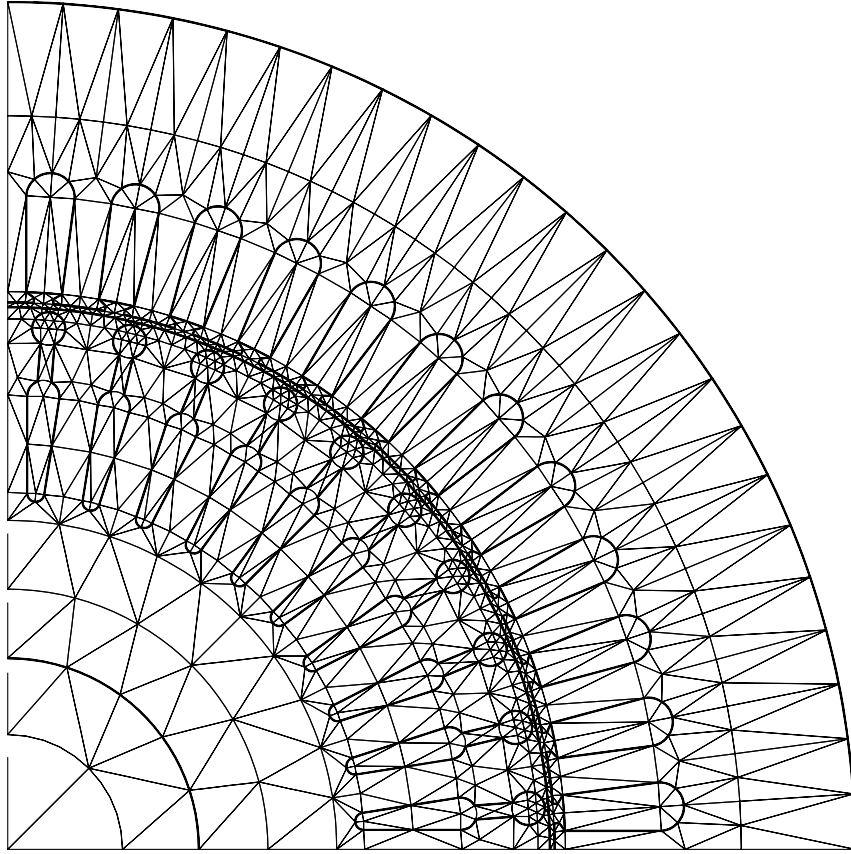


Figure 4.1: Finite element mesh of the cage induction motor.

equation. In the circuit parameter approach, the definition of  $\mathbf{e}_{ws}$  is slightly different, but the equations are in the same form.

When an ideal voltage supply is assumed, the circuit equation of the stator winding in star connection is

$$\mathbf{u}_{ws} = \mathbf{e}_{ws} + \mathbf{R}_{ws}\mathbf{i}_{ws} + \mathbf{L}_{ws} \frac{d\mathbf{i}_{ws}}{dt} \quad (4.1)$$

where  $\mathbf{u}_{ws}$  is the stator voltage vector,  $\mathbf{i}_{ws}$  the stator current vector,  $\mathbf{R}_{ws}$  the stator resistance matrix and  $\mathbf{L}_{ws}$  the stator inductance matrix. Because the sum of the stator currents is zero in the star connection, one of the currents can be eliminated from the equations by

$$\mathbf{i}_{ws} = \mathbf{K}_{ws}^T \mathbf{i}'_{ws} \quad (4.2)$$

where  $\mathbf{i}'_{ws}$  is the vector of independent stator currents and the connection matrix  $\mathbf{K}_{ws}^T$  for a three-phase system is defined by

$$\mathbf{K}_{ws}^T = \begin{bmatrix} 1 & 0 \\ 0 & 1 \\ -1 & -1 \end{bmatrix} \quad (4.3)$$

If the neutral is not connected, line-to-line voltage  $\mathbf{v}_{ws}$  is known instead of line-to-neutral voltage  $\mathbf{u}_{ws}$ . In such a case, we can use the relation

$$\begin{bmatrix} 1 & 0 & -1 \\ 0 & 1 & -1 \end{bmatrix} \mathbf{u}_{ws} = \begin{bmatrix} 1 & 1 & 0 \\ 0 & 1 & 0 \end{bmatrix} \mathbf{v}_{ws} \quad (4.4)$$

or, in simpler form,

$$\mathbf{K}_{ws} \mathbf{u}_{ws} = \mathbf{M}_{ws} \mathbf{v}_{ws} \quad (4.5)$$

By combining equations (4.1), (4.2) and (4.5), the circuit equation of the cage induction motor becomes

$$\mathbf{M}_{ws} \mathbf{v}_{ws} = \mathbf{K}_{ws} \mathbf{e}_{ws} + \mathbf{K}_{ws} \mathbf{R}_{ws} \mathbf{K}_{ws}^T \mathbf{i}'_{ws} + \mathbf{K}_{ws} \mathbf{L}_{ws} \mathbf{K}_{ws}^T \frac{d\mathbf{i}'_{ws}}{dt} \quad (4.6)$$

### Grid and compensation capacitors

Figure 4.2 presents the circuit model of the whole system with grid and compensation capacitors. The grid is modelled as a simple Thevenin equivalent, where  $\mathbf{v}_{gs}$  is the grid voltage,  $\mathbf{R}_{gs}$  the line resistance and  $\mathbf{L}_{gs}$  the line inductance. Now we can define the stator voltage as

$$\mathbf{M}_{ws} \mathbf{v}_{ws} = \mathbf{M}_{ws} \mathbf{v}_{gs} - \mathbf{K}_{ws} \mathbf{R}_{gs} \mathbf{K}_{ws}^T \mathbf{i}'_{gs} - \mathbf{K}_{ws} \mathbf{L}_{gs} \mathbf{K}_{ws}^T \frac{d\mathbf{i}'_{gs}}{dt} \quad (4.7)$$

After connecting the compensating capacitors, more equations are needed. Current  $\mathbf{i}_{cs}$  through the capacitance  $\mathbf{C}_{ws}$  in the delta connection is

$$\mathbf{i}_{cs} = \mathbf{C}_{ws} \frac{d\mathbf{v}_{cs}}{dt} \quad (4.8)$$

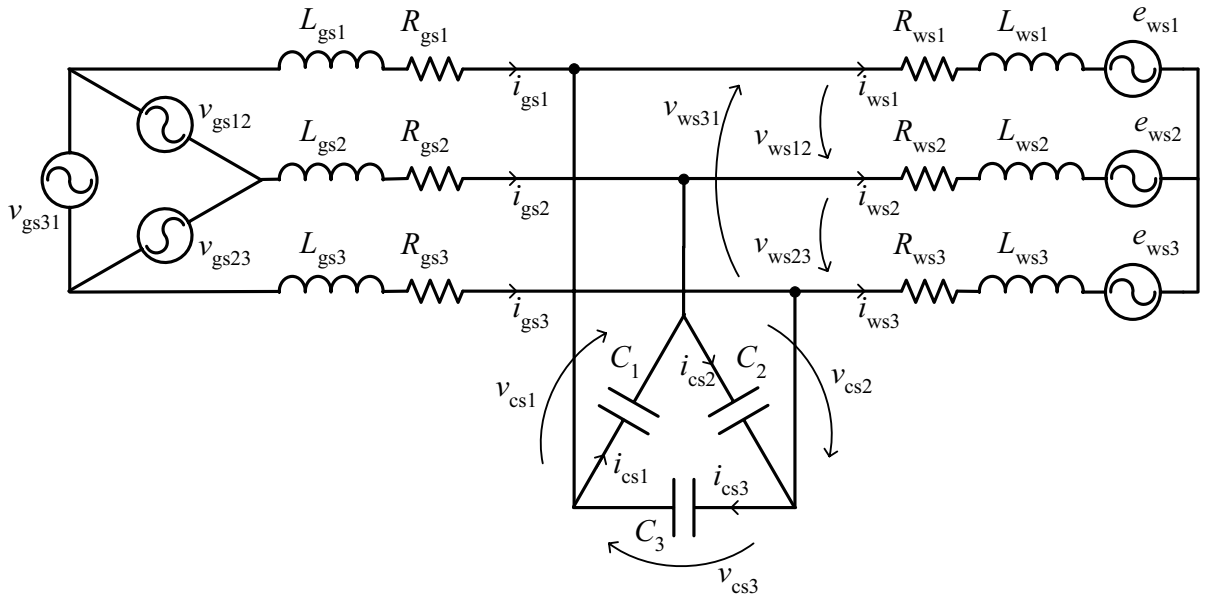


Figure 4.2: Circuit model of the cage induction motor, grid and compensating capacitors.

where  $\mathbf{v}_{cs}$  is the voltage and  $\mathbf{i}_{cs}$  the current of the capacitors in the delta connection. In order to relate the capacitor current with the currents in grid and stator, a transformation similar to (4.5) is needed. Combining (4.8) with Kirchhoff's current law gives

$$\mathbf{P}_{ws} \mathbf{K}_{ws}^T \mathbf{i}'_{ws} - \mathbf{P}_{ws} \mathbf{K}_{ws}^T \mathbf{i}'_{gs} + \mathbf{K}_{ws} \mathbf{C}_{ws} \mathbf{K}_{ws}^T \frac{d\mathbf{v}'_{cs}}{dt} = 0 \quad (4.9)$$

where  $\mathbf{v}'_{cs}$  is the vector of independent capacitor voltages and the connection matrix  $\mathbf{P}_{ws}$  is

$$\mathbf{P}_{ws} = \begin{bmatrix} 1 & 0 & 0 \\ 1 & 1 & 0 \end{bmatrix} \quad (4.10)$$

Setting the stator voltage  $\mathbf{v}_{ws}$  equal to the capacitor voltage  $\mathbf{K}_{ws}^T \mathbf{v}'_{cs}$  and coupling (4.6), (4.7) and (4.9) gives the system of equations

$$\mathbf{K}_{ws} \mathbf{e}_{ws} + \mathbf{K}_{ws} \mathbf{R}_{ws} \mathbf{K}_{ws}^T \mathbf{i}'_{ws} + \mathbf{K}_{ws} \mathbf{L}_{ws} \mathbf{K}_{ws}^T \frac{d\mathbf{i}'_{ws}}{dt} - \mathbf{M}_{ws} \mathbf{K}_{ws}^T \mathbf{v}'_{cs} = 0 \quad (4.11)$$

$$\mathbf{K}_{ws} \mathbf{R}_{gs} \mathbf{K}_{ws}^T \mathbf{i}'_{gs} + \mathbf{K}_{ws} \mathbf{L}_{gs} \mathbf{K}_{ws}^T \frac{d\mathbf{i}'_{gs}}{dt} + \mathbf{M}_{ws} \mathbf{K}_{ws}^T \mathbf{v}'_{cs} = \mathbf{M}_{ws} \mathbf{v}_{gs} \quad (4.12)$$

$$\mathbf{P}_{ws} \mathbf{K}_{ws}^T \mathbf{i}'_{ws} - \mathbf{P}_{ws} \mathbf{K}_{ws}^T \mathbf{i}'_{gs} + \mathbf{K}_{ws} \mathbf{C}_{ws} \mathbf{K}_{ws}^T \frac{d\mathbf{v}'_{cs}}{dt} = 0 \quad (4.13)$$

To sum up, equation (4.6) governs the cage induction motor with the ideal voltage supply. In order to model the whole system containing the cage induction motor, grid and compensating capacitors, the solution of equations (4.11), (4.12) and (4.13) is required.

## 4.2 Simulation models

### 4.2.1 Current output approach

Equation (4.6) is already included in the FEM computation when the current output approach is used for the coupling. Therefore, the simulation with the ideal voltage supply is straightforward. As Fig. 4.3 shows, a sinusoidal voltage signal is given as input for the FEM block and a current signal is obtained from the output. There are no feedback loops in the system and the model is, as a matter of fact, equivalent to the directly coupled model.

The simulation model for the system with grid and compensating capacitors (4.11)–(4.13) is presented in Fig. 4.4. The state variables in the system are the grid current  $\mathbf{i}'_{gs}$  and the capacitor voltage  $\mathbf{v}'_{cs}$ . Their values are obtained by numerical integration from

$$\frac{d\mathbf{i}'_{gs}}{dt} = \left( \mathbf{K}_{ws} \mathbf{L}_{gs} \mathbf{K}_{ws}^T \right)^{-1} \left[ \mathbf{M}_{ws} \left( \mathbf{v}_{gs} - \mathbf{K}_{ws}^T \mathbf{v}'_{cs} \right) - \mathbf{K}_{ws} \mathbf{R}_{gs} \mathbf{K}_{ws}^T \mathbf{i}'_{gs} \right] - \alpha \mathbf{i}'_{gs} \quad (4.14)$$

$$\frac{d\mathbf{v}'_{cs}}{dt} = \left[ \left( \mathbf{K}_{ws} \mathbf{C}_{ws} \mathbf{K}_{ws}^T \right)^{-1} \mathbf{P}_{ws} \mathbf{K}_{ws}^T \left( \mathbf{i}'_{gs} - \mathbf{i}'_{ws} \right) \right] - \alpha \mathbf{v}'_{cs} \quad (4.15)$$

while the stator current  $\mathbf{i}'_{ws}$  is defined by the FEM block. The high-pass filter with cutoff frequency  $\alpha$  is used for drift compensation, as in Section 3.

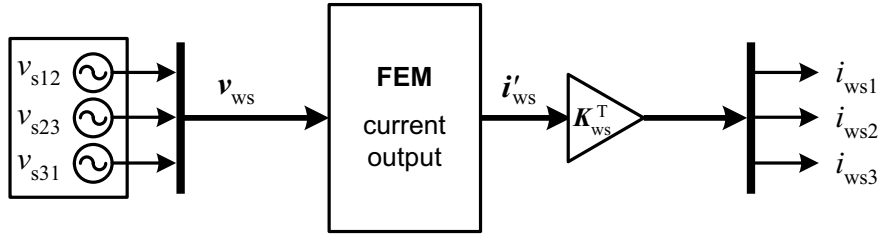


Figure 4.3: Simulation model of the cage induction motor with ideal voltage supply using the current output approach.

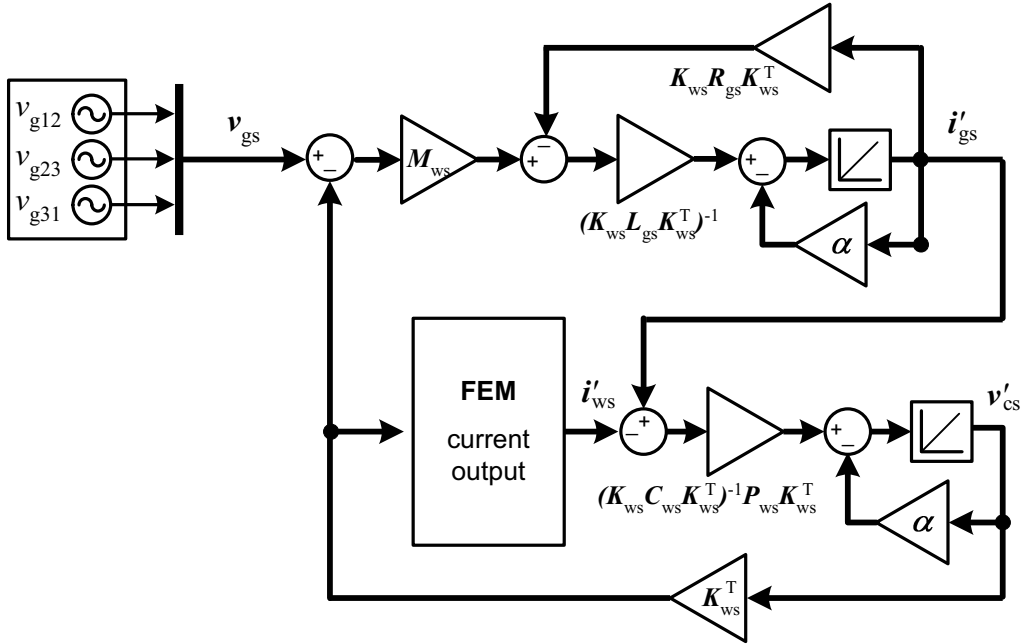


Figure 4.4: Simulation model of the system consisting of the FEM model of cage induction motor, grid and compensating capacitors using the current output approach.

## 4.2.2 Circuit parameter approach

The simulation model for the cage induction motor with an ideal voltage supply using the circuit parameter approach is presented in Fig. 4.5. The motor is modelled by the electromotive force  $e_{ws}$ , resistance  $R_{ws}$  and the dynamic inductance  $L_{ws}^{dyn}$ . These parameters are obtained at each time step from the FEM block and used in the circuit model based on (4.6).

When the whole system with grid and compensating capacitors is modelled, both currents  $i'_{ws}$  and  $i'_{gs}$  and capacitor voltage  $v'_{cs}$  are required as state variables and therefore they are subject to numerical integration. Besides (4.14) and (4.15), the stator current is integrated from

$$\frac{di'_{ws}}{dt} = \left( K_{ws} L_{ws}^{dyn} K_{ws}^T \right)^{-1} \left[ M_{ws} K_{ws}^T v'_{cs} - K_{ws} e_{ws} - K_{ws} R_{ws} K_{ws}^T i'_{ws} \right] - \alpha i'_{ws} \quad (4.16)$$

The simulation model for a system simulator is presented in Fig. 4.6.

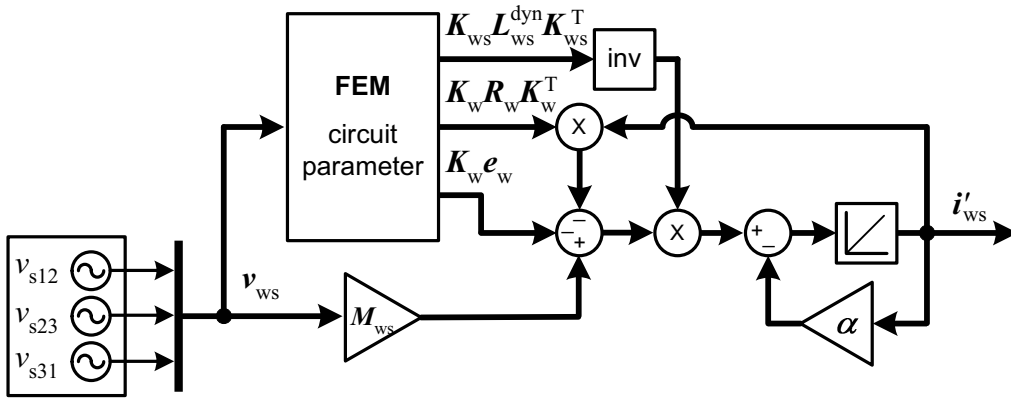


Figure 4.5: Simulation model of the cage induction motor with an ideal voltage supply using the circuit parameter approach.

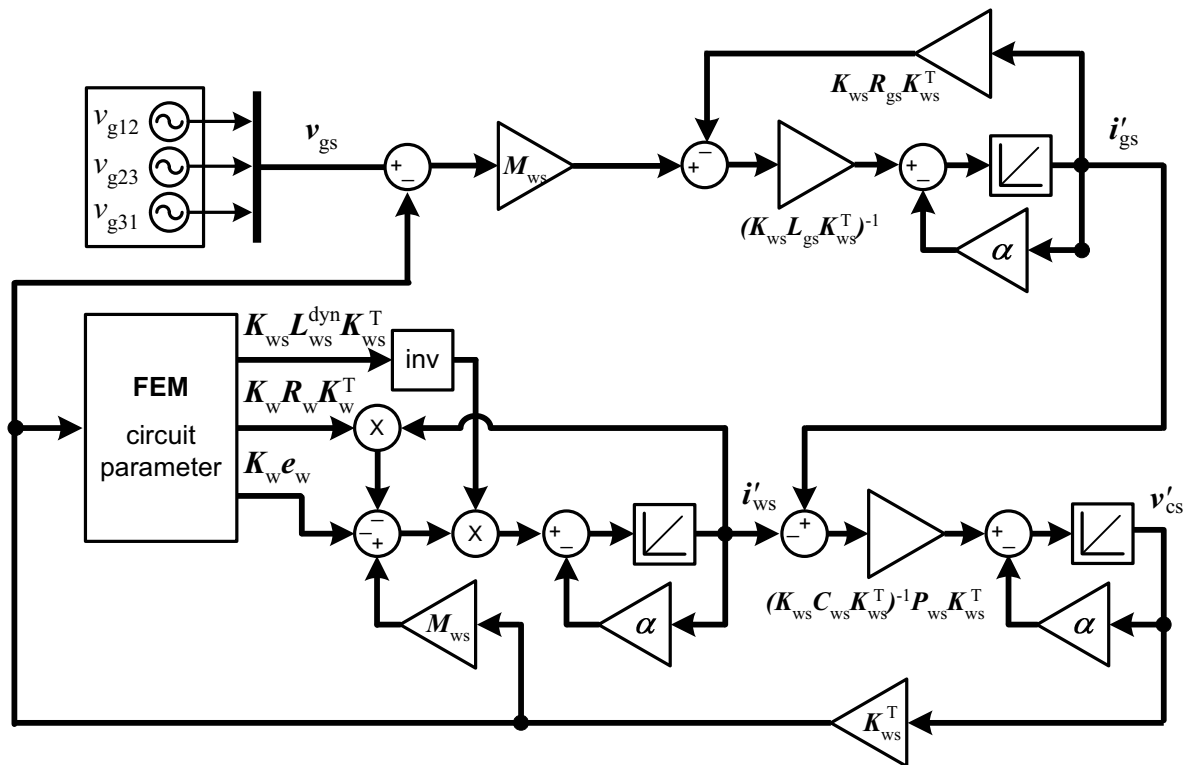


Figure 4.6: Simulation model of the system consisting of the FEM model of cage induction motor, grid and compensating capacitors using the circuit parameter approach.

### 4.2.3 Direct coupling

The directly coupled field and circuit equations of the system are formulated in order to verify the results of the current output approach and the circuit parameter approach. The simulation method is the same as described in Section 2.1, but the external circuit equations are added into the system of equations. The cage induction motor is modelled by (2.25), (2.26) and (2.27) on page 24 and the external circuit is modelled by (4.12) and (4.13). Applying the trapezoidal

approximation for the derivatives gives

$$\begin{aligned} \mathbf{r}_f &= \mathbf{S}\mathbf{a}^k + \mathbf{F}_b^T \mathbf{u}_b^k + \mathbf{F}_{ws}^T \mathbf{K}_{ws}^T \mathbf{i}'^k \\ &+ \mathbf{S}_0 \mathbf{a}^{k-1} + \mathbf{F}_b^T \mathbf{u}_b^{k-1} + \mathbf{F}_{ws}^T \mathbf{K}_{ws}^T \mathbf{i}'^{k-1} = 0 \end{aligned} \quad (4.17)$$

$$\mathbf{r}_b = \mathbf{F}_b \mathbf{a}^k + \mathbf{B} \mathbf{u}_b^k - \mathbf{F}_b \mathbf{a}^{k-1} + \mathbf{B} \mathbf{u}_b^{k-1} + \mathbf{Q}_{b0} \mathbf{i}_b^{k-1} = 0 \quad (4.18)$$

$$\begin{aligned} \mathbf{r}_{ws} &= \mathbf{K}_{ws} \mathbf{F}_{ws} \mathbf{a}^k + \mathbf{K}_{ws} \mathbf{W}_s \mathbf{K}_{ws}^T \mathbf{i}'^k + \mathbf{Q}_{ws} \mathbf{K}_{ws}^T \mathbf{v}'^k \\ &- \mathbf{K}_{ws} \mathbf{F}_{ws} \mathbf{a}^{k-1} + \mathbf{K}_{ws} \mathbf{W}_{s0} \mathbf{K}_{ws}^T \mathbf{i}'^{k-1} + \mathbf{Q}_{ws} \mathbf{K}_{ws}^T \mathbf{v}'^{k-1} = 0 \end{aligned} \quad (4.19)$$

$$\begin{aligned} \mathbf{r}_{gs} &= \mathbf{K}_{ws} \mathbf{G}_{gs} \mathbf{K}_{ws}^T \mathbf{i}'^k - \mathbf{Q}_{ws} \mathbf{K}_{ws}^T \mathbf{v}'^k + \mathbf{M}_{ws} \mathbf{v}_{gs}^k \\ &- \mathbf{K}_{ws} \mathbf{G}_{gs0} \mathbf{K}_{ws}^T \mathbf{i}'^{k-1} - \mathbf{Q}_{ws} \mathbf{K}_{ws}^T \mathbf{v}'^{k-1} + \mathbf{M}_{ws} \mathbf{v}_{gs}^{k-1} = 0 \end{aligned} \quad (4.20)$$

$$\begin{aligned} \mathbf{r}_{cs} &= \mathbf{K}_{ws} \mathbf{Q}_{ws}^T \mathbf{i}'^k - \mathbf{K}_{ws} \mathbf{Q}_{ws}^T \mathbf{i}'_{gs}^k + \mathbf{K}_{ws} \mathbf{G}_{cs} \mathbf{K}_{ws}^T \mathbf{v}'^k \\ &+ \mathbf{K}_{ws} \mathbf{Q}_{ws}^T \mathbf{i}'^{k-1} - \mathbf{K}_{ws} \mathbf{Q}_{ws}^T \mathbf{i}'_{gs}^{k-1} - \mathbf{K}_{ws} \mathbf{G}_{cs} \mathbf{K}_{ws}^T \mathbf{v}'^{k-1} = 0 \end{aligned} \quad (4.21)$$

where (4.17)–(4.19) characterize the cage induction motor and (4.20)–(4.21) represent the grid and compensation capacitors. Coefficients  $\mathbf{S}$ ,  $\mathbf{S}_0$ ,  $\mathbf{F}_b$ ,  $\mathbf{F}_{ws}$ ,  $\mathbf{B}$ ,  $\mathbf{W}_s$ ,  $\mathbf{W}_{s0}$ ,  $\mathbf{Q}_{b0}$  and  $\mathbf{Q}_{ws}$  are determined in Section 2.1.2 on pages 24–25, and connection matrices  $\mathbf{K}_{ws}$  and  $\mathbf{M}_{ws}$  are determined by (4.3) and (4.4), respectively. Coefficients  $\mathbf{G}_{gs}$ ,  $\mathbf{G}_{gs0}$  and  $\mathbf{G}_{cs}$  are defined by

$$\mathbf{G}_{gs,ii} = -\frac{R_{g,i} \Delta t + 2L_{g,i}}{2\gamma l_{ws}} \quad (4.22)$$

$$\mathbf{G}_{gs0,ii} = -\frac{R_{g,i} \Delta t - 2L_{g,i}}{2\gamma l_{ws}} \quad (4.23)$$

$$\mathbf{G}_{cs,ii} = \frac{C_i}{\gamma l_{ws}} \quad (4.24)$$

where  $l_{ws}$  is the length of the coil and  $\gamma$  the number of symmetry sectors in the finite element model.

Using the nonlinear Newton–Raphson iteration, the field and circuit variables are solved from

$$\begin{bmatrix} \mathbf{J}(\mathbf{a}^{k,n}) & \mathbf{F}_b^T & \mathbf{F}_{ws}^T \mathbf{K}_{ws}^T & \mathbf{0} & \mathbf{0} \\ \mathbf{F}_b & \mathbf{B} & \mathbf{0} & \mathbf{0} & \mathbf{0} \\ \mathbf{K}_{ws} \mathbf{F}_{ws} & \mathbf{0} & \mathbf{K}_{ws} \mathbf{W}_s \mathbf{K}_{ws}^T & \mathbf{0} & \mathbf{Q}_{ws} \mathbf{K}_{ws}^T \\ \mathbf{0} & \mathbf{0} & \mathbf{0} & \mathbf{K}_{ws} \mathbf{G}_{gs} \mathbf{K}_{ws}^T & -\mathbf{Q}_{gs} \mathbf{K}_{ws}^T \\ \mathbf{0} & \mathbf{0} & \mathbf{K}_{ws} \mathbf{Q}_{ws}^T & -\mathbf{K}_{ws} \mathbf{Q}_{gs}^T & \mathbf{K}_{ws} \mathbf{G}_{cs} \mathbf{K}_{ws}^T \end{bmatrix} \begin{bmatrix} \Delta \mathbf{a}^{k,n} \\ \Delta \mathbf{u}_b^{k,n} \\ \Delta \mathbf{i}'_{ws}^{k,n} \\ \Delta \mathbf{i}'_{gs}^{k,n} \\ \Delta \mathbf{v}'_{cs}^{k,n} \end{bmatrix} = - \begin{bmatrix} \mathbf{r}_f^n \\ \mathbf{r}_b^n \\ \mathbf{r}_{ws}^n \\ \mathbf{r}_{gs}^n \\ \mathbf{r}_{cs}^n \end{bmatrix} \quad (4.25)$$

which is an extension of (2.43) on page 26.

## 4.3 Simulation results

In order to see the difference between the methods, the system was modelled at different levels of complexity. At first, the cage induction motor was connected to an ideal supply only in order to evaluate the circuit parameter approach with respect to direct coupling. The ideal model was simulated in steady state and during start-up. In the simulation of the whole system with grid and capacitors, the current output approach was also utilized and all the three methods were compared with each other using several different values for the external circuit parameters.

### 4.3.1 Ideal voltage supply

Simulation with the ideal sinusoidal voltage supply was carried out by the circuit parameter approach and direct coupling. Again, the current output approach is equivalent to the direct coupling, since the model does not contain any additional circuit elements besides the stator winding. The effective value of the supply voltage was 400 V and the frequency was 50 Hz. In the circuit parameter approach, the FEM computation is processed at 50  $\mu\text{s}$  major steps and the circuit model is integrated at 10  $\mu\text{s}$  minor steps. The time step in the directly coupled simulation was 50  $\mu\text{s}$ . The cutoff frequency  $\alpha$  for the numerical integration was 15 Hz in the steady-state simulation. When simulating the start-up of the motor,  $\alpha$  was set to zero.

Figure 4.7 presents the waveforms of the steady-state stator current at no load, half load (18.5 kW) and full load (37 kW). When the methods are compared, the shapes of the waveforms differ slightly, although the agreement is excellent in terms of amplitude and effective value.

Figure 4.8 presents the current during the start-up with no load, also obtained by the circuit parameter approach and direct coupling. The difference between the methods is presented as a separate plot, since it would not be visible otherwise. According to the results, the absolute difference remains in the range from  $-15$  A to  $+15$  A, regardless of the current amplitude.

The influence of the minor step size is illustrated by Fig. 4.9. As observed with the doubly-fed induction generator, changing the size of the minor steps changes slightly the results, but does not greatly improve the accuracy. In this case, however, the difference between the waveforms is more visible. Possible reasons for this could be smaller ratings and the cage winding in the rotor. As described in Section 2.4.1, the damping effect of the cage winding is only present in the electromotive force that is held constant between the major steps. Therefore, the numerical integration of the current does not incorporate the rotor bars, but only the dynamic inductance of the stator winding. On the other hand, the agreement in the results is still satisfactory regardless of the simplified approach.

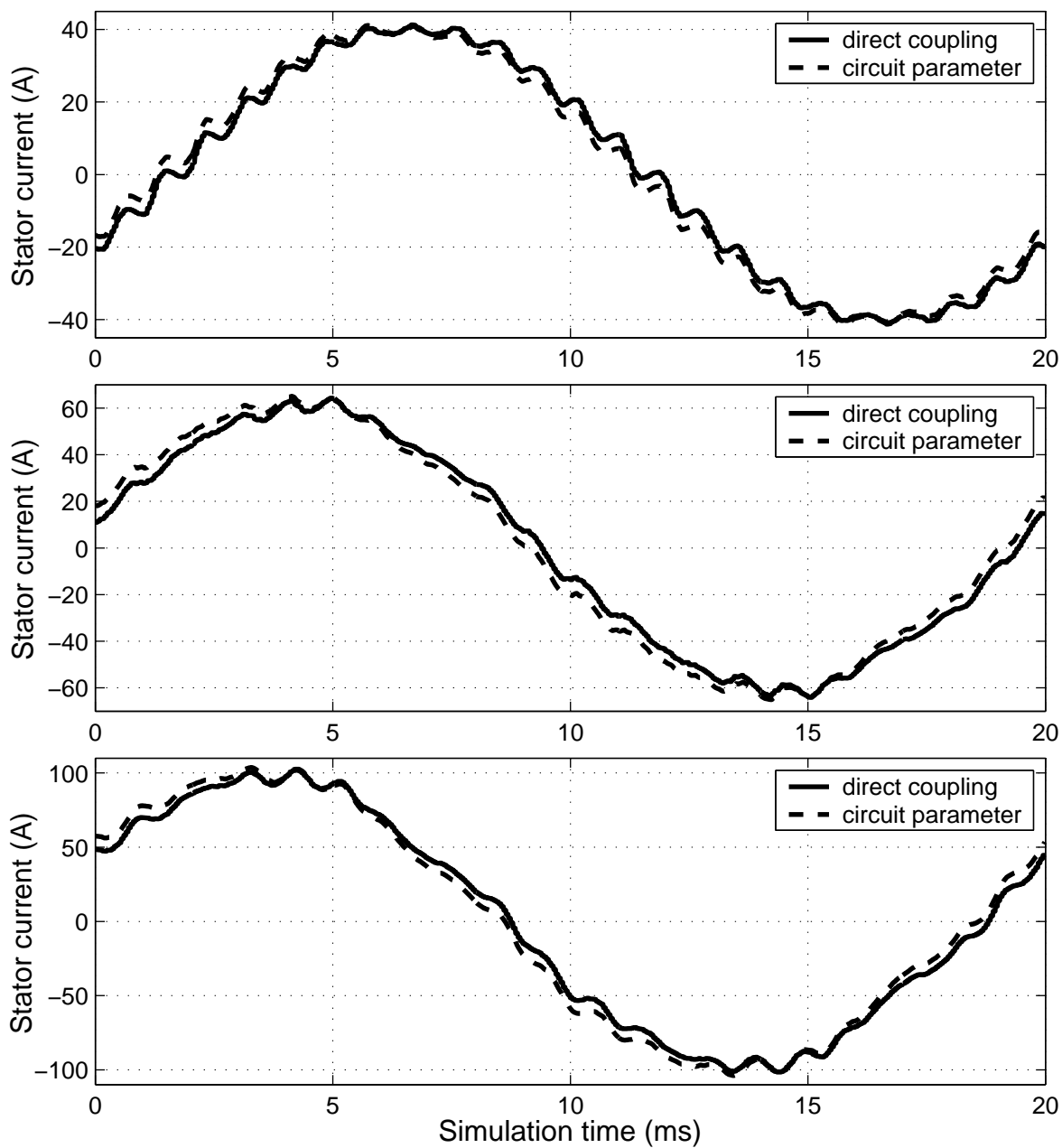


Figure 4.7: Steady-state stator current at no load, half load (18.5 kW) and full load (37 kW) obtained by circuit parameter approach and direct coupling.

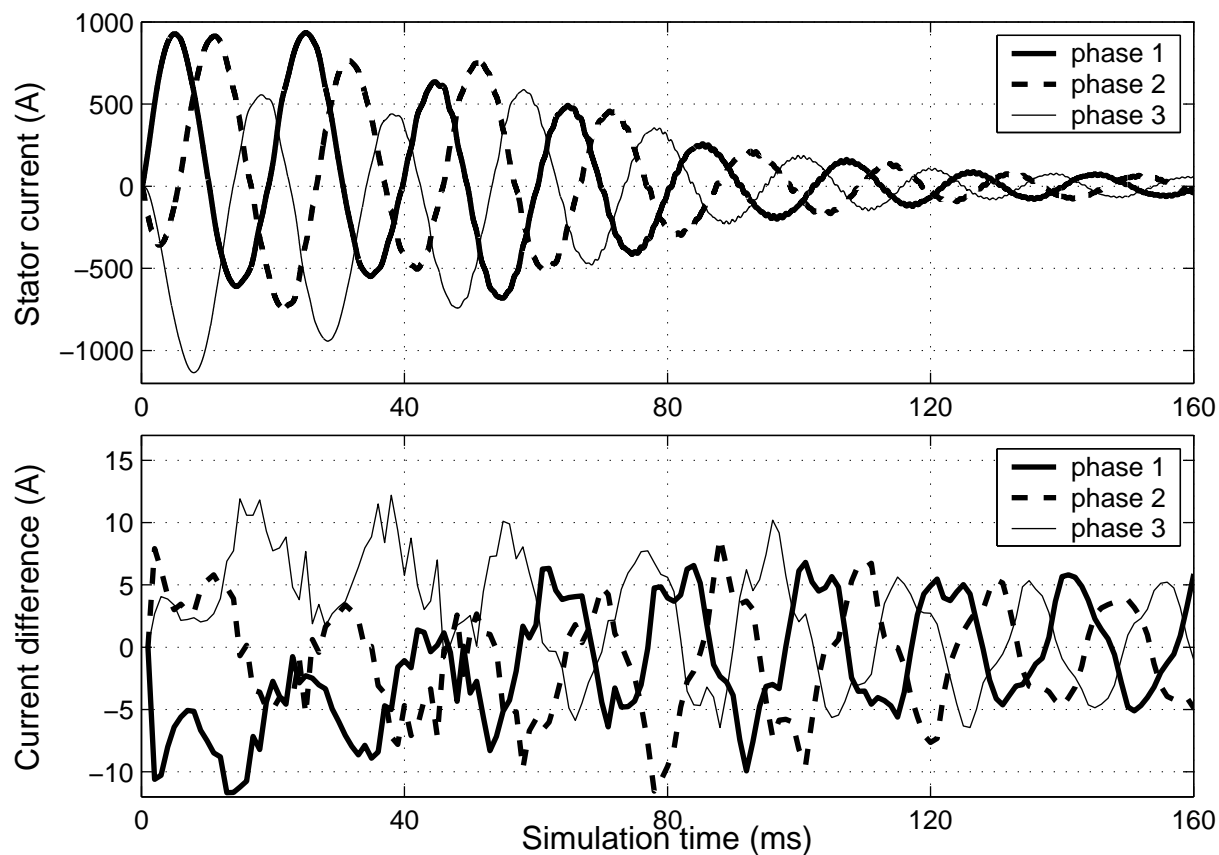


Figure 4.8: Stator current during start-up transient obtained by circuit parameter approach, and the absolute difference with respect to direct coupling.

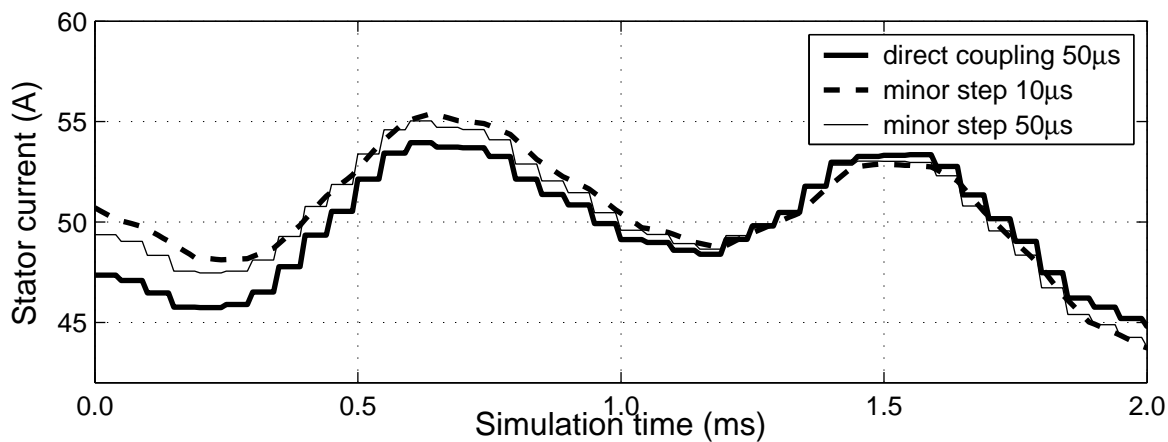


Figure 4.9: Influence of the minor step size on the stator current.

### 4.3.2 Grid and compensating capacitors

The simulation of the whole system model with grid and compensating capacitors is carried out by the circuit parameter approach, current output approach and direct coupling. The supply voltage, time steps and cutoff frequency for the numerical integration had the same values as the steady-state simulation above. Two different grid models and three values for the compensating capacitance were used in the simulation. In the following, grid 1 refers to the parameters  $L_g = 1$  mH,  $R_g = 2.2$  m $\Omega$  and grid 2 to the parameters  $L_g = 7$  mH,  $R_g = 35$  m $\Omega$ . In terms of short-circuit power, grid 1 corresponds to 500 kVA and grid 2 to 70 kVA. The capacitance values are  $C_1 = 67$   $\mu$ F,  $C_2 = 134$   $\mu$ F and  $C_3 = 200$   $\mu$ F, which correspond to 10, 20 and 30 kVAr reactive power, respectively. The parameter values are selected to correspond to the laboratory setup that was used for experimental validation of the simulation models (Section 4.4).

Table 4.2 presents the effective (RMS) values of stator current  $i_s$ , grid current  $i_g$  and stator voltage  $v_s$ , obtained by the circuit parameter approach (circ), current output approach (cur) and direct coupling (dir). In general, both current output approach and circuit parameter approach agree well with the direct coupling, except in the cases producing very low grid current (typed in boldface). Furthermore, a closer inspection reveals that the results obtained by the current output approach are slightly closer to the results of directly coupled simulation.

The differences between the methods are also illustrated in Fig. 4.10, which presents the waveforms of the stator current, grid current and stator voltage during one period of the supply frequency, when the motor is connected to grid 2 and capacitance  $C_2$  and operates at full load. In addition, detailed plots of the results are presented in Fig. 4.11.

The results obtained by the different methods are very similar in terms of both the effective values and waveforms, but it is also shown that the methods are not equivalent to each other. There is a clear distinction between the direct and indirect coupling because of the one-step delay between the FEM computation and circuit simulation, but the two indirect approaches produce almost identical waveforms. Nevertheless, inspection of the effective values in Table

T 4.2: C

	grid 1: no load			grid 2: no load			grid 1: full load			grid 2: full load		
	$C_1$	$C_2$	$C_3$	$C_1$	$C_2$	$C_3$	$C_1$	$C_2$	$C_3$	$C_1$	$C_2$	$C_3$
$i_s^{\text{cur}}$ [A]	27.2	28.8	30.4	22.9	29.1	38.0	66.1	68.9	69.4	52.2	56.7	61.5
$i_s^{\text{circ}}$ [A]	27.2	28.8	30.3	22.8	29.5	38.1	67.8	70.6	71.7	52.8	57.2	62.2
$i_s^{\text{dir}}$ [A]	27.5	28.9	30.5	23.4	29.2	38.1	66.3	68.0	69.5	51.2	56.5	62.0
$i_g^{\text{cur}}$ [A]	13.0	<b>1.6</b>	14.9	9.7	<b>1.3</b>	9.8	60.0	59.8	58.8	47.3	48.1	53.4
$i_g^{\text{circ}}$ [A]	13.1	<b>4.3</b>	15.8	9.8	<b>6.2</b>	12.75	62.7	63.5	64.3	48.8	50.7	57.1
$i_g^{\text{dir}}$ [A]	13.2	<b>0.9</b>	14.7	10.3	<b>0.4</b>	9.5	59.6	57.0	57.3	45.6	47.4	52.0
$v_s^{\text{cur}}$ [V]	393	400	408	363	400	436	386	397	401	309	334	365
$v_s^{\text{circ}}$ [V]	393	400	408	363	397	434	386	397	401	308	331	359
$v_s^{\text{dir}}$ [V]	393	400	408	361	399	436	386	394	401	306	336	369

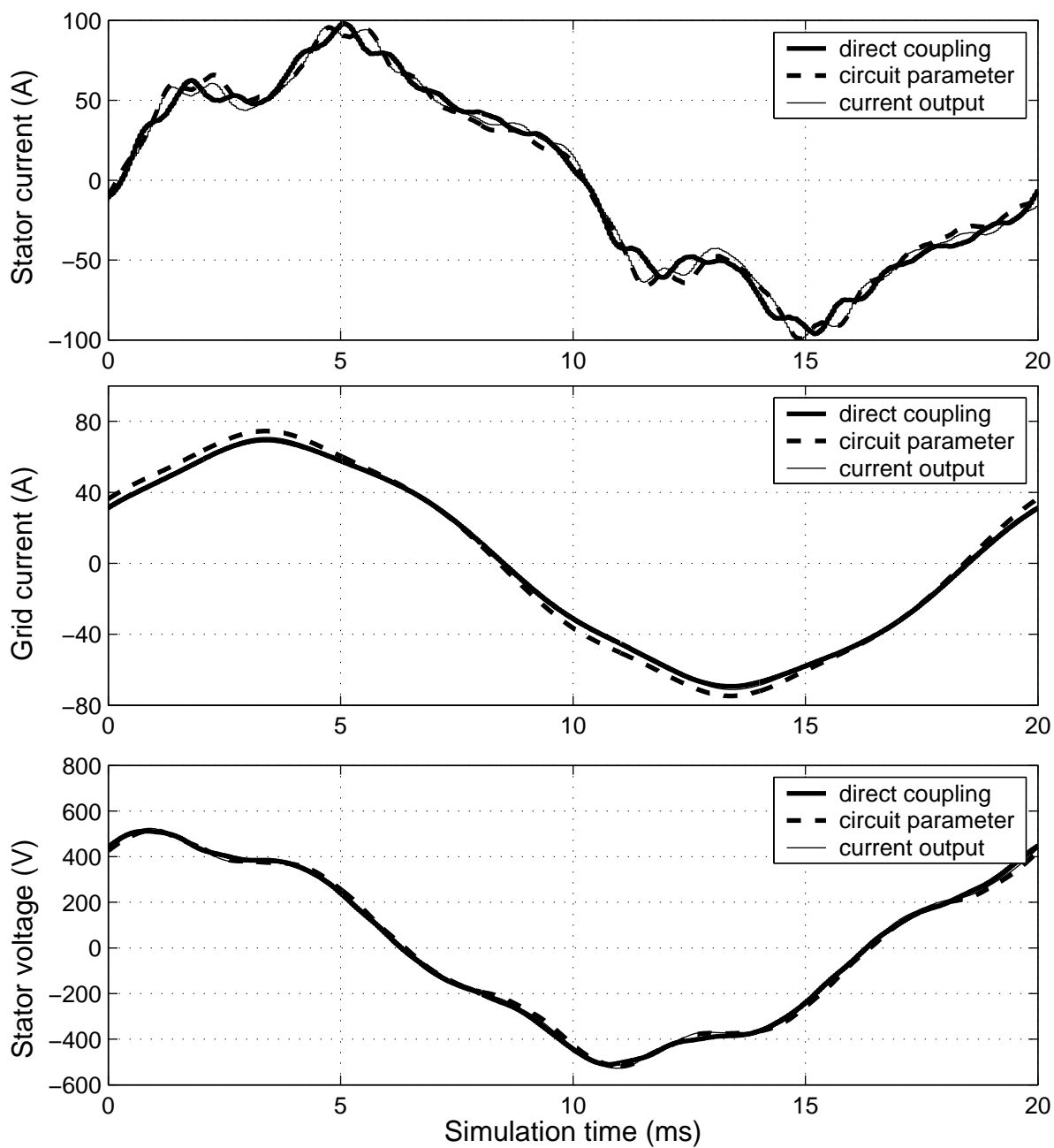


Figure 4.10: Comparison of the stator current, grid current and stator voltage obtained by direct coupling, circuit parameter approach and current output approach.

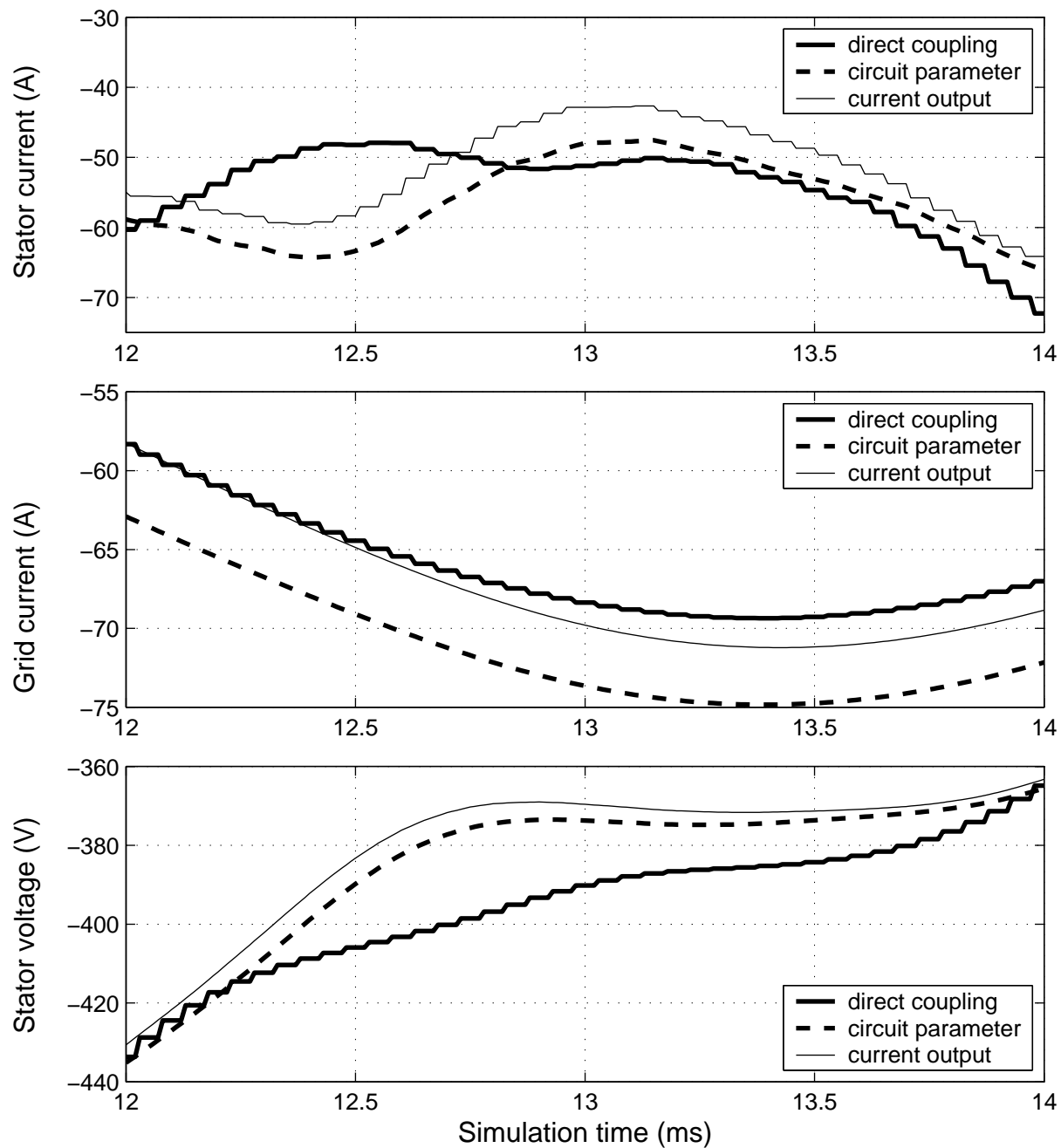


Figure 4.11: Details of the simulation results in Fig. 4.10.



The characteristics of the generators G1 and G2 correspond as closely as possible to grid 1 and grid 2 used in the simulation models. However, both of the generators had automatic voltage control systems that kept the stator voltage nearly constant regardless of the capacitance value in the stator. The DC generator G3 was supplied by a thyristor rectifier with speed control and excited by a constant field current.

The stator voltage was measured between phases A–B and C–B by a Tektronix A6907 voltage isolator. The currents in the grid and stator were measured from phases A and B by a LEM LT-300 Hall sensors. The effective values were calculated from the measured waveforms and double-checked by a NORMA D6100 power analyzer. The shaft torque and rotational speed were measured by a HOTTINGER T30FNA torque transducer, but the results were only used for ensuring the correct operation point of the system. The waveforms of the results were stored by a KONTRON WW700 transient recorder. The temperature of the cage induction motor was measured at the end-windings and outer surface of the stator core in order to ensure that the conditions do not change during the measurements.

#### 4.4.2 Measured results

Using a 400 V supply voltage with 50 Hz frequency, the steady-state operation of the system was measured at no load and full load with one, two or three capacitor banks in the stator. However, generator G2 was not applicable for the full load, because the required field current would have been over the ratings. The results are presented in Table 4.3, together with corresponding results from the directly coupled simulation. Because of the automatic voltage control in the laboratory setup, not all the simulation results are fully comparable with the measurements. For those cases, in which the measured and simulated stator voltages are close to each other, the stator currents are also close enough to show the validity of the FEM model. The differences in the grid current are in the same range, except for the no-load cases with full compensation. However, these cases were also shown to be problematic in the comparison of the direct and indirect simulation methods above.

Figure 4.13 shows an example of the waveform comparison, when the motor was supplied by generator G1, operating at full load, and the reactive power was compensated by capacitance

T 4.3: E

	G1: no load			G2: no load			G1: full load		
	$C_1$	$C_2$	$C_3$	$C_1$	$C_2$	$C_3$	$C_1$	$C_2$	$C_3$
$i_s^{\text{meas}}$ [A]	28.6	28.6	28.6	28.4	28.0	29.4	66.6	66.6	66.6
$i_s^{\text{dir}}$ [A]	27.5	28.9	30.5	23.4	29.2	38.1	66.3	68.0	69.5
$i_g^{\text{meas}}$ [A]	15.3	3.8	14.9	15.6	4.5	14.9	59.7	55.5	55.6
$i_g^{\text{dir}}$ [A]	13.2	0.9	14.7	10.3	0.4	9.5	59.6	57.0	57.3
$v_s^{\text{meas}}$ [V]	397	397	398	393	391	394	394	397	397
$v_s^{\text{dir}}$ [V]	393	400	408	361	399	436	386	394	401

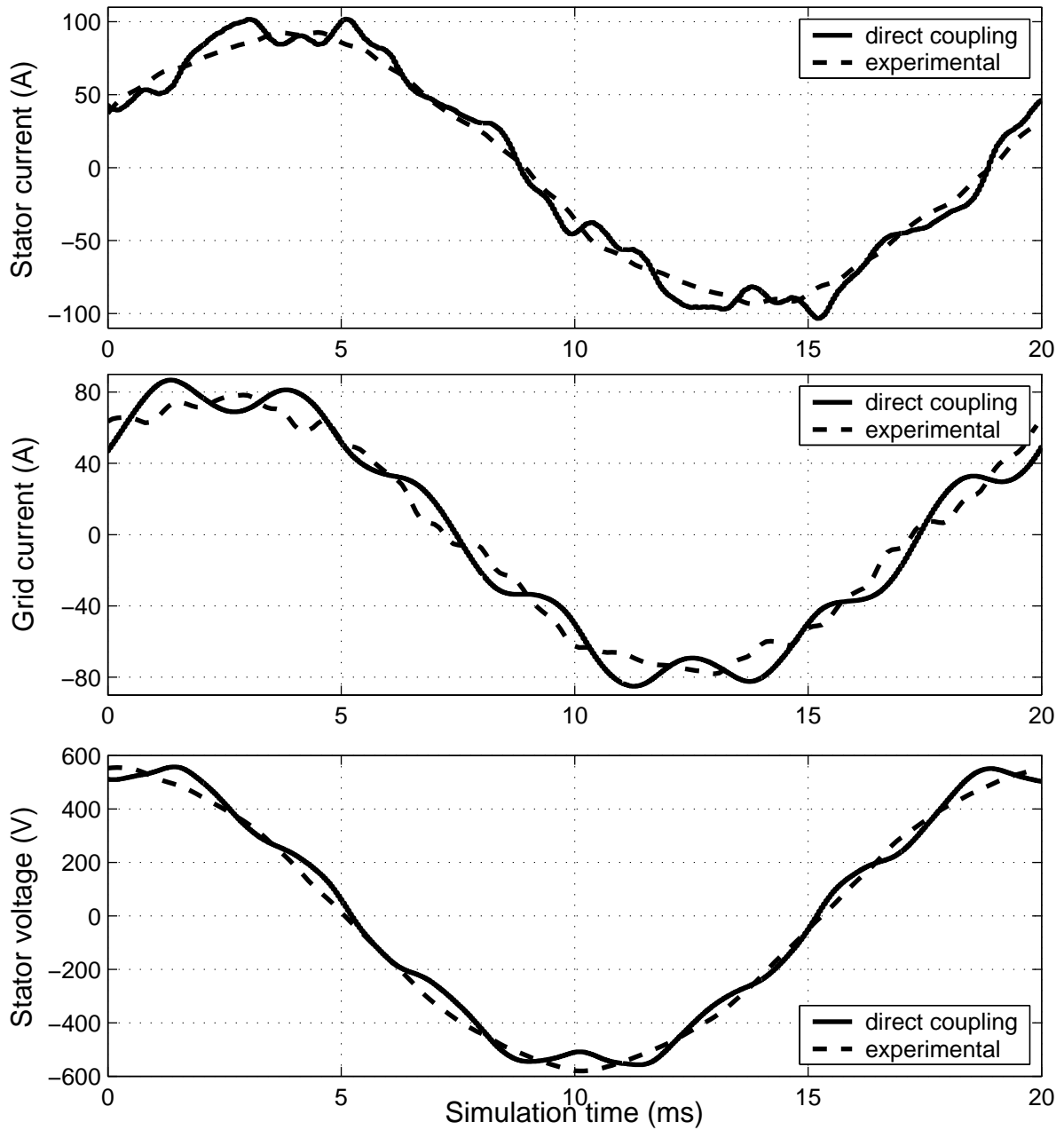


Figure 4.13: Measured and simulated waveforms of stator current, grid current and stator voltage.

$C_2$ . The comparison shows that both the amplitudes and phases of the stator voltage and the currents are nearly the same in the measured and simulated results.

## 4.5 Discussion

In this example, the FEM model of the cage induction motor was connected with the circuit model of a grid and compensating capacitors. The system was simulated by the current output

approach and circuit parameter approach, both of which utilize an indirect coupling between the FEM model and the external circuit model. The results of each approach were compared with the results of directly coupled simulation, showing good agreement. In addition, the FEM model with directly coupled circuit equations was validated by experimental results.

Based on the results of this example, the conclusions of Chapter 3 can be extended as follows:

1. The applicability of the circuit parameter approach is also shown for electrical machines with cage rotor.
2. Both the current output approach and circuit parameter approach are applicable for non-iterative indirect coupling with external circuit models.
3. The difference between the waveforms obtained by indirectly and directly coupled simulation is visible, but not significant in most cases.

As distinct from the previous example, it is now possible to evaluate the interaction between the models of the electrical machine and the external circuit. Regardless of the good agreement between indirect and direct coupling, the observed differences reveal that even a simple circuit model is rather sensitive to any inaccuracy in the computation. This can be explained by considering the magnetic field and electrical circuit as two domains of the electromagnetic system, having strong physical coupling by nature. Separation of the domains for non-iterative simulation breaks the physical coupling by introducing a delay of one time step between the field and circuit models. Therefore, the length of the time step must be chosen carefully considering the time constants in the physical system, in order to keep the accuracy at a reasonable level.

The comparison between the indirect approaches did not reveal significant differences in the accuracy. When considering the applicability and flexibility in model construction, however, the approaches differ from each other to some extent. In general, modelling circuit equations in a system simulator is not as simple as it would be in a circuit simulator. Similarly, the current output approach is more convenient to use in a system simulator, but the circuit parameter approach would be more appropriate in a circuit simulator. Hence, selection of the approach for indirect coupling should be based on the software to be used for the circuit simulation.

On the basis of the above conclusions, the most appropriate approach for combining a FEM model with electrical circuit simulation is still direct or iterative coupling, which preserves the strong coupling between the field and circuit domains. Nevertheless, implementation of a new circuit topology always requires new circuit equations, which are tedious to write manually in the program code. The process can be simplified by automatic construction of the coupled equations, as presented by Väänänen (1996) or Kuo-Peng et al. (1997). In some cases, however, coupling with an external simulator provides such flexibility for model construction that it is truly advantageous to utilize the indirect approaches instead of direct coupling. Examples of such applications are presented in the next chapter.

## **5 Case studies of controlled frequency converter supply**

This chapter reviews two case studies concerning frequency converter models coupled with the finite element analysis. In the first case, an induction motor drive using the direct torque control (DTC) algorithm is modelled in SIMULINK and coupled with the FEM computation by the current output approach. The second case presents an application of a doubly-fed induction generator in a variable-speed wind turbine, in which the rotor is supplied by a frequency converter and protected against sudden faults by a passive crowbar. The system is modelled in SIMULINK and the coupling with the FEM computation is carried out by both the current output approach and the circuit parameter approach, giving a comparative analysis. The purpose of this chapter is to show that indirect coupling, especially by the current output approach, provides good results with complex frequency converter models.

### **5.1 Induction motor drive with detailed DTC algorithm**

This example presents the simulation of a 2 MW cage induction motor drive with a detailed control system model corresponding to a real product (ACS6000) as closely as possible. The drive model is implemented in SIMULINK and the coupling with the FEM model is carried out by the current output approach. The system was simulated in steady state and compared with an analytical model and experimental results, showing good agreement. The work was carried out in co-operation between the university and an industrial partner, and is originally reported in (Kanerva et al., 2004).

#### **5.1.1 Background**

This study was accomplished in co-operation between the university, the drives manufacturer and the machine factory. The main objectives of this case were the validation of the method by experiments and creation of the coupled simulation environment providing opportunity to share the expertise between the designers of frequency converters and electrical machines. In this case, the model of the frequency converter was created by the drives manufacturer and the FEM model of the motor was provided by the machine factory. Therefore, it was possible to obtain close agreement between the simulation model and the real application. The contribution of the author of this thesis has been to provide the computational methods for the finite element analysis, and, together with other parties, to analyze the results and draw conclusions.

### 5.1.2 Description of the system model

The fundamental structure of the drive model is similar to the basic scheme of the direct torque control (DTC) (Takahashi and Noguchi, 1986; Depenbrock, 1988), but the digital control system is modelled in detail by several discrete functions on different time levels, as in the real application. Figure 5.1 presents the top level schematic of the drive model, showing the main functions for torque control and speed control modes. Originally, the simulation model was developed for an analytical motor model, but the FEM model was simply included by replacing the block of the analytical motor model with the block of the FEM model. The fundamental time step for the frequency converter model was  $12.5 \mu\text{s}$ ; its multiples were used in the parts of the model requiring slower sampling. The major step for the FEM computation was  $100 \mu\text{s}$ ; the coupling was accomplished by the current output approach. The selection of the time steps is based on finding an optimum between reasonable simulation time and adequate accuracy.

The cage induction motor in the drive system has 3 phases, 6 poles and 86 non-skewed rotor bars. The ratings of the motor and the frequency converter are presented in Table 5.1. The finite element mesh of the machine comprises 13143 nodes and 6518 quadratic elements, as illustrated by Fig. 5.2.

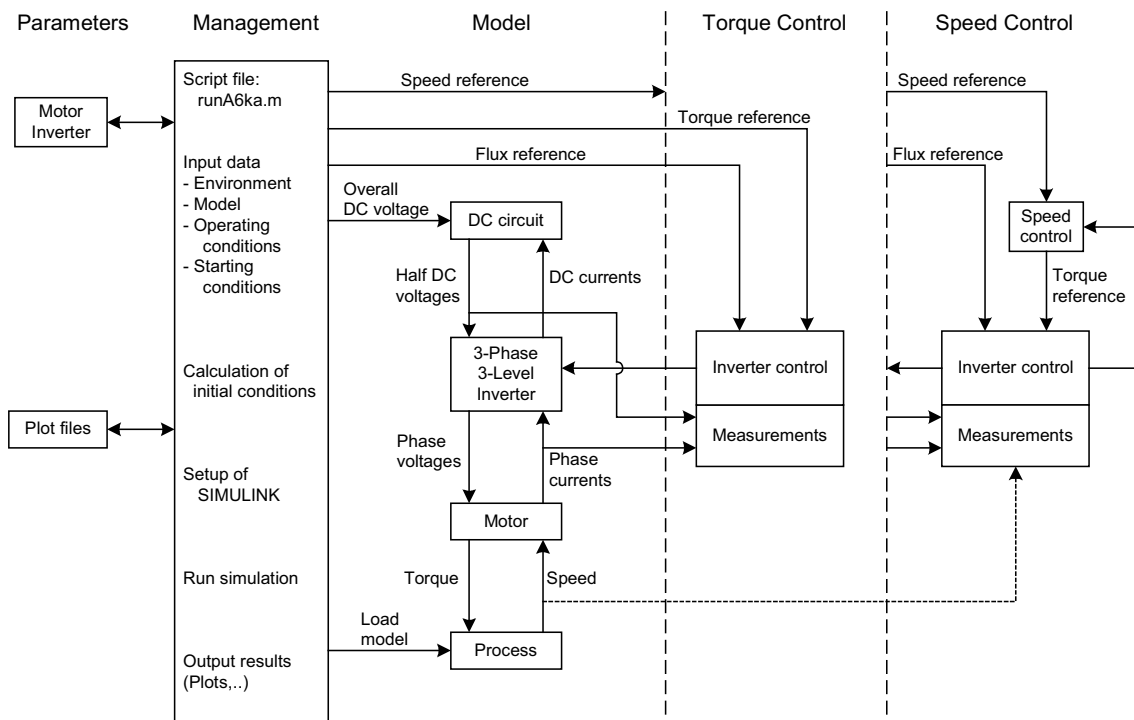


Figure 5.1: Schematic of the detailed DTC drive model (Kanerva et al., 2004).

T 5.1: R

Cage induction motor			Frequency converter		
$P_N$	rated power	2 MW	$P_{\max}$	maximum power	9 MW
$U_N$	rated voltage	3150 V	$U_{\max}$	maximum voltage	3300 V
$I_N$	rated current	436 A	$I_{\max}$	maximum current	1645 A
$f_N$	rated frequency	40 Hz	$f_{\min} \dots f_{\max}$	frequency range	0...75 Hz
$n_N$	nominal speed	792 rpm			

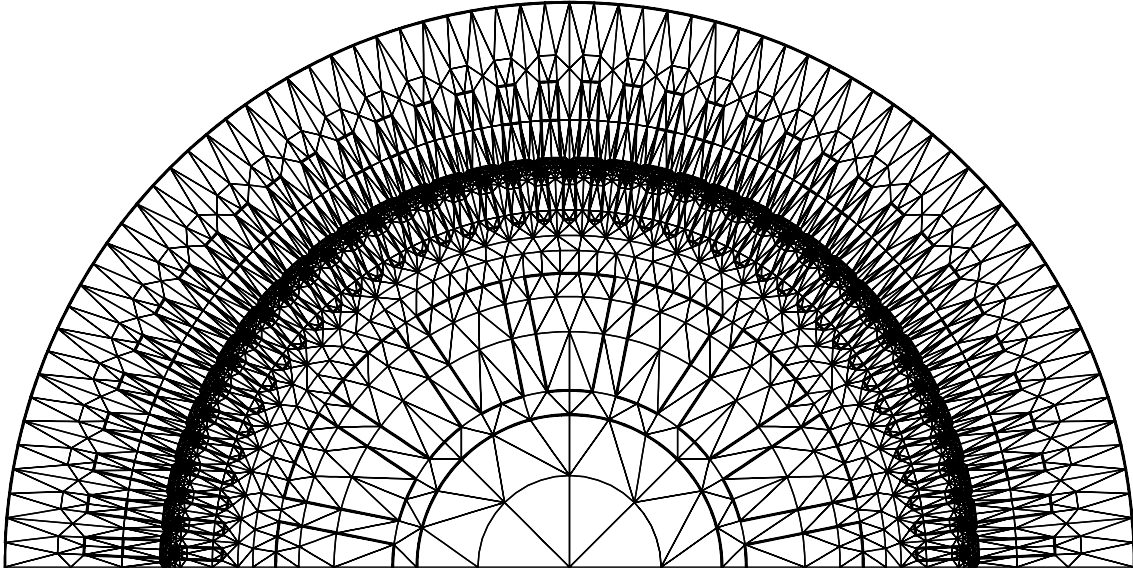


Figure 5.2: Finite element mesh of the 2 MW cage induction motor.

### 5.1.3 Results

In order to study the agreement of the simulation model with the real drive application, the system was simulated in steady state at 600 rpm rotational speed and full load. The simulation was run for several periods of the fundamental frequency and the Fourier analysis was applied to the results in order to find out the harmonic contents of the voltage and current waveforms. Due to the stochastic nature of the control strategy, pure comparison of the waveforms does not give much information, so the frequency components of the voltage and current are studied instead.

The results obtained by the FEM model and analytical model were compared with the experimental results in terms of the frequency components. Figure 5.3 presents the voltage spectrum without the fundamental component, showing good agreement between measurements and simulation by the both models. This shows that the analytical model is alone sufficient for analyzing the control system itself. As illustrated by Fig. 5.4, however, there is a clear difference between the analytical and FEM models in the current spectrum. As compared with the measurements, the results from the FEM model provide very close agreement with the real drive. In addition, the impedance of the motor is calculated from the frequency components and

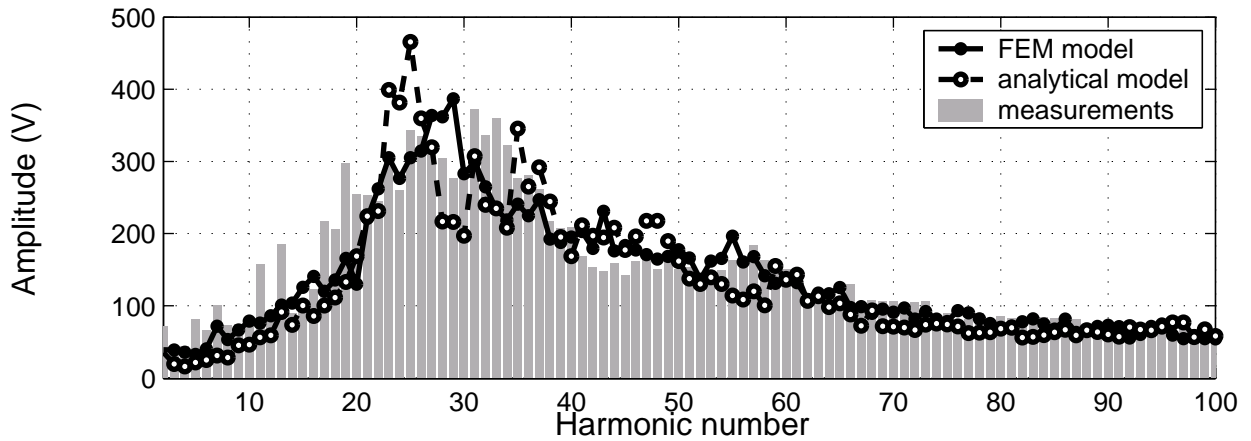


Figure 5.3: Comparison of the voltage spectrum obtained by the FEM model, analytical model and measurements.

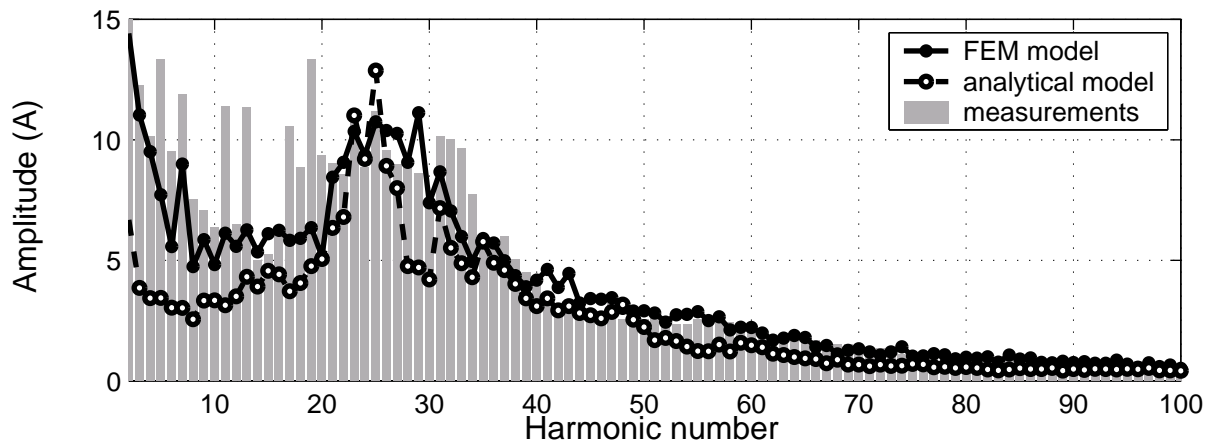


Figure 5.4: Comparison of the current spectrum obtained by the FEM model, analytical model and measurements.

presented in Fig. 5.5.

Besides the steady state, the transient operation was also tested by simulating rapid load changes. Figure 5.6 presents the electromagnetic torque and the stator current when the load is first increased from zero to nominal and decreased to half the nominal after 40 ms. In the simulation with the FEM model, the control system responds very well to the changes.

### 5.1.4 Conclusion

The results of this example show the capability of the current output approach for coupling the FEM model of the electrical machine with a frequency converter model and a closed-loop control system. The operation of the drive system was purely based on a stochastic closed-loop control. In comparison with the static control presented widely in the literature, the simulation model of this example requires proper feedback from the FEM computation to the converter

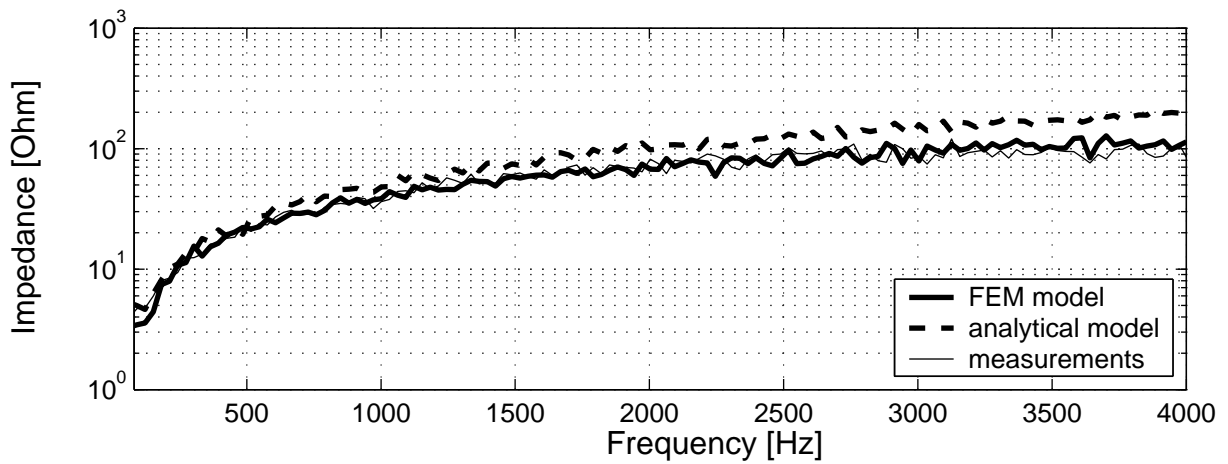


Figure 5.5: Comparison of the motor impedance obtained by the FEM model, analytical model and measurements.

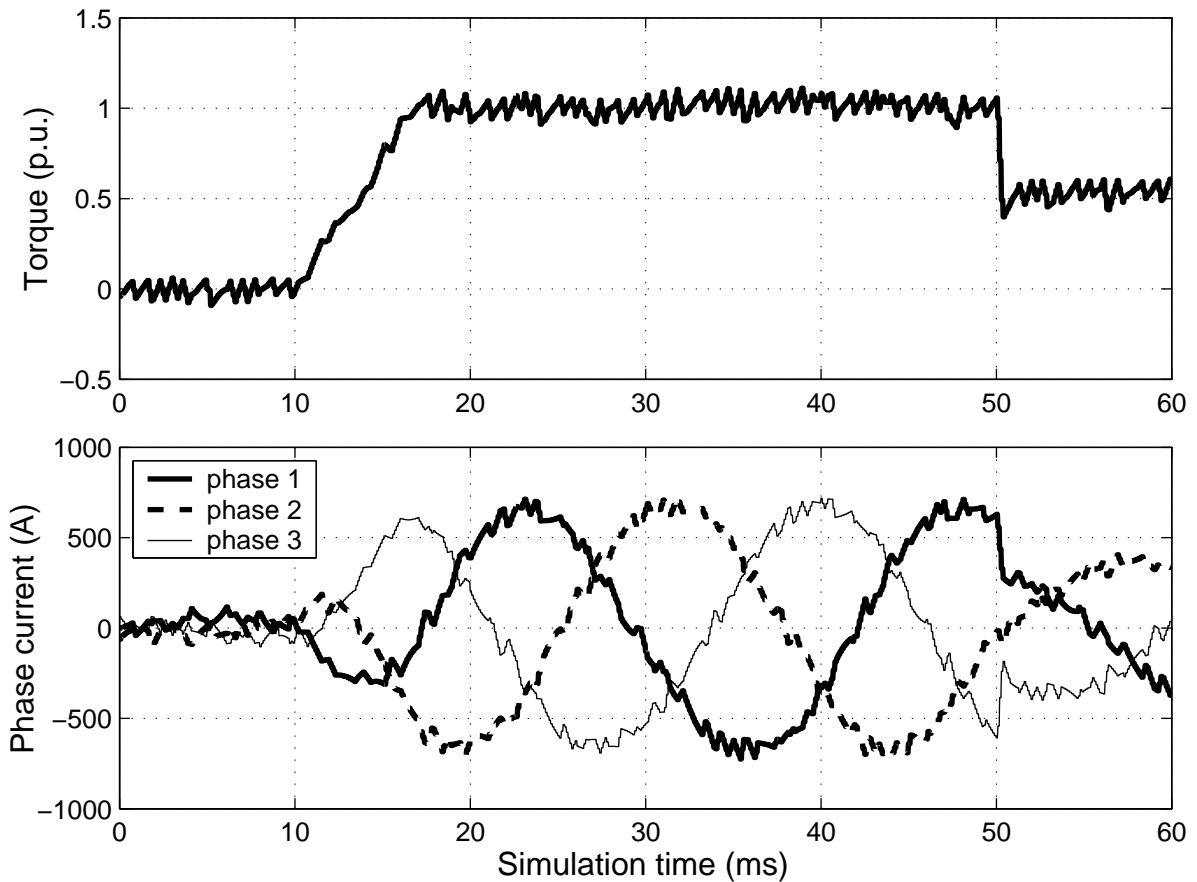


Figure 5.6: Simulated electromagnetic torque and stator current during load steps.

model. It was shown that the implementation of such a closed-loop model is also possible when indirect coupling is utilized between the FEM model and control system model. In addition, it is possible to use a longer time step in the time-consuming FEM computation than is required for the control system; when used, this provides a significant saving in simulation time with

respect to the direct coupling.

Because the output of the inverter model is an ideal voltage source and the estimates for torque and flux are based on the stator current, the current output approach is an ideal method for coupling the FEM model within the system model. The effect of the one-step delay due to indirect coupling is not significant, because the current measurement in the actual control system also works with a delay.

In this example, a real industrial application was modelled with numerous details and the results were validated by experiments. A special feature of this case is that the original drive model was developed by an industrial partner as a part of the product development activity, and the inclusion of the FEM model was simply carried out by replacing the analytical motor model with the FEM block. This allows the designers of frequency converters and the designers of electrical machines, typically working at different locations, to combine their expertise and construct detailed simulation models for large systems.

## **5.2 Doubly-fed induction generator in a variable-speed wind turbine**

This case study presents the simulation of a doubly-fed induction generator in a variable-speed wind turbine. The rotor of the generator is supplied by a frequency converter providing the speed control, stator voltage control and power factor control. A crowbar circuit is connected to the rotor for overcurrent protection. The system model is implemented in SIMULINK and both the current output approach and circuit parameter approach were used for coupling the FEM model of the generator with the system model. The operation of the system was simulated in steady state and during a symmetric grid fault. On the basis of the comparison between the coupling methods and analytical generator model, it was shown that the current output approach was more stable and accurate than the circuit parameter approach. The example case is originally reported in (Semán et al., 2004) and (Kanerva et al., 2005).

### **5.2.1 Background**

In the background of this case were the regulations for wind parks, where several wind turbines operate together like one large power plant. It was required that a wind park must not be disconnected from the grid in the case of sudden voltage drop, if the fault lasts only for a short period of time. Therefore, the manufacturers of the wind generators must know the consequences of such faults and design the control systems that will not only protect the generators but also support the grid during short voltage dips.

A simulation environment was built for a doubly-fed induction generator, comprising models for the generator, frequency converter and the control system. Originally, an analytical model was used for the generator in order to ensure quick simulation for testing the influence of different control settings. The analytical model was then replaced by the FEM model, because it was

necessary to have as accurate a model as possible for the fault simulation. On the other hand, simulation with the FEM model also provides a good basis for evaluating the accuracy of the analytical generator model and improving the model according to the results. The contribution of the author of this thesis has been to provide the computational methods for the finite element analysis, and, together with other parties, to analyze the results and draw conclusions.

## 5.2.2 Description of the system model

The schematic of the system is presented in Fig. 5.7. The grid is modelled by a sinusoidal voltage source with an inductance and resistance in series, and the transformer (TR) model comprises the short-circuit inductance, resistance and the leakage capacitance. The frequency converter model comprises two back-to-back connected voltage source inverters and a DC link. The stator-side converter is modelled as a simple first-order filter that controls the DC-link voltage with a PI controller. The rotor-side converter is supplied from the common DC link and the switches are assumed to be ideal. The control of the inverter is based on direct torque control (DTC), where the estimates of flux linkage and torque are calculated from constant equivalent circuit parameters and the currents obtained from the generator model. The over-current protection circuit (crowbar) consists of a diode bridge, a resistor, and a thyristor that connects the rectified rotor voltage to the resistor, when the fault occurs.

Models of the grid, transformer, frequency converter and crowbar are implemented in SIMULINK, while the FEM model of the generator is coupled with the system model by both the current output approach and circuit parameter approach. An analytical generator model with constant parameters was used for the design of the control system and for comparison with the FEM model. The generator is the same as presented in Table 3.1 on page 34. In the simulation, the major time step for the FEM computation was  $50 \mu\text{s}$  and the frequency converter model was simulated using  $0.5 \mu\text{s}$  steps. In the circuit parameter approach, the minor time step for

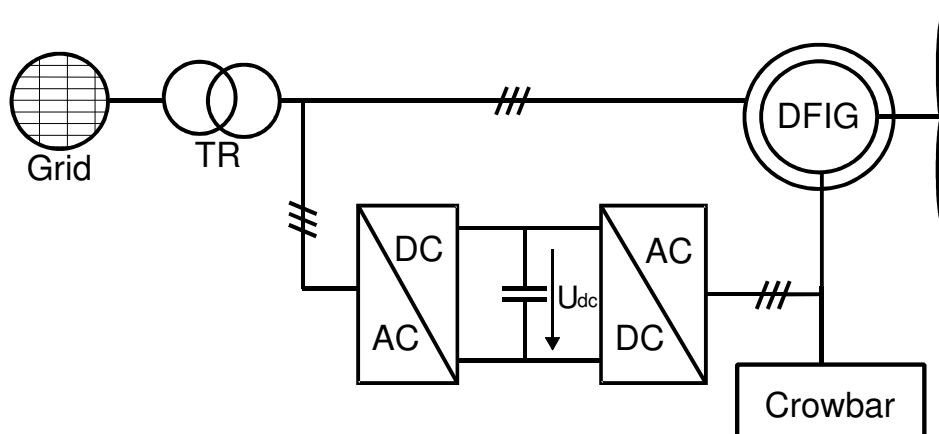


Figure 5.7: Schematic of the variable-speed wind turbine with doubly-fed induction generator (DFIG), rotor-side frequency converter, overcurrent protection circuit (crowbar), transformer (TR) and grid (Seman et al., 2004).

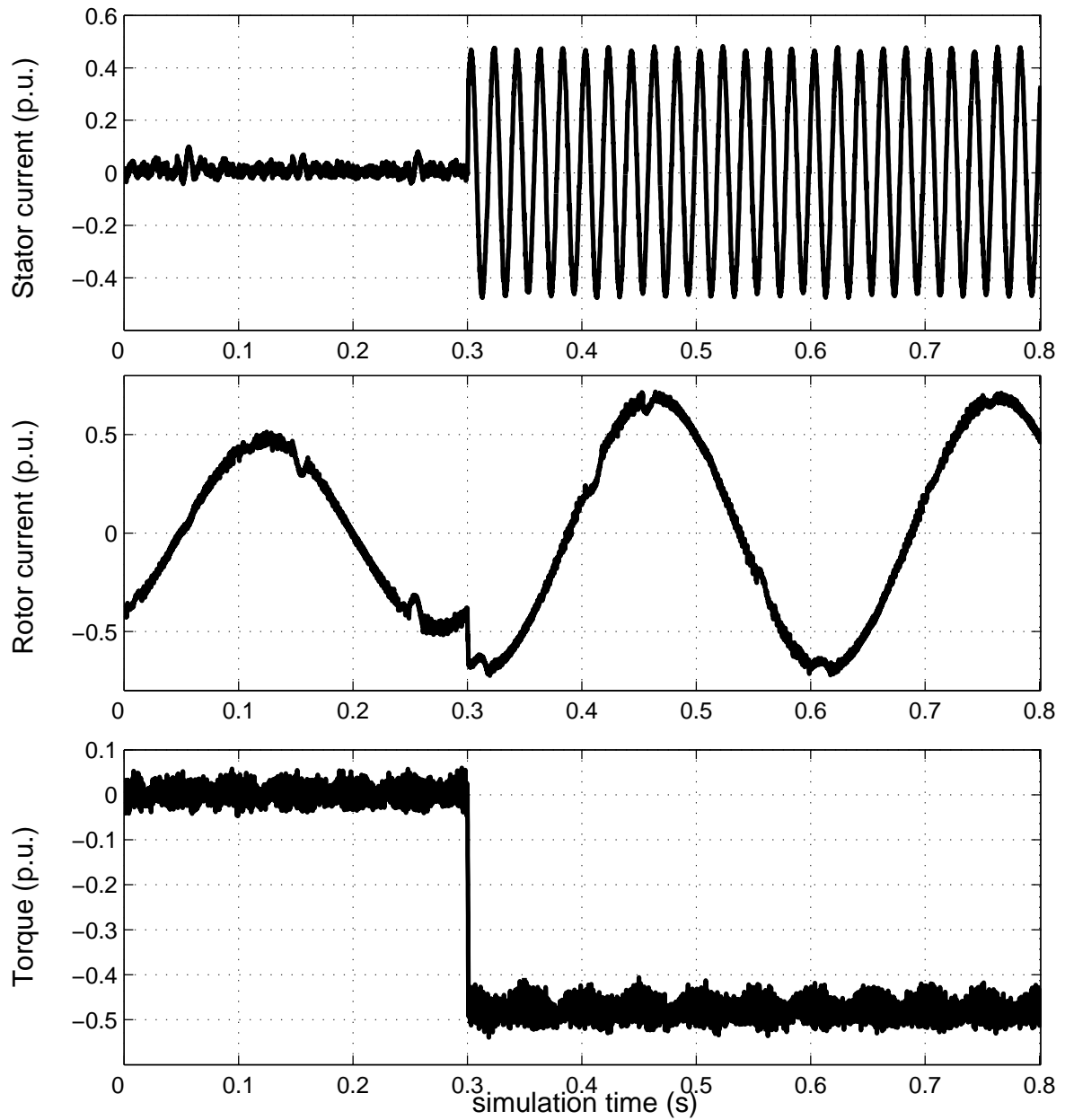
integrating the phase currents was  $10 \mu\text{s}$ . Again, optimal time steps were chosen to provide a reasonable computation time and accurate results. It should be noted that even though there is a significant difference in the minor and major time steps, no numerical problems were introduced. The parameters of the control system were tuned according to the test simulations with the analytical generator model; the same settings were used in all the simulations.

### 5.2.3 Results

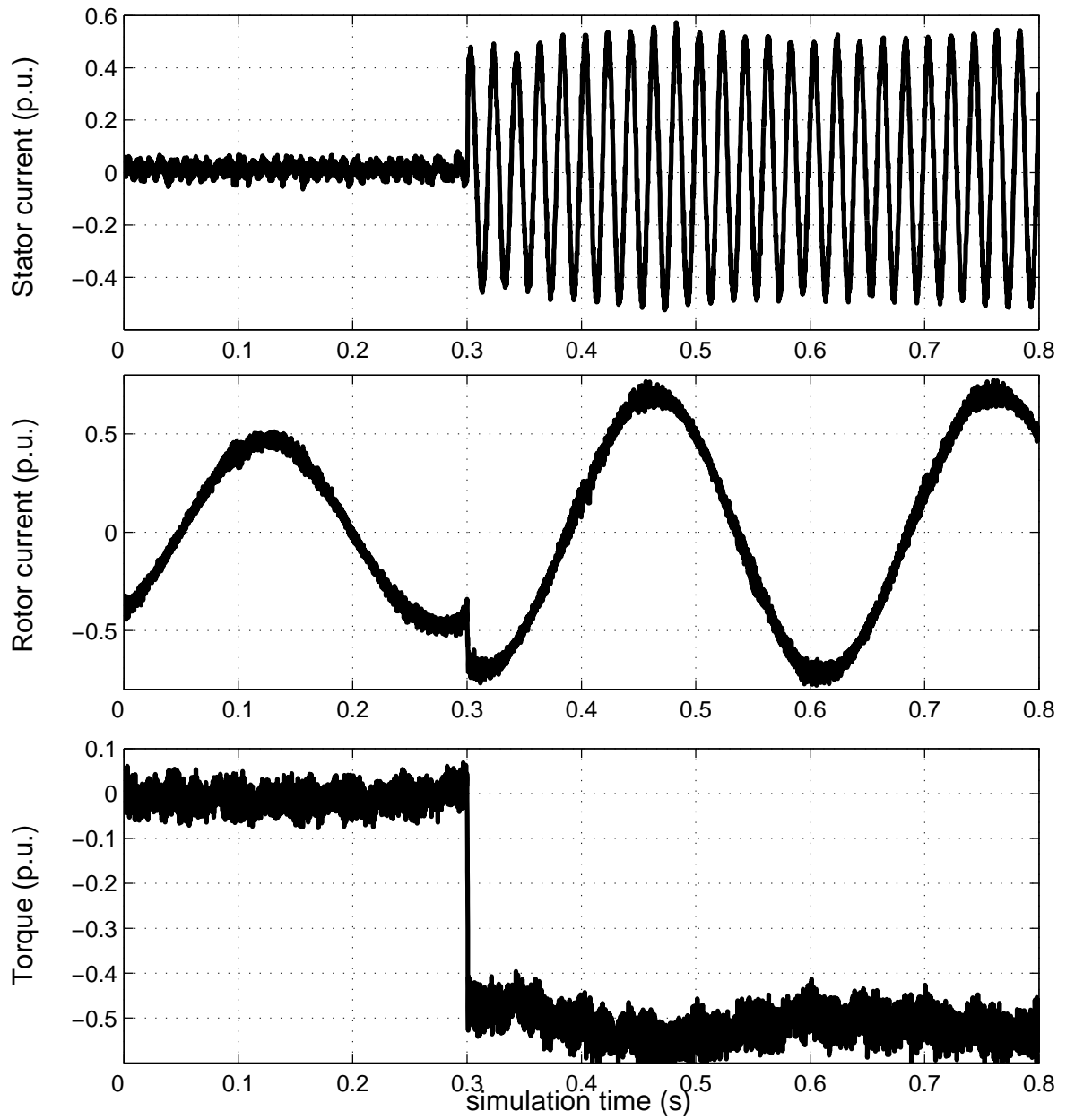
The system was simulated in steady-state, during a load step and during a symmetric grid fault. A constant rotational speed was assumed in all the cases because of the large moment of inertia of the rotor and turbine. Figure 5.8 presents the stator current, rotor current and electromagnetic torque in a transient from no-load to half-load operation, simulated by the current output approach. Due to the DTC algorithm, the rotor supply is controlled to produce the desired torque in all operating conditions. As shown by the results, the obtained torque is very stable and the response to the reference change is rapid.

Figure 5.9 presents the corresponding case simulated by the circuit parameter approach. The settings for the control system were the same as with the current output approach. With the circuit parameter approach, however, the operation is not as stable and accurate as it is with the current output approach. An obvious reason for this is the error in the phase current integration, already reported in Section 3.3, which gives faulty information to the control system resulting in visible oscillation in the stator current and electromagnetic torque. The effect on the control is also illustrated by Fig. 5.10, which presents an example of the output voltage of the rotor-side converter using both the current output approach and circuit parameter approach. The switching in the latter case is very rapid, which is a result of faulty operation of the control. This causes higher ripple in the rotor current, but also removes the small notches, as seen in Fig. 5.8. However, the notches are not critical to the operation of the system, since the primary control variable is the flux linkage.

The operation of the system during a sudden grid fault was also simulated. The amplitude of the stator voltage was dropped to 35 % of the nominal value when the generator was running at half load. Because of the fault, the control system disconnects the rotor-side converter and the crowbar is triggered in order to protect the rotor winding. In the simulation, both the current output approach and the circuit parameter approach were used for the FEM model, and the results were compared with each other and the ones obtained by the analytical generator model. Figure 5.11 presents the stator and rotor current obtained by all the three methods. The difference between the analytical and FEM models is relatively large during the first periods, because the analytical model does not include the effects of saturation and slotting. However, the waveforms get closer as the transient decays. The difference between the current output approach and the circuit parameter approach is also clear and can be explained in the same way as the steady-state simulation.



*Figure 5.8: Stator current, rotor current and electromagnetic torque during a load step obtained by the current output approach.*



*Figure 5.9: Stator current, rotor current and electromagnetic torque during a load step obtained by the circuit parameter approach.*

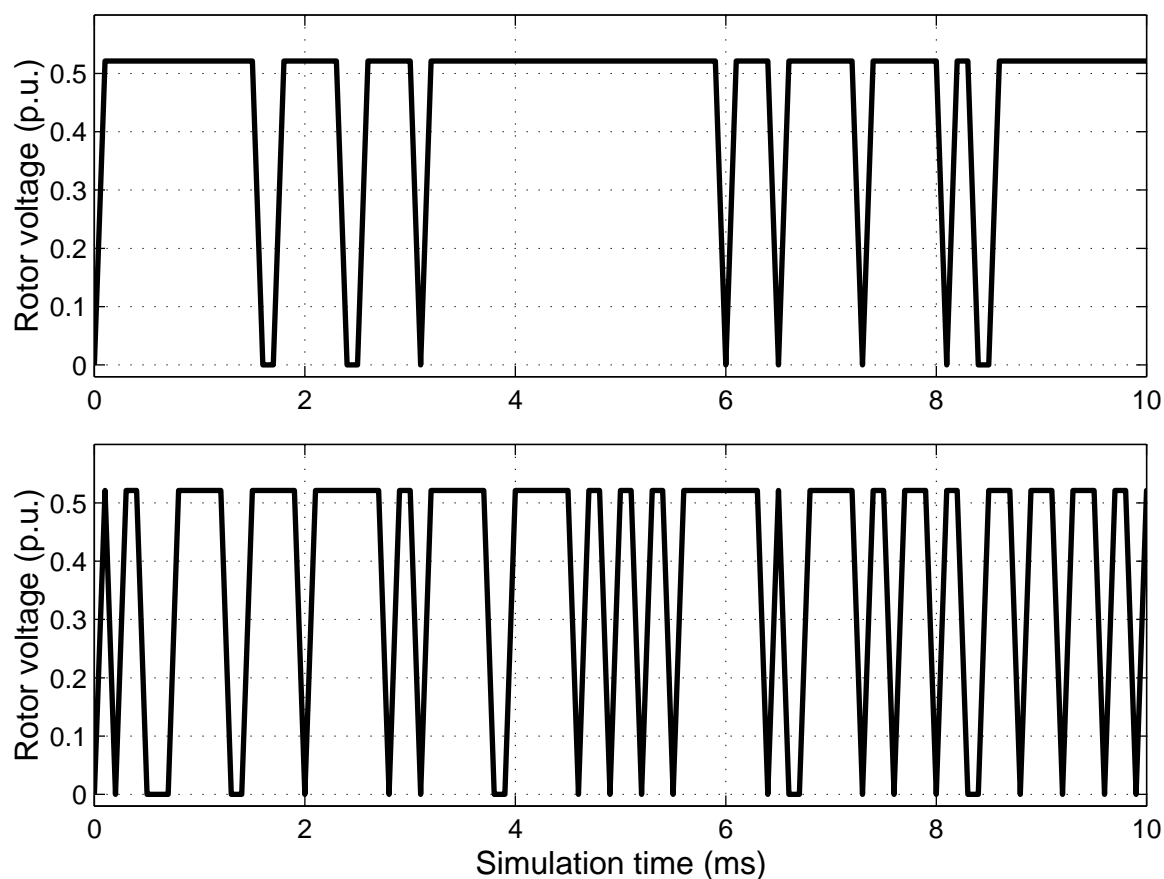


Figure 5.10: Output voltage of the rotor-side converter using current output approach (upper) or circuit parameter approach (lower).

## 5.2.4 Conclusion

As in the drive example, a controlled system with a frequency converter supply was also presented in this case. Therefore, the conclusions presented in Section 5.1.4 also apply to this case, confirming the applicability of the current output approach for simulating such systems. In addition, the circuit parameter approach was also applied to the same system, but its performance was not as good as that obtained with the current output approach. This is mainly due to the error in the phase current, which was also presented in Chapters 3 and 4. Therefore, the circuit parameter approach cannot be recommended for coupling controlled frequency converter models with the FEM computation. Comparison with the analytical model showed that the FEM model can provide more accurate results for simulating the consequences of sudden faults. On the other hand, it was shown that a simple analytical model is accurate enough for the control system design, but the FEM model can be used for ensuring the correct operation of the system during different transients and faults.

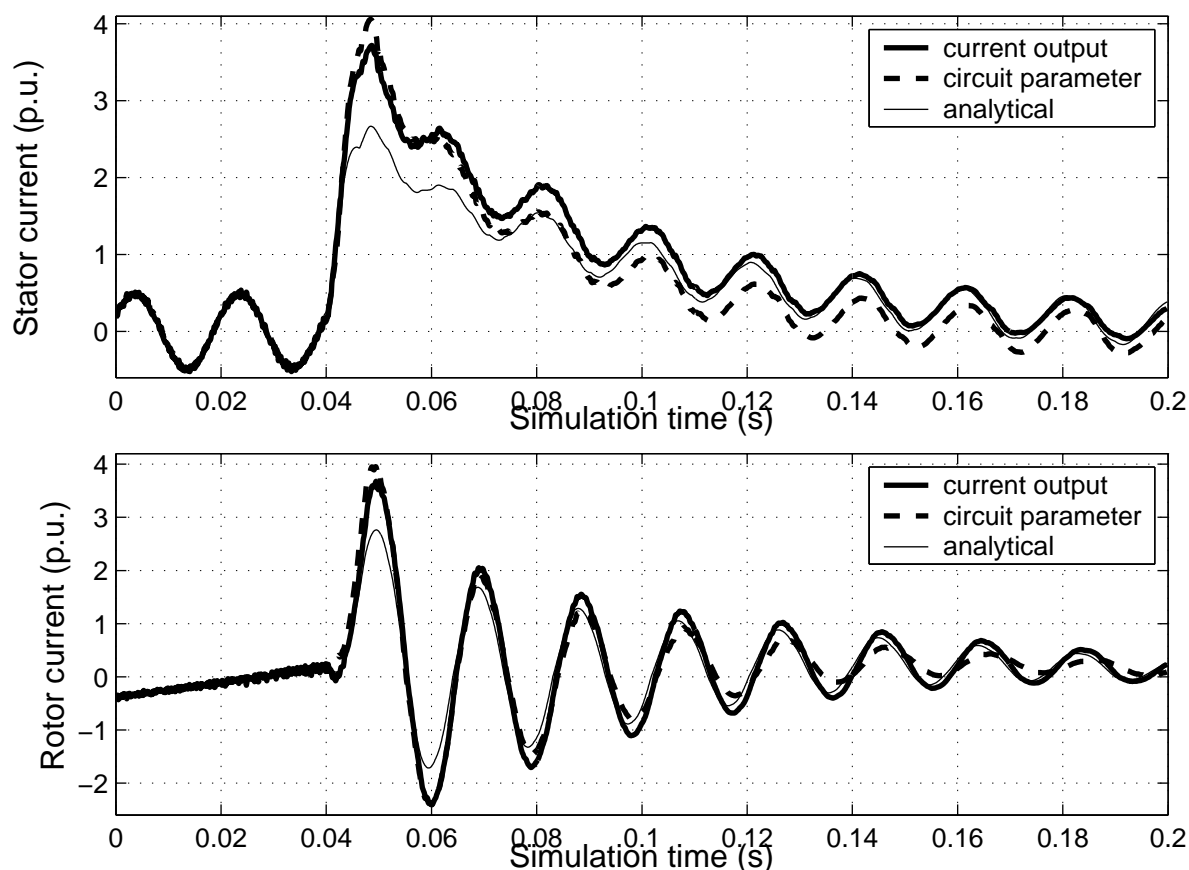


Figure 5.11: Stator and rotor current during a symmetric stator fault obtained by the current output approach, circuit parameter approach and analytical generator model.

### 5.3 Discussion

In this chapter, two examples relating to frequency converter supply of electrical machines were presented. As the previous chapters concentrated on the basic electric circuits, the models in these examples comprised mostly control systems. Since the switching components in all cases were modelled by ideal switches, there were practically no additional circuit equations to be coupled with the FEM computation, but only the control system equations. Therefore, it can be stated that this chapter presented FEM-control coupling instead of FEM-circuit coupling.

In both the examples, the current output approach was shown to be appropriate for simulating coupled FEM-control models; however, the circuit parameter approach did not perform as well. This can be explained by the direct or indirect coupling between the field and circuit equations. In the current output approach, the field-circuit coupling is direct, whereas it is indirect in the circuit parameter coupling. This causes an error in the phase currents, which was also discussed in Chapter 3. In sensitive control systems, this error is large enough to cause oscillation and inaccurate operation. However, it was shown that direct coupling is not necessarily required between the FEM model and control system, since the indirect coupling resulted in good response and accurate simulation. This can be explained by the fact that the physical coupling between the control system and electromagnetic system is actually weak, since the actions in

the control system and the response of the electromagnetic system always follow each other in a chain and there is always a delay between the actions.

The examples presented in this chapter also emphasize the main benefits of the indirect coupling. Since the models of the real frequency converter are relatively large and complex, it is convenient to construct the models in a system simulator software with a graphical user interface. By using the current output approach, inclusion of the FEM model into the converter model is as simple as using an analytical model. Another major advantage of the indirect coupling is the possibility of using different time steps in the control system model and the FEM model. In the presented examples, the time steps for the control system were remarkably shorter than for the time-consuming FEM computation, which resulted in computation-effective simulation.

The computational time was not analyzed, because there were no corresponding cases to be compared with. The time required by the FEM computation would have been similar to the cases presented in Chapters 3 and 4, but the simulations were run by another computer. In both case studies, the control system models were implemented for SIMULINK as compiled S-functions written in C or Fortran. Therefore, the simulation time was significantly shorter than it would be with corresponding models constructed from single blocks.

Based on the results of the case studies and the above discussion, the following conclusions can be drawn in reference to the frequency converter supply:

1. The current output approach is shown to be suitable for simulating electrical machines with frequency converters; this has been validated by experimental results.
2. Simulation of closed-loop control systems with a FEM model of an electrical machine does not necessarily require direct coupling.
3. The applicability of the method was proved by modelling real applications and studying actual problems in co-operation with industrial partners.
4. The circuit parameter approach is not recommended for simulating controlled frequency converters with electrical machines.

Finally, it should be noted that both the examples in this chapter were based on real applications, and also that they were accomplished in co-operation with industry. The method for coupling FEM computation with the frequency converter models has proved to be useful for the industrial partners and provided them with new knowledge.

## 6 Discussion

The aim of this chapter is to summarize and discuss the results of this thesis. The current output approach and the circuit parameter approach are analyzed in terms of their suitability for modelling and simulating electrical machines with circuits and control systems. The significance of the work is evaluated with respect to the literature reviewed in Chapter 1. On the basis of the results of this work and other research in this field, an optimal simulation environment and methodology is proposed for large-scale systems consisting of electrical machines, circuits and control systems.

### 6.1 Summary of the results

Two different approaches were presented for coupling the time-stepping finite element analysis with a system simulator SIMULINK. Because of the indirect coupling, it is possible to build the whole large-scale model in SIMULINK, whereas the FEM model of the electrical machine is represented by a functional block with a few input and output variables. The main advantages achieved by such coupling are the simple model construction, when separate parts of the system can be designed by experts in different fields and coupled simply in the simulator software, and the possibility of using different time steps for the FEM computation and the rest of the system, which results in computationally effective simulation.

The current output approach is based on directly coupled field and circuit equations, resolving the magnetic field in the cross section and the circuit quantities of the windings. In SIMULINK, the functional block performing the FEM computation passes the phase current values as output, when the supply voltage values are given as input. The coupling with external circuits and control systems using the current output approach was studied through examples involving an induction motor with grid and compensation capacitors, an induction motor drive with a frequency converter, and a doubly-fed induction generator with a frequency converter. The applicability of the method was shown in all cases, resulting in good accuracy and flexible model construction.

In the circuit parameter approach, the coupling with SIMULINK is similar but the outputs of the block are the electromotive force, dynamic inductance and resistance. These parameters are included as a part of the external circuit model and are updated at each time step. Contrary to the current output approach, the coupling between the magnetic field equations and the circuit equations of the windings is indirect in this method. The accuracy of the circuit parameter approach was studied by simulating a doubly-fed induction generator and a cage induction motor with sinusoidal supply. In comparison with the results of the directly coupled simulation, a clear difference was discovered due to the one-step delay in the coupling and the open-loop

integrators utilized in the circuit simulation. The method was also applied in the cases involving an induction motor with grid and compensation capacitors and a doubly-fed induction generator with a frequency converter. In the case of grid and capacitors, the results were similar to those obtained by the current output approach. In the case with a frequency converter, however, the results were not satisfactory due to problems in the control system model.

In order to draw some general conclusions from the results, the coupling mechanisms between the magnetic field, circuits and control systems must be analyzed. The electromagnetic coupling between the magnetic core of the electrical machine, windings and external circuits is physically strong, which explains the differences between the two indirect approaches and the directly coupled approach. Discrete operation of the switching components and control systems, however, introduces a numerically weak coupling between the electromagnetic system and the control system, which actually explains the good performance of the current output approach in the examples involving controlled frequency converters. On the other hand, the unsatisfactory performance of the circuit parameter approach in similar situations is mainly explained by the errors in the current integration, which gives a faulty reference to the control system.

## 6.2 Significance of the work

This work contributes to the simulation of electrical machines, external circuits and control systems, especially motors and generators connected with frequency converters. The main problem related to the simulation has been that, while each part of the system requires a different modelling approach, suitable simulation software for coupling these subsystems has not been available. The coupling between finite element analysis and circuit simulation has been studied widely, but the inclusion of closed control loops cannot any longer be regarded as trivial. The challenges in the control loop implementation are related to the coupling mechanisms and model description. The direct coupling between the FEM computation and control systems requires equal time steps for the whole system model, but the indirect coupling would allow different time scales for the subsystems. The type of coupling accurate enough for the coupled simulation, however, has not been studied. Another issue of consideration is, whether the control system model can be described as a block diagram or state graph and efficiently translated into the format required by the coupled simulation software. In this work, solutions to these problems are sought from a combination of private FEM code and a commercial system simulator.

The new methods presented in this work are based on indirect coupling, the performance of which is also compared with direct coupling. It is shown that direct coupling is required between the magnetic field equations and the circuit equation of the windings, but indirect coupling is adequate for controlled converter models. The applicability of the indirect coupling between electrical machines and external circuits depends on the difference between the time constants, and therefore it is subject to the studied case. The results of this work, however, support the usage of indirect coupling in many cases and will possibly give rise to further studies in this field.

In most of the references in this field, authors have utilized program code owned by the university. Commercial software is not always sufficient for the specific research interests and licence

fees may be unaffordable, but they often provide excellent user interface and post-processing routines. A combination of university code and commercial software, as presented in this work, also combines the advantages. On the one hand, the program code for the finite element analysis is optimized for electrical machines and can be modified if necessary; on the other, construction of large-scale system models in SIMULINK is simple and there are several block libraries and functions available, including all functions and post-processing routines of MATLAB. Consequently, the simulation models can be designed in collaboration between several experts, each of whom is only responsible for one part of the overall simulation model.

Numerical coupling between time-stepping finite element analysis and circuit simulation has been presented widely in the literature, and some references also include control systems in the simulation model. However, the control systems presented for frequency converters have been very simple and only operating in open-loop mode. The studies presenting closed-loop control systems, on the other hand, have only considered simple inductors or relays. Using the current output approach presented in this work, large control systems can be modelled together with FEM in a relatively simple manner because of the flexible coupling with a system simulator and the possibility of simulating each part of the model with different time steps. As a result, complex models of frequency converters including the closed-loop control system were coupled with the FEM computation in the examples involving a drive application and a wind generator. Similar cases have not been reported in the literature, since appropriate methods have not been available earlier. In addition, the industrial partners involved with the example cases have been satisfied with the methods and have also obtained new knowledge from the results.

The software related to this work was developed as a combination of specific FEM code and SIMULINK, which naturally has required several tailored solutions in the programming. Nevertheless, the methods themselves are universal and therefore applicable to other software, too. Many circuit simulators or system simulators provide the possibility of linking existing program code to the simulation. In this respect, this work will be an encouraging example, showing the possibilities of coupling FEM code with commercial simulator software.

### **6.3 Optimal environment for the coupled simulation of electrical machines, circuits and control systems**

According to the literature review and the results of this work, it is possible to outline an optimal simulation environment for electrical machines, circuit and control systems. A fundamental assumption for doing so is that the emphasis of the simulation will be on the operation of the whole system and the interaction between the components, as well as on the behaviour and design of each component separately. Therefore, the optimal solution must contain two or three different tools operating firmly together. The finite element method is a natural choice for the electrical machine, while the electrical circuits are most fluently modelled by a circuit simulator providing a user interface and an extensive component library. The control systems are usually modelled as block diagrams, which may require a separate system simulator depending on the features of the circuit simulator.

As stated earlier, direct numerical coupling, which requires strong interaction between the FEM

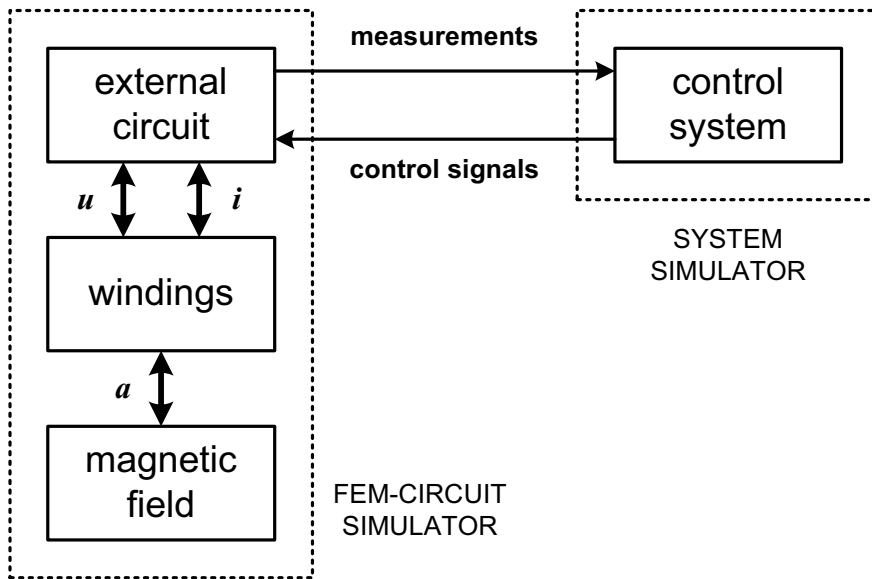


Figure 6.1: Outline of an optimal methodology for a coupled simulation of electrical machines, circuits and control systems.

computation and circuit simulation, is proposed for the field and circuit equations. To achieve this, the computation of fields and circuits must be integrated, which has usually been the case in the previous studies reported in the literature. Since the indirect coupling between the field-circuit models and control systems is adequate, and even more efficient due to the different time scale, an external simulator can be utilized for control system simulation.

To conclude the above discussion, outline of an optimal methodology for a coupled simulation of electrical machines, circuits and control systems is presented in Fig. 6.1. The equations of the magnetic field, windings and external circuits are coupled directly and solved in a FEM-circuit simulator. The variables in the coupled system of equations are the nodal values of magnetic vector potential  $a$ , the vector of currents  $i$  and the vector of voltages  $u$ . The control system is modelled in a system simulator, which is connected indirectly with the FEM-circuit simulator by the measurement signals and switch control signals. Because of the indirect coupling, different time steps may be used in the FEM-circuit simulator and the system simulator.

For modelling the switching elements, several approaches can be used. Accordingly, the selected approach also affects the time-stepping scheme. If the switches are considered as binary-valued resistors, the control signals are used for triggering the resistance value and forcing a new time step for the directly coupled FEM-circuit simulation. A similar procedure is required when the switching is modelled by changing the circuit topology. In such cases, a procedure for variable time steps is required. In the approach utilized in the case studies of Chapter 5, however, the control system and the switches are modelled together with the voltage source inverter; the effects of the switching are thus present in the voltage input of the FEM model. Because the inverter model is detached from the FEM model, the time steps need not be synchronized and constant steps can be utilized.

## 7 Conclusion

The aim of this study was to develop a simulation environment for electrical machines, circuits and control systems. To achieve this, a methodology was presented for coupling finite element analysis with a system simulator SIMULINK. Two indirect approaches were developed: the current output approach and circuit parameter approach. Performance of both these methods were studied by example cases of varying complexity.

The computational algorithms for modelling the magnetic field in the electrical machine are based on a two-dimensional finite element method (FEM), coupled with the circuit equations of the windings. The methods are implemented for SIMULINK as S-functions, which provide functional blocks for the FEM computation. Because of the indirect coupling, time steps of different lengths can be used in the model. Another benefit of using a system simulator is that the large-scale system model can be composed of parts designed by several experts in different fields and connected simply in the block structure.

The current output approach is based on direct coupling between the field and circuit equations relating to the cross section and windings of the electrical machine. In SIMULINK, the electrical machine is represented by a block, which solves the phase currents from the given supply voltages. In the circuit parameter approach, the electrical machine is characterized by the electromotive force, dynamic inductance and resistance, which are solved by FEM at each time step. The inputs for the functional block in SIMULINK are the supply voltages, while the outputs are the above-mentioned circuit parameters.

In the first case study, a doubly-fed induction generator was modelled by FEM and simulated in steady-state and fault operations using an ideal voltage supply. The results obtained by the circuit parameter approach were compared with those obtained by the directly coupled simulation, revealing some differences due to the indirect coupling mechanism. In the circuit parameters solved by FEM, there was a delay of one time step that cannot be removed, but the error in the simulation results can be decreased by shortening the time step.

In the second case study, the circuit parameter approach was applied to a cage induction motor, giving results similar to those obtained for the doubly-fed induction generator. The FEM model of the cage induction motor was also coupled with an external circuit model comprising grid and compensating capacitors. The system was simulated using the current output approach, circuit parameter approach and directly coupled FEM-circuit model, and the simulation models were validated by experimental results. The results obtained by the three methods were similar but not identical, indicating that the indirect coupling of the field and circuit equations may give results that are relatively accurate, but not as reliable as the directly coupled simulation.

Two examples, relating to a motor drive and a wind generator with controlled frequency converters, were also presented. In the first example, a FEM model of a cage induction motor was

coupled with a detailed model of a frequency converter with direct torque control. The current output approach was used for the simulation and the results were compared to measurements. In the second example, a FEM model of a doubly-fed induction generator was coupled with models of a frequency converter, grid, transformer, overcurrent protection circuit and a control system. A simulation was run using both the current output approach and circuit parameter approach. The results of both examples confirmed that the performance of the current output approach was excellent in the coupled simulation of an electrical machine, frequency converter and a closed-loop control system. The circuit parameter approach, however, was not suitable for simulating such systems.

On the basis of the results and the literature study, an optimal environment was proposed for coupled simulation of electrical machines, circuits and control systems. In such an environment, there would be direct coupling between the field and circuit equations, and indirect coupling between the field-circuit model and control system model. This could be accomplished by a FEM-circuit simulator coupled indirectly to a system simulator.

## References

Abe, N.M. and Cardoso, J.R. 1998: “Coupling Electric Circuit and 2D-FEM Model With Dommel’s Approach for Transient Analysis”, *IEEE Transactions on Magnetics*, Vol. 34, No. 5, September 1998, pp. 3487–3490.

Ahn, S.C., Lee, J.H., and Hyun, D.S. 2000: “Dynamic Characteristic Analysis of LIM Using Coupled FEM and Control Algorithm”, *IEEE Transactions on Magnetics*, Vol. 36, No. 4, July 2000, pp. 1876–1880.

Albanese, R. and Rubinacci, G. 1992: “Numerical Procedures for the Solution of Nonlinear Electromagnetic Problems”, *IEEE Transactions on Magnetics*, Vol. 28, No. 2, March 1992, pp. 1228–1231.

Ansoft 2005: <http://www.ansoft.com/> (5.2.2005).

Ansys 2005: <http://www.ansys.com/> (5.2.2005).

Arkkio, A. 1987: “Analysis of Induction Motors Based on the Numerical Solution of the Magnetic Field and circuit Equations”, Electrical Engineering Series, No. 59, Acta Polytechnica Scandinavica, Helsinki, 97 p., available: <http://lib.hut.fi/Diss/198X/isbn951226076X/> (5.2.2005).

Arkkio, A. 1990: “Finite Element Analysis of Cage Induction Motors Fed by Static Frequency Converters”, *IEEE Transactions on Magnetics*, Vol. 26, No. 2, March 1990, pp. 551–554.

Bedrosian, G. 1993: “A New Method for Coupling Finite Element Field Solutions with External Circuits and Kinematics”, *IEEE Transactions on Magnetics*, Vol. 29, No. 2, March 1993, pp. 1664–1668.

Cedrat 2005: <http://www.cedrat.com/> (5.2.2005).

Cervera, M., Codina, R., and Galindo, M. 1996: “On the Computational Efficiency and Implementation of Block-Iterative Algorithms for Nonlinear Coupled Problems”, *Engineering Computations*, Vol. 13, No. 6, June 1996, pp. 4–30.

Charpentier, J.F., Lefèvre, Y., and Piquet, H. 1998: “An Original and Natural Method of Coupling Electromagnetic Field Equations with Circuit Equations Put in a State Form”, *IEEE Transactions on Magnetics*, Vol. 34, No. 5, September 1998, pp. 2489–2492.

Comsol 2005: <http://www.comsol.com/> (5.2.2005).

Costa, M.C., Nabeta, S.I., and Cardoso, J.R. 2000: “Modified Nodal Analysis Applied to Electric Circuits Coupled with FEM in the Simulation of a Universal Motor”, *IEEE Transactions on Magnetics*, Vol. 36, No. 4, July 2000, pp. 1431–1434.

Coulomb, J.L. 1983: “A Methodology for the Determination of Global Electromechanical Quantities from a Finite Element Analysis and Its Application to the Evaluation of Magnetic Forces, Torques and Stiffness”, *IEEE Transactions on Magnetics*, Vol. MAG-19, No. 6, November 1983, pp. 2514–2519.

De Gersem, H., Mertens, R., Lahaye, D., Vandewalle, S., and Hameyer, K. 2000: “Solution Strategies for Transient, Field-Circuit Coupled Systems”, *IEEE Transactions on Magnetics*, Vol. 36, No. 4, July 2000, pp. 1531–1534.

Demenko, A. 1994: “Time-Stepping FE Analysis of Electric Motor Drives with Semiconductor Converters”, *IEEE Transactions on Magnetics*, Vol. 30, No. 5, September 1994, pp. 3264–3267.

Demerdash, N. and Nehl, T. 1999: “Electric Machinery Parameters and Torques by Current and Energy Perturbations from Field Computations – Part I: Theory and Formulation”, *IEEE Transactions on Energy Conversion*, Vol. 14, No. 4, December 1999, pp. 1507–1513.

Depenbrock, M. 1988: “Direct Self-Control (DSC) of Inverter-Fed Induction Machine”, *IEEE Transactions on Power Electronics*, Vol. 3, No. 4, October 1988, pp. 420–429.

Dommel, H.W. 1969: “Digital Computer Solution of Electromagnetic Transients in Single- and Multiphase Networks”, *IEEE Transactions on Power Apparatus and Systems*, Vol. PAS-88, No. 4, April 1969, pp. 388–399.

Driesen, J., Belmans, R., and Hameyer, K. 1999: “Adaptive Relaxation Algorithms for Thermo-Electromagnetic FEM Problems”, *IEEE Transactions on Magnetics*, Vol. 35, No. 3, May 1999, pp. 1622–1625.

Driesen, J., Belmans, R., and Hameyer, K. 2002: “Computation Algorithms for Efficient Coupled Electromagnetic-Thermal Device Simulation”, *IEE Proceedings – Science, Measurement & Technology*, Vol. 149, No. 2, March 2002, pp. 67–72.

Eustache, P., Meunier, G., and Coulomb, J.L. 1996: “Finite Element Toolbox for Generic Coupling (magnetic, thermal, etc.)”, *IEEE Transactions on Magnetics*, Vol. 32, No. 3, May 1996, pp. 1461–1464.

Fu, W.N., Zhou, P., Lin, D., Stanton, S., and Cendes, Z.J. 2004: “Modeling of Solid Conductors in Two-Dimensional Transient Finite-Element Analysis and Its Application to Electric Machines”, *IEEE Transactions on Magnetics*, Vol. 40, No. 2, March 2004, pp. 426–434.

Fujiwara, K., Nakata, T., Okamoto, N., and Muramatsu, K. 1993: “Method for Determining Relaxation Factor for Modified Newton-Raphson Method”, *IEEE Transactions on Magnetics*, Vol. 29, No. 2, March 1993, pp. 1962–1965.

Gear, C.W. 1971: “Numerical Initial Value Problems in Ordinary Differential Equations”, Prentice-Hall, Englewood Cliffs, New Jersey.

Hameyer, K., Driesen, J., De Gersem, H., and Belmans, R. 1999: “The Classification of Coupled Field Problems”, *IEEE Transactions on Magnetics*, Vol. 35, No. 3, May 1999, pp. 1618–1621.

Ho, S.L., Fu, W.N., Li, H.L., Wong, H.C., and Tan, H. 2001: "Performance Analysis of Brushless DC Motors Including Features of the Control Loop in the Finite Element Modeling", *IEEE Transactions on Magnetics*, Vol. 37, No. 5, September 2001, pp. 3370–3374.

Infolytica 2005: <http://www.infolytica.com/> (5.2.2005).

Ito, M., Kawabata, K., Tajima, F., and Motoi, N. 1997: "Coupled Magnetic Field Analysis with Circuit and Kinematics Modelings of Brushless Motors", *IEEE Transactions on Magnetics*, Vol. 33, No. 2, March 1997, pp. 1702–1705.

Jabbar, M.A., Phyu, H.N., and Liu, Z.J. 2004: "Analysis of the Starting Process of a Disk Drive Spindle Motor by Time Stepping Finite Element Method", *IEEE Transactions on Magnetics*, Vol. 40, No. 4, July 2004, pp. 3204–3206.

Kanerva, S. 2001: "Implementation of Two-Dimensional Finite Element Method in System Simulator", Report 67, Helsinki University of Technology, Laboratory of Electromechanics, 49 p.

Kanerva, S., Stulz, C., Gerhard, B., Burzanowska, H., Järvinen, J., and Seman, S. 2004: "Coupled FEM and System Simulator in the Simulation of Asynchronous Machine Drive with Direct Torque Control", *International Conference on Electrical Machines ICEM 2004*. Cracow, Poland, September 5–8, 2004.

Kanerva, S., Seman, S., and Arkkio, A. 2005: "Inductance Model for Coupling Finite Element Analysis with Circuit Simulation", to be published in *IEEE Transactions on Magnetics*, Vol. 41, No. 3, May 2005.

Kuo-Peng, P., Sadowski, N., Bastos, J.P.A., Carlson, R., Batistela, N.J., and Lajoie-Mazenc, M. 1997: "A General Method for Coupling Static Converters with Electromagnetic Structures", *IEEE Transactions on Magnetics*, Vol. 33, No. 2, March 1997, pp. 2004–2009.

Kuo-Peng, P., Bastos, J.P.A., Sadowski, N., and Carlson, R. 1999: "Analysis of a Combined Converter-Electromagnetic Device by Taking into Account its Control Loop", *IEEE Transactions on Energy Conversion*, Vol. 14, No. 4, December 1999, pp. 1430–1434.

Kuo-Peng, P., Sadowski, N., Batistela, N.J., and Bastos, J.P.A. 2000: "Coupled Field and Circuit Analysis Considering the Electromagnetic device Motion", *IEEE Transactions on Magnetics*, Vol. 36, No. 4, July 2000, pp. 1458–1461.

Lombard, P. and Meunier, G. 1993: "A General Purpose Method for Electric and Magnetic Combined Problems for 2D, Axisymmetric and Transient Systems", *IEEE Transactions on Magnetics*, Vol. 29, No. 2, March 1993, pp. 1737–1740.

Luomi, J., Niemenmaa, A., and Arkkio, A. 1986: "On the Use of Effective Reluctivities in Magnetic Field Analysis of Induction Motors Fed from a Sinusoidal Voltage Source", *Proceedings of International Conference On Electrical Machines (ICEM) '86*. München, Germany, September 8–10, 1986, pp. 706–709.

MagneForce 2005: <http://www.magneforcess.com> (5.2.2005).

Manot, G., Lefèvre, Y., Piquet, H., and Richardeau, F. 2002: “Integration of Control Loops in Coupled Field Circuit Model to Study Magnetic Devices Supplied by Power Electronic Converter and Their Control”, *COMPEL: International Journal for Computation and Mathematics in Electrical and Electronic Engineering*, Vol. 21, No. 4, September 2002, pp. 563–572.

Meunier, G., Shen, D., and Coulomb, J.L. 1988: “Modelisation of 2D and Axisymmetric Magnetodynamic Domain by the Finite Elements Method”, *IEEE Transactions on Magnetics*, Vol. 24, No. 1, January 1988, pp. 166–169.

Nakata, T., Takahashi, N., Fujiwara, K., Okamoto, N., and Muramatsu, K. 1992: “Improvements of Convergence Characteristics of Newton-Raphson Method for Nonlinear Magnetic Field Analysis”, *IEEE Transactions on Magnetics*, Vol. 28, No. 2, March 1992, pp. 1048–1051.

O’Dwyer, J. and O’Donnell, T. 1995: “Choosing the Relaxation Parameter for the Solution of Nonlinear Magnetic Field Problems by the Newton-Raphson Method”, *IEEE Transactions on Magnetics*, Vol. 31, No. 3, May 1995, pp. 1484–1487.

Oliveira, A.M., Kuo-Peng, P., Ferreira da Luz, M.V., Sadowski, N., and Bastos, J.P.A. 2001: “Generalization of Coupled Circuit-Field Calculation for Polyphase Structures”, *IEEE Transactions on Magnetics*, Vol. 37, No. 5, September 2001, pp. 3444–3447.

Oliveira, A.M., Kuo-Peng, P., Sadowski, N., de Andrade, M.S., and Bastos, J.P.A. 2002: “A Non-a priori Approach to Analyze Electrical Machines Modeled by FEM Connected to Static Converters”, *IEEE Transactions on Magnetics*, Vol. 38, No. 2, March 2002, pp. 933–936.

Piriou, F. and Razek, A. 1988: “Coupling of Saturated Electromagnetic Systems to Non-Linear Power Electronic Devices”, *IEEE Transactions on Magnetics*, Vol. 24, No. 1, January 1988, pp. 274–277.

Piriou, F. and Razek, A. 1990a: “A Model for Coupled Magnetic-Electric Circuits in Electric Machines with Skewed Slots”, *IEEE Transactions on Magnetics*, Vol. 26, No. 2, March 1990, pp. 1096–1100.

Piriou, F. and Razek, A. 1990b: “Numerical Simulation of a Non-Conventional Alternator Connected to a Rectifier”, *IEEE Transactions on Energy Conversion*, Vol. 5, No. 3, September 1990, pp. 512–518.

Piriou, F. and Razek, A. 1993: “Finite Element Analysis in Electromagnetic Systems Accounting for Electric Circuits”, *IEEE Transactions on Magnetics*, Vol. 29, No. 2, March 1993, pp. 1669–1675.

Preston, T.W., Reece, A.B.J., and Sangha, P.S. 1988: “Induction Motor Analysis by Time-Stepping Techniques”, *IEEE Transactions on Magnetics*, Vol. 24, No. 1, January 1988, pp. 471–474.

Preston, T.W., Reece, A.B.J., and Sangha, P.S. 1991a: “Analysis of Switched Reluctance Drives by the Finite Element Time-Stepping Method”, *IEE Fifth International Conference on Electrical Machines and Drives*. London, UK, September 11–13, 1991, pp. 81–85.

Preston, T.W., Sturgess, J.P., and Tarkanyi, M. 1991b: “Finite-Element Simulation of a Generator Feeding into a Rectified Load”, *IEE Fifth International Conference on Electrical Machines and Drives*. London, UK, September 11–13, 1991, pp. 311–315.

Roel Ortiz, J.L., Sadowski, N., Kuo-Peng, P., Batistela, N.J., and Bastos, J.P.A. 2001: “Coupling Static Converter With Control Loop and Non-Linear Electromagnetic Devices”, *IEEE Transactions on Magnetics*, Vol. 37, No. 5, September 2001, pp. 3514–3517.

Sadowski, N., Carly, B., Lefevre, Y., Lajoie-Mazenc, M., and Astier, S. 1993: “Finite Element Simulation of Electrical Motors Fed by Current Inverters”, *IEEE Transactions on Magnetics*, Vol. 29, No. 2, March 1993, pp. 1683–1688.

Sadowski, N., Carlson, R., Arruda, S.R., da Silva, C.A., and Lajoie-Mazenc, M. 1995: “Simulation of Single-phase Induction Motor by a General Method Coupling Field and Circuit Equations”, *IEEE Transactions on Magnetics*, Vol. 31, No. 3, May 1995, pp. 1908–1911.

Salon, S.J., DeBortoli, M.J., and Palma, R. 1990: “Coupling of Transient Fields, Circuits, and Motion Using Finite Element Analysis”, *Journal of Electromagnetic Waves and Applications*, Vol. 4, No. 11, November 1990, pp. 1077–1106.

Seman, S., Kanerva, S., Niiranen, J., and Arkkio, A. 2004: “Transient Analysis of Doubly Fed Wind Power Induction Generator Using Coupled Field-Circuit Model”, *International Conference on Electrical Machines ICEM 2004*. Cracow, Poland, September 5–8, 2004.

Shen, D., Meunier, G., Coulomb, J.L., and Sabonnadiere, J.C. 1985: “Solution of Magnetic Fields and Electrical Circuits Combined Problems”, *IEEE Transactions on Magnetics*, Vol. MAG-21, No. 6, November 1985, pp. 2288–2291.

Silvester, P.P. and Ferrari, R.L. 1990: “Finite Elements for Electrical Engineers”, Second Edition, Cambridge University Press, New York, 344 p.

Simulink 2005: “SIMULINK Online documentation”, MathWorks, Inc., <http://www.mathworks.com/access/helpdesk/help/toolbox/simulink/> (5.2.2005).

Smith, A.C., Williamson, S., and Smith, J.R. 1990: “Transient Currents and Torques in Wound-Rotor Induction Motors Using the Finite-Element Method”, *IEE Proceedings B*, Vol. 137, No. 3, May 1990, pp. 160–173.

Strangas, E.G. and Theis, K.R. 1985: “Shaded Pole Motor Design and Evaluation Using Coupled Field and Circuit Equations”, *IEEE Transactions on Magnetics*, Vol. MAG-21, No. 5, September 1985, pp. 1880–1882.

Strangas, E.G. 1985: “Coupling the Circuit Equations to the Non-Linear Time Dependent Field Solution in Inverter Driven Induction Motors”, *IEEE Transactions on Magnetics*, Vol. MAG-21, No. 6, November 1985, pp. 2408–2411.

Strangas, E.G. and Ray, T. 1988: “Combining Field and Circuit Equations for the Analysis of Permanent Magnet AC Motor Drives”, *IEEE Industry Applications Society Annual Meeting*, volume 1. Pittsburgh, USA, October 2–7, 1988, pp. 7–10.

- Takahashi, I. and Noguchi, T. 1986: "A New Quick-Response and High-Efficiency Control Strategy of an Induction Motor", *IEEE Transactions on Industry Applications*, Vol. IA-22, No. 5, September/October 1986, pp. 820–827.
- Tsukerman, I.A., Konrad, A., and Lavers, J.D. 1992: "A Method for Circuit Connections in Time Dependent Eddy Current Problem", *IEEE Transactions on Magnetics*, Vol. 28, No. 2, March 1992, pp. 1701–1704.
- Tsukerman, I.A., Konrad, A., Meunier, G., and Sabonnadiere, J.C. 1993: "Coupled Field-Circuit Problems: Trends and Accomplishments", *IEEE Transactions on Magnetics*, Vol. 29, No. 2, March 1993, pp. 1701–1704.
- Vande Sande, H., De Gersem, H., and Hameyer, K. 2003: "Solving Nonlinear Magnetic Problems Using Newton Trust Region Methods", *IEEE Transactions on Magnetics*, Vol. 39, No. 3, May 2003, pp. 1709–1712.
- Vassent, E., Meunier, G., and Foggia, A. 1991a: "Simulation of Induction Machines Using Complex Magnetodynamic Finite Element Method Coupled with the Circuit Equations", *IEEE Transactions on Magnetics*, Vol. 27, No. 5, September 1991, pp. 4246–4249.
- Vassent, E., Meunier, G., Foggia, A., and Reyne, G. 1991b: "Simulation of Induction Machine Operation Using a Step by Step Finite Element Method Coupled with the Circuits and Mechanical Equations", *IEEE Transactions on Magnetics*, Vol. 27, No. 6, November 1991, pp. 5232–5234.
- Väänänen, J. 1994: "Combination of Power Electronic Models with the Two-Dimensional Finite-Element Analysis of Electrical Machines", *International Conference on Electrical Machines ICEM 1994*. Paris, France, September 5–8, 1994, pp. 99–104 (Vol. 3).
- Väänänen, J. 1996: "Circuit Theoretical Approach to Couple Two-Dimensional Finite Element Models with External Circuit Connections", *IEEE Transactions on Magnetics*, Vol. 32, No. 2, March 1996, pp. 400–410.
- Wang, J.S. 1996: "A Nodal Analysis Approach for 2D and 3D Magnetic-Circuit Coupled Problems", *IEEE Transactions on Magnetics*, Vol. 32, No. 3, May 1996, pp. 1074–1077.
- Williamson, S. and Ralph, J.W. 1983: "Finite-Element Analysis of an Induction Motor fed from a Constant-Voltage Source", *IEE Proceedings B*, Vol. 130, No. 1, January 1983, pp. 18–24.
- Williamson, S. and Begg, M.C. 1985: "Analysis of Cage Induction Motor - A Combined Fields and Circuits Approach", *IEEE Transactions on Magnetics*, Vol. MAG-21, No. 6, November 1985, pp. 2396–2399.
- Williamson, S., Lim, L.H., and Robinson, M.J. 1990: "Finite-Element Models for Cage Induction Motor Analysis", *IEEE Transactions on Industry Applications*, Vol. 26, No. 6, November/December 1990, pp. 1007–1017.
- Williamson, S. and Volschenk, A.F. 1995: "Time-Stepping Finite Element Analysis for a Synchronous Generator Feeding a Rectifier Load", *IEE Proceedings – Electric Power Applications*, Vol. 142, No. 1, January 1995, pp. 50–56.

# A Implementation of the FEM computation in Simulink

This annex describes briefly how the numerical methods of Chapter 2 are implemented in Simulink. The original Fortran code has been rearranged and some new interfacing subroutines have been programmed according to the specifications of Simulink. The following sections present some general information about S-functions, the structure of the S-function for the FEM computation and the methodology for the data transfer between the S-function and Simulink. The objective of this annex is to provide some practical information for the researchers who might be interested in combining their own code with Simulink.

## A.1 S-functions in general

The purpose of an S-function is to describe the operation of a functional block in Simulink using Matlab's command language, C, C++, Ada or Fortran. The detailed structure and operation of the S-functions are presented in the documentation of Simulink (Simulink, 2005). However, the most relevant features with respect to the FEM implementation are described briefly in this section.

The computational routines inside the S-function must be formulated in terms of the discrete or continuous state-space approach. The input, output and state variables are managed by Simulink, but the data transfer routines and memory allocation must be programmed in the source code of the S-function using specific subroutines that are delivered with Simulink.

The basic procedure of calling the S-functions is based on flag variables that invoke different operations during the simulation. Consequently, the S-function code must be organized in subroutines performing the desired operations. The flags and the corresponding operations are listed below:

- **flag=0:** Initialization
- **flag=1:** Calculate the derivatives of the continuous state variables
- **flag=2:** Calculate the discrete state variables
- **flag=3:** Calculate the output variables
- **flag=4:** Determine the next sample time hit
- **flag=9:** End of the simulation

When existing program code is transformed into an S-function, it is not always easy to formulate the code according to the specifications of Simulink, because the number of variables cannot be very high and the numerical algorithms of the original code do not necessarily match with Simulink. It should be noted, therefore, that the implementation described in the following section is a unique case and may not be directly applicable to other computational software.

## A.2 S-function for the FEM computation

### A.2.1 Exceptional concepts

The main objective of implementing the FEM computation as an S-function has been the coupling with Simulink. Therefore, all the numerical algorithms have been conserved as closely as possible and only the inevitable modifications have been carried out. As a result, the implemented S-function does not comply perfectly with the concept and rules of Simulink, but it gives trustworthy results in comparison with the original program. In order to achieve this, certain exceptional concepts were required as listed below:

- **Internal variables:** Although the time-stepping simulation is basically governed by Simulink, the numerical algorithms are completely independent from the methods selected in Simulink. Accordingly, all the variables related with the computation are managed inside the S-function using internal memory space, which is not visible in Simulink.
- **State variables:** The natural choice for the state variables would have been the nodal values of the magnetic vector potential, but it turned out that Simulink is not capable of handling such a number of states. As a result, the vector potential values are considered as internal variables.
- **Direct feedthrough:** In order to prevent any non-converging iteration loops in the model, the output of the S-function must be delayed for one step with respect to the input by setting the parameter called ‘direct feedthrough’ to zero during the initialization. As a result, however, Simulink does not send the input variables for the calculation of outputs (flag=3), but the input values must be stored into the internal memory space during the calculation of state variables (flag=2).

### A.2.2 Outline of the implementation

Since the original FEM code (FCSMEK) is intended for stand-alone computation, it carries out all the simulation stages including initialization, time stepping and storage of the results. When the code is transformed into an S-function, the main program must be split into separate subroutines that are called by Simulink according to the flag variables. The following list describes the main operations performed on different flag values:

- **flag=0:** At the beginning of the simulation, the input data and simulation variables are read from the files and the internal variables of the S-function are initialized. In addition, the number of inputs and outputs are determined at this stage. Although the state variables are not utilized in the analysis, one meaningless discrete state is defined in order to manage the input variables at flag value 2.
- **flag=1:** Since there are no continuous states, this flag invokes no actions.
- **flag=2:** This flag is originally intended for calculating the discrete state variables, but is now only used for storing the input variables into the internal memory.
- **flag=3:** This flag invokes the FEM computation. The computational routines remain mostly unchanged, but now the analysis is only run for one time step.
- **flag=4:** The next sample time hit is based on the constant time step length, which is defined during the initialization.
- **flag=9:** At the end of the simulation, the results are prepared for post processing and stored into a file.

### A.2.3 Data transfer methodology

As the simulation variables are managed by Simulink, they are transferred directly with the function calls. However, the types and sizes of the input, output and state variables must be carefully determined and sufficient memory must be allocated in the S-function. For this purpose, a file template is delivered with Simulink in order to ensure the correct form of the code. The data pointers and variables are handled by specific subroutines, which are also delivered with Simulink.

Besides the simulation variables, which are passed at each time step, there are several parameters that are only needed for initialization. These parameters are read from a specific file at the initialization stage. In order to make the simulation more fluent, the custom masking properties of Simulink can be utilized in the creation of the parameter file. Details of this feature are presented in the documentation of Simulink.



ISBN 951-22-7609-7  
ISBN 951-22-7610-0 (PDF)  
ISSN 1795-2239  
ISSN 1795-4584 (PDF)